STIMULUS- AND CONTEXT-DEPENDENT TEMPORAL FILTERING IN THE AUDITORY PATHWAY OF THE LOCUST

Dissertation
zur Erlangung des akademischen Grades
doctor rerum naturalium
(Dr. rer. nat.)
im Fach Biologie

eingereicht an der

Lebenswissenschaftlichen Fakultät
der Humboldt-Universität zu Berlin

von
Dipl.-Biol. Sarah Kaarina Wirtssohn

Präsident der Humboldt-Universität zu Berlin

Prof. Dr. Jan-Hendrik Olbertz

Dekan der Lebenswissenschaftlichen Fakultät

Prof. Dr. Richard Lucius

Gutachter: 1. Prof. Dr. Bernhard Ronacher
2. Prof. Dr. Andreas Stumpner
3. Prof. Dr. Martin Nawrot

Eingereicht am: 06.10.2015
Tag der mündlichen Prüfung: 08.12.2015

"Die Natur und ihre Machenschaften wären ja auch eine ganz schöne Aufgabe zur Beschreibung."

—Thomas Bernhard

ABSTRACT

Temporal filtering of sensory input is crucial for the recognition of many sensory stimuli. Auditory neurons perform various computations and signal transformations to accomplish temporal filtering of acoustic input, comprising temporal integration, temporal resolution, and temporal feature selection. To test whether temporal filtering processes within a neuron type depend on stimulus features, such as intensity, and on context, such as temperature, I conducted neurophysiological recordings from neurons in the auditory pathway of migratory locusts.

First, I examined temporal integration in receptors and interneurons. The time course and extent of integration of subthreshold acoustic stimuli were neuron-specific. While peripheral sensory neurons acted as energy integrators, interneurons showed different temporal integration profiles, enabling neuron-specific temporal filtering. The analysis of postsynaptic potentials elucidated implemented mechanisms, suggesting that temporal integration is based on neuron-specific presynaptic and neuron-intrinsic computations.

Second, I studied the response recovery of receptors and interneurons to the second stimulus in a stimulus pair, separated by a few milliseconds. This revealed the effect of acute, short-term adaptation and thus indicated the maximal temporal resolution of these neurons. In the sensory periphery response recovery was shaped by moderate adaptation and an exponential recovery. In many interneurons non-linear effects occurred, comprising a suppression of the response to the second stimulus and a response gain.

Third, I tested the effect of temperature on temporal filtering. Temporal feature selectivity of interneurons was examined at cold and warm temperatures. With increasing temperature, the neurons preferred a temporally compressed feature. Temperature-dependent changes in temporal feature selectivity might thus contribute to temperature coupling of the sender and the receiver of the poikilothermic grasshoppers.

Keywords: insects, auditory system, temporal filtering, temporal integration, adaptation, temperature, neuroscience

ZUSAMMENFASSUNG

Die zeitliche Filterung von sensorischem Input ist entscheidend für das Erkennen vieler Stimuli. Auditorische Neurone führen dazu mehrere Verarbeitungsschritte und Signaltransformationen durch, u. a. durch zeitliche Integration, zeitliche Auflösung und Selektion eines zeitlichen Merkmals. Um zu testen, ob zeitliche Filterung von Stimuluseigenschaften (Intensität) oder Kontext (Temperatur) abhängt, untersuchte ich Neurone in der Hörbahn der Wanderheuschrecke.

Zuerst untersuchte ich zeitliche Integration in Rezeptoren und Interneuronen. Zeitverlauf und Ausmaß der Integration waren Neuronen-spezifisch. Während periphere Neurone die akustische Energie integrierten, unterschied sich die zeitliche Integration der Interneuronentypen stark, was eine spezifische zeitliche Filterung ermöglicht. Die Analyse postsynaptischer Potentiale deckte presynaptische und intrinsische Mechanismen der Integration auf, was darauf hindeutet, dass Unterschiede zwischen Neuronen wahrscheinlich auf Typ-spezifischer Verarbeitung beruhen.

Zweitens erforschte ich die neuronale Antwort auf den zweiten Stimulus in einem Stimuluspaar mit einem Interstimulus-Intervall von wenigen Millisekunden. Die Veränderung der Antwort auf den zweiten im Vergleich zum ersten Stimulus zeigt den Effekt von akuter, kurzfristiger Adaptation und ist ein Maß für die maximale zeitliche Auflösung. In der sensorischen Peripherie trat moderate Adaptation auf, deren Einfluss exponentiell abfiel. Viele Interneurone zeigten dagegen nicht-lineare Effekte, wie die Unterdrückung oder Verstärkung der Antwort auf den zweiten Stimulus.

Drittens testete ich den Effekt von Temperatur auf zeitliche Filterung. Die Selektivität von Interneuronen für zeitliche Stimulusmerkmale wurde bei wechselnden Temperaturen untersucht. Mit steigender Temperatur präferierten Neurone ein zeitlich komprimiertes Merkmal. Diese temperaturabhängige Veränderung könnte zur Temperatur-Kopplung von Sender und Empfänger bei den wechselwarmen Heuschrecken beitragen.

Schlagwörter: Insekten, auditorisches System, zeitliche Filterung, zeitliche Integration, Adaptation, Temperatur, Neurowissenschaften

Contents

List of Figures

List of Tables

List of Abbreviations

AHP	afterhyperpolarization
AN	ascending neuron
BSN1	bisegmental neuron 1
BSN1$_{\mathbf{b}}$	bisegmental neuron 1, bursting subtype
BSN1$_{\mathbf{nb}}$	bisegmental neuron 1, non-bursting subtype
EPSP	excitatory postsynaptic potential
FDHM	full-duration-at-half-maximum
FDHMin	full-duration-at-half-minimum
ICI	interclick interval
IPSP	inhibitory postsynaptic potential
LN	local neuron
LN$_{\mathbf{phas}}$	unknown local neuron, phasic subtype
LN$_{\mathbf{ton}}$	unknown local neuron, tonic subtype
$m_{\mathbf{pos}}$	weight of the positive lobe of STA-filter
RN	receptor neuron
SD	standard deviation
SN	segmental neuron
STA	spike-triggered average
TN1	T-shaped neuron 1

1 General Introduction

1.1 Sensory filtering

What an animal perceives of the world is made available to its nervous system through various sensory organs. These sensory organs transduce a physical or chemical stimulus into electrical signals, which are transmitted from the peripheral receptor neurons to the central nervous system. In the brain these electrical signals (the *sensory input*) can be evaluated, and allow to create an internal representation of the surrounding external environment and the changes within it. Ultimately, the brain can then generate the appropriate reaction to an external stimulus, or use the internal representation to guide goal-directed behavior.

However, the world around us is practically infinite, and so are the potential stimuli. In contrast, sensory organs and the brain are finite. Hence the nervous system needs to filter the information that is biologically relevant for an animal's perception, its behavior, and ultimately for its survival. Only a part of the infinite physical stimulus space is thus mapped into the finite sensory space spanned by the neuronal structures.

Filtering can refer to the *stimulus modality*, such as light or pressure, and to a certain *stimulus range*. Mechanisms for filtering can be implemented both peripherally and centrally in the nervous system. Examples of different mechanisms are:

- The mechanics of the sensory organ or its receptive structures, which make a receptor selective for a specific stimulus property. For instance, in the vertebrate cochlea a sound pressure wave travels along the basilar membrane such that hair cells at different locations resonate strongest at specific carrier frequencies.

- The sensitivity of receptors, which selectively respond to a specific stimulus range. We cannot, e.g., perceive ultra-violet light, because the pigments in our visual receptors are not sensitive to light at such short wavelengths.

- The tuning of sensory neurons to stimulus properties like a specific temporal pattern. Auditory interneurons can be tuned to sound duration, for example.

- Adaptation, which allows the dynamic adjustment of the neuronal firing rate to the current stimulus intensity. In audition, adaptation occurs for instance in response to continuous acoustic stimulation.

- Cognitive mechanisms that temporarily suppress or enhance the processing of a stimulus. For instance, we can improve the perception of a certain stimulus modality by focusing our attention on it, while the perception of other sensory modalities can be impaired.

1.2 The significance of temporal filtering in audition

Acoustic stimuli are sound pressure waves propagated through air or water that are transduced by the mechanoreceptors of a hearing organ. Perceiving a sound can be very important for animals. For instance, many species use sound for intraspecific communication, or a sound may alert to an approaching threat. Both the carrier frequency and the temporal pattern of a sound can contain the relevant information for an animal. The auditory organ therefore has to be sensitive to the carrier frequency range of interest. As mentioned, this can be accomplished by the mechanics of the ear, and the sensitivity of receptor neurons. More complex processes underlie the decoding of temporal patterns. Acoustic signals are fast by nature, and accordingly an auditory system has to operate quickly to make sense of a sound stimulus. Thus, *temporal filtering* is particularly significant in audition in order to extract the decisive cues from the amplitude modulations of a sound envelope. Without adequate temporal filtering, humans would not be able to understand speech, and animals would not be able to extract meaningful signals from an incoming sound.

1.3 Grasshoppers: A suitable model organism to study temporal filtering

Studying temporal filtering in the auditory system of humans and vertebrates in general is hindered by the complexity of the underlying neuronal structures, by the large potential stimulus space, and often by the limitation of available and ethically appropriate experimental methods. But luckily, "simpler" organisms like many insects also possess hearing organs which aid them in finding mates or prey and in avoiding predators.

Among these insects, grasshoppers are particularly interesting because many species use acoustic communication for mating purposes, with a stereotyped species-specific acoustic signal generated by the sender and a stereotyped response of the receiver. Correctly recognizing and localizing an attractive conspecific signaler requires the adequate processing and filtering of the temporal structure of an incoming sound. This task is accomplished by a comparably small set of neurons, of which many are well-accessible for neurophysiological experiments. Therefore, the grasshopper auditory system is well-suited to study the various aspects of temporal filtering in sensory neurons.

1.4 The scope of this thesis

The present thesis concentrates on both the stimulus- and context-dependence of the temporal filtering capabilities of the neurons in the auditory pathway of grasshoppers. To this end, I studied the response properties of neurons stimulated with different sound intensities, under different states of neuronal adaptation, and at different temperatures. Specifically, I addressed:

- **Temporal integration**.
- **Response recovery**.
- **Temperature effects**.

These various aspects reflect and affect temporal filtering, implemented in a specific neuron type and/or at a certain processing level.

1.5 The thesis structure

All experiments were carried out on the migratory locust (*Locusta migratoria*), which belongs to the acridid grasshoppers. Hence, I give an overview of the auditory pathway of grasshoppers in chapter 2.

Electrophysiological procedures by which data from neurons in the grasshopper auditory pathway were obtained comprised intra- and extracellular recording methods. The experimental methods and the setups for acoustic stimulation partly overlap for the different experiments, thus the description of the recording and stimulation methods are pooled in chapter 3.

In chapter 4, I investigate the temporal integration in neurons at three consecutive processing stages of the auditory pathway. To this end, I determined detection thresholds for very brief single click and click pair stimuli. The neuron-specific mechanisms of temporal integration are addressed in chapter 5.

Chapter 6 describes the response recovery to short stimuli in auditory neurons. Emphasis lies on the recovery from acute adaptation, which is an important determinant of temporal resolution. Temporal resolution in turn determines potential temporal filtering properties of a neuron.

Chapter 7 tackles the temperature-dependence of neuronal feature selectivity and the resulting temporal filters. Temperature effects are particularly relevant for poikilothermic animals, like grasshoppers. The work in this chapter is based on a close collaboration with Frederic Roemschied from Prof. Susanne Schreiber's group "Computational Neurophysiology" at the Humboldt-Universität zu Berlin.

Finally, in chapter 8, I present the general conclusions and possible implications that can be derived from this thesis.

2 The Auditory Pathway of Grasshoppers: An Overview

As the reader may remember from strolling across a field or a meadow on a sunny summer afternoon, small grasshoppers are capable of making enormous noises. Grasshoppers sit in the grass and produce songs with a variety of rhythmic patterns to attract potential mates. These rhythmic patterns are species-specific, and in order to reproduce successfully the individual grasshopper has to detect this pattern despite of the background noise (produced, e.g., by heterospecific signalers). Further, the grasshopper needs to evaluate whether the signaler is attractive based on cues in the song, and, last but not least, localize the signal source. These tasks are accomplished by a rather small set of neurons, which are homologous in terms of physiology and morphology across individuals, and – at least at early processing stages – even across grasshopper species. This acoustic communication behavior and the (relative) simplicity of the underlying neuronal structures make the grasshopper an interesting model to study basic mechanisms of auditory function. In this thesis, the auditory pathway of the migratory locust, *Locusta migratoria*, served as the model system to investigate fundamental properties of neurons involved in auditory processing. I will therefore give a general introduction to the auditory pathway of grasshoppers here.

As outlined above, many grasshopper species rely on acoustic signaling for mating purposes. Typically, a male produces a species-specific calling song to which a female may respond, either by her own song or by a phonotactic approach towards the male (von Helversen, 1972, 1997). Therefore, the female has to recognize the signaler as a conspecific, and to evaluate the song with respect to the attractiveness of the male (von Helversen, 1997; Stange and Ronacher, 2012).

Grasshopper songs are typically sounds consisting of rather broadband carrier frequencies with a species-specific amplitude modulation of the sound envelope (Elsner, 1974; Stumpner and von Helversen, 1994; Meyer and Elsner, 1996). The decisive cues for species recognition are not provided by the spectral frequency content of the signal, but rather by the temporal structure of the amplitude-modulated sound envelope (fig. 2.1). Indeed the auditory system of grasshoppers is well-adapted to extract relevant cues from the temporal structure of a signal: it performs well at recognizing amplitude modulations at different time scales, but shows a relatively poor spectral frequency resolution (see Hennig et al. 2004 for a review, Schmidt et al. 2008).

Figure 2.1: **Example song of a grasshopper**. The song phrase of a *Chorthippus biguttulus* male. The decisive cues for species recognition lie rather in the temporal pattern of amplitude modulations of the sound envelope than in the spectral frequency content. Modified from von Helversen et al. (2004).

The ears of grasshoppers are found in the first abdominal segment. The neurons that constitute the first stages of the grasshopper auditory pathway are located in the metathoracic ganglion, and are strongly conserved across grasshopper species regarding their morphology and physiology (Römer and Marquart, 1984; Ronacher and Stumpner, 1988; Sokoliuk et al., 1989; Neuhofer et al., 2008). For this reason it is possible to use *L. migratoria* – a species that does not use acoustic communication for mating purposes – for neurophysiological experiments, and relate the findings to behavioral data obtained from other grasshopper species that communicate acoustically. Working with *L. migratoria* has decisive advantages: Locusts are large and thus easier to handle in experiments than many other species, and they can easily be obtained from commercial suppliers throughout the year.

The grasshopper's metathoracic auditory pathway is a three-layered, putatively purely feed-forward network. Its input layer is formed by $\sim$ 60-80 receptor neurons per ear that project onto $\sim$ 15 local neurons (LNs) via excitatory synapses. The LNs constitute the intermediate layer of the network and convey excitatory and inhibitory input onto the ascending neurons (ANs; Römer and Marquart 1984; Jacobs et al. 1999; Stumpner and von Helversen 2001; Vogel et al. 2005; Vogel and Ronacher 2007). These $\sim$ 20 ANs form the network output layer and transmit the information to the brain, where the song attractiveness is evaluated and ultimate behavioral decisions are triggered (Ronacher et al., 1986; Bauer and von Helversen, 1987). The network is putatively purely feed-forward and the connectivity within the layers is generally low; the BSN1 neuron however is a LN that receives input not exclusively from receptors, but also from within the LN layer via excitatory and inhibitory inputs. See fig. 2.2 for a schematic overview of the metathoracic network.

The auditory pathway is not a simple relay station for transmitting signals from the sensory periphery to the brain. In contrast, responses to auditory signals are preprocessed. The receptor neurons faithfully encode the amplitude modulations, that is, the envelope of an acoustic stimulus, in their spike patterns (e.g., Machens et al. 2001; Rokem et al. 2006). The ANs rather respond to distinct stimulus features and thus extract specific information from the incoming signal, such as, e.g., sound direction, or the duration of pauses (Ronacher and Stumpner, 1988; Stumpner et al.,

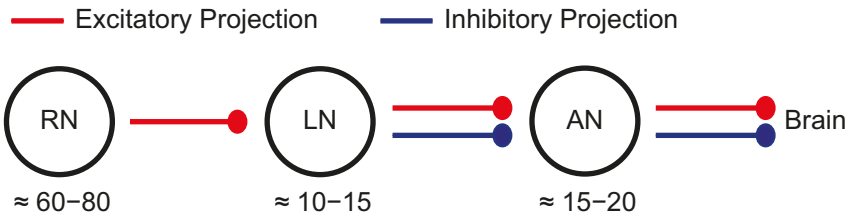

Figure 2.2: **Schematic overview of the metathoracic network in the locust auditory pathway.** RN = receptor neuron; LN = local neuron; AN = ascending neuron.

1991; Ronacher et al., 2004). Recent studies suggest that a change in coding strategy occurs in the metathoracic auditory network, namely from a summed population code with emphasis on spike timing, implemented in the receptors and most LNs, to a labeled-line code implemented in the ANs (Clemens et al., 2011, 2012; Meckenhäuser et al., 2014). Thus, ANs exhibit specific auditory filters with different shapes (for a review, see also Hildebrandt 2014). Generally, ANs can be grouped into direction-coding and pattern-coding neurons (Ronacher and Stumpner, 1993; Stumpner and Ronacher, 1994).

The data presented in this thesis stem from neurons of all three processing stages of the metathoracic network: Receptor neurons, local neurons and ascending neurons, and are referred to according to the nomenclature of Römer and Marquart (1984) and Stumpner and Ronacher (1991). In chapters 4, 5 and 6, neurons were individually identified according to their characteristic morphology and physiology (Stumpner and Ronacher, 1991). Here, the local neurons include: TN1 (T-shaped neuron 1), SN1 (segmental neuron 1), BSN1 (bisegmental neuron 1), and two groups of unspecified LNs. The ascending neurons are abbreviated with AN and a number; the ANs investigated in this thesis include the AN1, AN2, AN3, AN10, AN11 and AN12. In chapter 7, extracellular recordings were conducted, and neurons were not individually identified. Since recordings were obtained from the neck connectives, only neurons with axons ascending to the brain were recorded here.

3 Material and Methods

Adult migratory locusts (*Locusta migratoria*) of both sexes were used for all experiments. The locusts were obtained from commercial suppliers and housed at room temperature with *ad libitum* food and water supply. Neuronal signals from the auditory pathway of the locust were obtained by electrophysiological recordings. The data in chapters 4, 5 and 6 stem from intracellular recordings in the metathoracic ganglion. The data in chapter 7 was collected with extracellular recordings from the connectives which ascend from the prothoracic to the suboesophageal ganglion. The applied acoustic stimuli and data analysis methods will be described in each chapter separately.

3.1 Intracellular recording and acoustic stimulation setup

Animal preparation. For intracellular recordings, the head, legs and wings of the animal were removed. The last 1-2 abdominal segments were cut off and the gut was pulled out. The torso was waxed ventral side down on an animal holder using a wax-resin mixture. The thorax was opened dorsally to expose the thoracic ganglia. The connectives ascending from the mesothoracic ganglion were cut, as well as the descending connectives from the first three abdominal ganglia that are fused with the metathoracic ganglion. The meso- and metathoracic ganglia were lifted on a small NiCr-spoon for stabilization during the recording procedure. The torso was filled with locust ringer solution (Pearson and Robertson, 1981) to prevent drying-out. The temperature of the preparation was kept at a constant temperature of 30 $\pm$ 2°C by means of a Peltier element glued to the animal holder. This preparation procedure does not fundamentally alter the physiology of the metathoracic auditory neurons, because they exhibit the same properties as neurons recorded with an intact thorax (Wolf, 1986; Krahe, 1997; Kutzki, 2012).

Data acquisition. Sharp microelectrodes were used for recordings from single auditory neurons in the metathoracic ganglion. The electrodes were made from glass borosilicate capillaries (GC100F-10, Harvard Apparatus) with a horizontal puller (P87 or P-2000, Sutter Instruments) and were filled with 3-5 % Lucifer Yellow in 0.5 M LiCl (Carl Roth). The electrode impedance ranged from $\sim$ 25-120 MΩ, though most electrodes had impedances between $\sim$ 50-90 MΩ. The intracellular signals were amplified (SEC05LX, npi electronic) and digitized (A/D converter PCI-MIO-16E-4, National Instruments) with a sampling rate of 80 kHz. In parallel, the envelope of the digital output signal (i.e., the acoustic stimulus) was recorded to ob-

tain the exact stimulus timing with absolute precision. By this procedure, an error resulting from a jitter introduced by the recording software was avoided (for instance, online loading a stimulus could sometimes take a few milliseconds longer or shorter). Since the acoustic stimuli presented were extremely short, the unusually high sampling rate of 80 kHz was necessary. The membrane voltage and the acoustic stimuli were stored via a custom-made program (LabView 7, National Instruments) on a regular personal computer. Spikes were detected offline by applying a voltage threshold in Matlab (The Mathworks, Inc.). After recording, Lucifer Yellow was injected via the recording electrode by applying negative current pulses with amplitudes ranging from -1.5 nA to -5 nA for several minutes. The meta- and mesothoracic ganglia were removed, fixated in 4 % paraformaldehyde or 10 % formalin, dehydrated in ethanol (with ascending concentration: 50 %, 70 %, 80 %, 96 %, 100 %, each for 10-12 minutes), and cleared in methylsalicylate for 10-15 minutes. The neurons were then identified under a fluorescence microscope, based on their characteristic morphology following the nomenclature of Stumpner and Ronacher (1991).

Setup for acoustic stimulation. All sounds were generated on a standard personal computer using a custom-made program written in Matlab (The MathWorks, Inc.). The signals were converted via a 100 kHz D/A-converter (PCI-MIO-16E-4, National Instruments) and attenuated (ATN-01M, npi electronic). An amplifier (Mercury 2000, Jensen) delivered the signal to two speakers (RT-7 Pro, Expolinear), which were each placed at a distance of ~ 40 cm, positioned at angles of $\pm 90°$ with respect to the longitudinal axis of the animal. A microphone (1/2 in, type 4133, Brüel & Kjær) and a measuring amplifier (type 2209, Brüel & Kjær) were used to calibrate sound intensity at the position of the preparation.

3.2 Extracellular recording and acoustic stimulation setup

Animal preparation. The antennae, legs and wings were removed. The animal was waxed dorsal side down on a Peltier element glued to an animal holder. Three small cuts were made into the cuticle of the first abdominal segment, such that a cuticle flap was formed. Special attention was paid to not damage the hearing structures. The flap was pulled aside to form a window in the abdominal cuticle. Through this window, the descending connectives from the first three abdominal ganglia were cut. The window in the abdomen was closed by replacing the cuticle flap and sealing it with wax-resin. The maxillae were removed, the labium was lifted and the gut was cut below the esophagus. The thin neck cuticle and the labial structure were removed to assess the connectives ascending from the prothoracic ganglion (in the following referred to as “neck connectives”). The tip of the abdomen was removed and the gut pulled out through the hole, such that the cavity below the connectives

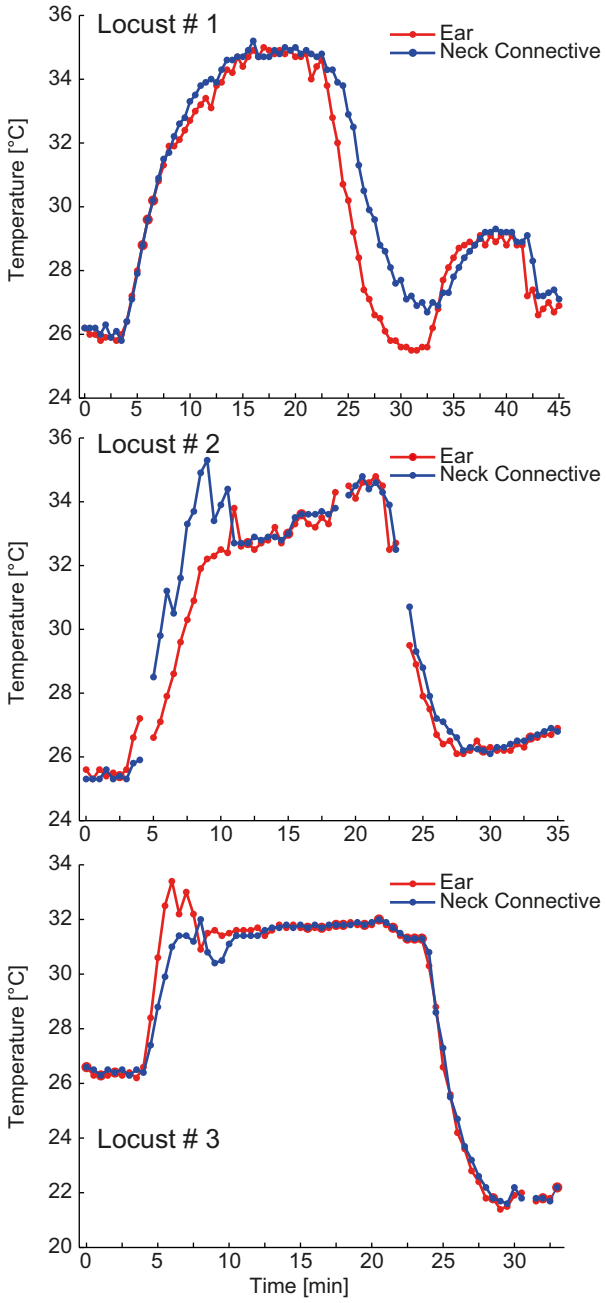

Figure 3.1: **Temperature measured simultaneously at the neck connectives (recording site) and the ears of three locusts.** After strong changes in temperature, a temperature equilibrium is quickly re-established. During maintenance of stable temperatures the temperature difference between neck and ear was negligible.

could be filled with a mixture of vaseline and mineral oil (Carl Roth). Two hook electrodes were placed around one of the connectives. To reduce noise, the connective was then cut below the subesophageal ganglion. The hook electrodes and the connectives were coated with vaseline for electrical isolation and to prevent a drying-out.

Data acquisition. As mentioned above, recordings were made with two hook electrodes made from tungsten wire, placed in parallel around one of the two neck connectives. Signals were differentially amplified (EXT-10C, npi electronic) and band-pass filtered with cut-off frequencies of 0.3 and 3 kHz (DPA-2FX, npi electronic) before digitization with a sampling rate of 20 kHz (PCI-MIO-16E-1, National Instruments) and storage on a personal computer.

Setup for acoustic stimulation. All sounds were generated on a standard personal computer using a custom-made program written in Matlab (The MathWorks, Inc.). The signals were converted via a 100 kHz D/A-converter (PCI-MIO-16E-1, National Instruments), attenuated (PA5, Tucker-Davis Technologies) and delivered by an amplifier (GTA 2100B, Blaupunkt) to one of two speakers (D21, Dynaudio). The speakers were each positioned at a distance of $\sim$ 35 cm at an angle of $\pm$ 90°with respect to the longitudinal axis of the animal. A microphone (1/2 in, type 4133, Brüel & Kjær) and a measuring amplifier (type 2209, Brüel & Kjær) were used to calibrate sound intensity at the position of the preparation.

Temperature control and monitoring. The temperature of the preparation was controlled by means of a Peltier element. In four recording sessions, the temperature was measured with two thermocouples. One was placed in the abdomen in the vicinity of the ear, and the other in the vicinity of the neck connectives, close to the recording site. The thermocouples where each connected to a thermometer with a measuring resolution of 0.5 °C (Greisinger, type GTH 1150). Of these specimens, three were recorded at cold and warm temperature, with ΔT of at least 5 °C. In eight recording sessions, the temperature was measured with one thermocouple in the thorax, close to the recording site, with a thermometer with a resolution of 0.05 °C (Greisinger, type GMH 3210). In these sessions, the recording temperature was maintained constant with a median standard deviation $<$ 0.11 °C. Control experiments showed that while maintaining a stable temperature, the temperature difference between the recording site and the ear was negligible (fig. 3.1). After a drastic temperature change a temperature equilibrium between the abdomen and the thorax was established after a few minutes. It was therefore sufficient to measure temperature only in the thorax close to the recording site during the experiments, and acoustic stimulation was started after waiting several minutes when the target temperature was reached.

4 Temporal Integration at Consecutive Processing Stages in the Locust Auditory Pathway

In this chapter, I will investigate temporal integration at the three consecutive processing stages of the locust auditory pathway. I will examine the time course and extent of temporal integration found in different neuron types. Large parts of this chapter were published in Wirtssohn and Ronacher (2015).

4.1 Introduction

The ability of an auditory system to summarize input over time is known as "temporal integration". It has traditionally been studied with so-called duration/intensity trade off-experiments, in which the detection threshold intensity is measured as a function of stimulus duration. In various species the detection threshold intensity decreases with increasing stimulus duration, for instance in humans (Plomp and Bouman, 1959), birds (Okanoya and Dooling, 1990), rodents (Viemeister et al., 1992), insects (Faure and Hoy, 2000) and marine mammals (Kastelein et al., 2010). These experiments usually reveal long integration time constants of up to several hundred milliseconds. However, other experimental paradigms, such as, e.g., gap detection and modulation transfer function measurements, describe a high temporal resolution of the auditory system, in the range of a few milliseconds. How can a system on one hand integrate over hundreds of milliseconds, but on the other hand have a temporal resolution of a few milliseconds? After all, the underlying neuronal structures processing acoustic input are the same, irrespective of the stimulus at hand. This puzzling problem has been termed the temporal integration-resolution paradox (De Boer, 1985; Green, 1985).

Different solutions to this paradox have been proposed. Many authors have argued that temporal integration in peripheral neurons occurs at short time scales, and that long time scale temporal integration is generated centrally in higher order brain regions (Viemeister and Wakefield, 1991; Lütkenhöner, 2011; Saija et al., 2014). It has also been proposed that the threshold reduction with increasing stimulus length is based on a summation of detection probability over time (Tougaard, 1998; Heil et al., 2008). Another possible solution for the integration-resolution paradox was introduced by Heil and colleagues: The first spike generation as a response to a sound in an auditory afferent fiber can be regarded as the accumulation of several independent sub-events, possibly point processes, such as, e.g., calcium-binding steps in synaptic processing. With increasing sound duration the mean rate of

these sub-events increases, until, eventually, a spike response is generated (for a review, see Heil 2004). With high sound amplitude the mean accumulation rate is high, yielding a high temporal resolution. The lower sound amplitude, the lower the mean accumulation rate and thereby temporal resolution, while temporal summation time measured as first-spike latency increases (Heil and Neubauer, 2003). Heil and Neubauer proposed that the integrator is located peripherally, namely in the synapse between the inner hair cell and the auditory nerve fiber. This theory opposes the notion that long term integration is generated centrally.

Psychoacoustic experiments on humans have indicated that detection thresholds depend on energy integration, suggesting that the auditory system has an intensity threshold; these findings have been traditionally described by leaky integrator models (e.g., Garner 1947; Plomp and Bouman 1959; Zwislocki 1960). More recent studies suggested that the detection threshold of sounds in vertebrate ears, cortical neurons and on the perceptual level is based on sound pressure integration, rather than energy integration (Heil and Neubauer, 2001). In insect ears, however, auditory receptor neurons act as energy detectors (Surlykke et al., 1988; Tougaard, 1996; Gollisch et al., 2002). The same is suggested for interneurons in the auditory pathway of katydids (Faure and Hoy, 2000) and crickets (Sabourin et al., 2008). Anatomical differences in the vertebrate and invertebrate ear may be the cause for the integration of different sound properties: In locusts, for instance, the receptors are directly attached to the tympanic membrane and the receptor axons form the fibers of the auditory nerve (e.g., Michelsen 1971). Using a two click-paradigm, Gollisch and Herz (2005) described the auditory transduction in the locust ear with an energy integration model. The model comprised a series of two linear filters, being the mechanical oscillation of the tympanum and the electrical integration at the neuronal membrane, and two nonlinear transformations.

Remarkably, detection threshold intensities are also decreased when two clicks (or other very brief stimuli) are presented, compared to the presentation of a single click (e.g., Viemeister and Wakefield 1991; Surlykke and Bojesen 1996; Tougaard 1996; Gollisch and Herz 2005; Heil et al. 2013). Those experiments often revealed temporal integration time constants of only a few milliseconds, which correspond well to the time constants found with other paradigms, e.g., with gap detection, and hence are more in line with the temporal resolution capabilities of auditory systems. The click pair paradigm is therefore a suitable experimental procedure to study temporal integration in an auditory system. A leaky energy integration model can be applied in a click pair paradigm; see fig. 4.1 for the effect predicted by the model on the detection threshold (compare Tougaard 1996). The basic idea of leaky energy integration is that the proportion to which the energy of sound is integrated decays monotonically (that is, in a “leaky” fashion) with time. At small intervals, the threshold reduction approaches -3 dB, since a doubling of sound energy, two clicks vs. a single click, yields an intensity increase of 3 dB. Over time,

the detection threshold reduction decreases monotonically. When the maximum integration time is reached there is no further improvement on detection threshold, and the detection threshold intensity is the same for a click pair as for a single click.

While there exist several studies investigating the temporal resolution capacities of auditory neurons of grasshoppers (e.g., Franz and Ronacher 2002; Prinz and Ronacher 2002; Ronacher et al. 2008), data on temporal integration are rare (but see Tougaard 1996, 1998; Gollisch et al. 2002; Gollisch and Herz 2005). Neurons in the metathoracic auditory pathway exhibit specified temporal filters, and particularly the ascending neurons (ANs) respond to specific features in a sound (Stumpner et al. 1991; Ronacher et al. 2004; Clemens et al. 2011, 2012; Meckenhäuser et al. 2014; see also chapter 2). It is therefore unlikely that there exists a uniform temporal integration time constant for all neurons of the auditory pathway. In contrast, neuron-specific temporal integration properties could enable temporal filtering. Studying temporal integration at consecutive stages in the auditory pathway may therefore help to reveal temporal filters as well as temporal limitations on auditory processing, and may give hints to the underlying mechanisms.

I therefore conducted intracellular recordings from morphologically identified neurons at the three subsequent processing stages in the metathoracic ganglion of *Locusta migratoria*, the migratory locust. The detection thresholds for single clicks and click pairs with varying interclick intervals were determined as a measure for temporal integration.

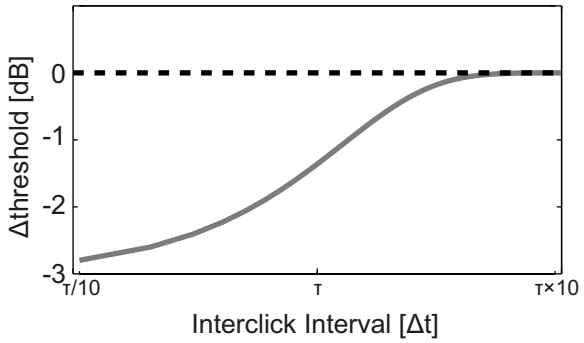

Figure 4.1: **The relative detection threshold, $\Delta threshold$, for a click pair as a function of the interclick interval, Δt, as described by the leaky integrator model** (gray line). At $\Delta threshold = 0$ (dashed line), the detection threshold for a click pair is equal to the single click detection threshold; τ is the time constant of the integrator.

4.2 Material and methods

4.2.1 Stimulus protocols and experimental procedure

Single clicks and click pairs were applied during intracellular recordings to obtain detection thresholds for different neuron types. The clicks were extremely short, with a duration of 40 μs, and the interclick interval (ICI) was systematically varied. The ICIs tested were 1, 2, 3, 4, 6, 8, 10, 20 and 30 ms. See fig. 4.2 for the digital waveforms of the click stimuli, and the air pressure fluctuations at the site of the animal's ear.

Once a stable recording was established, a rate-intensity response curve was measured by presenting 100 ms-noise pulses (5-40 kHz) from the left and the right loudspeaker separately. The pulses were presented in 8 dB-steps, from 32 dB to 88 dB, and repeated at least three times. The click stimuli were then presented from the more effective side, that is, the side from which stimulation at lower intensities evoked a spike response.

I then obtained the detection threshold for single clicks and click pairs with varying ICIs. To this end, 5 single click repetitions were presented in 8 dB-steps from 32 dB SPL to 88 dB SPL, in order to get a rough estimate for the approximate range of the detection threshold. This was evaluated online by visually monitoring post-stimulus spiking activity displayed on a standard oscilloscope. For the fine estimation of the detection threshold, single clicks (5 or 10 repetitions) and click pairs with varying ICIs (10 repetitions per ICI) were presented around the rough threshold estimate, such that usually a range of 10-16 dB in 2 dB-steps was covered.

For a detailed description of recording procedures and the setup for acoustic stimulation see chapter 3.

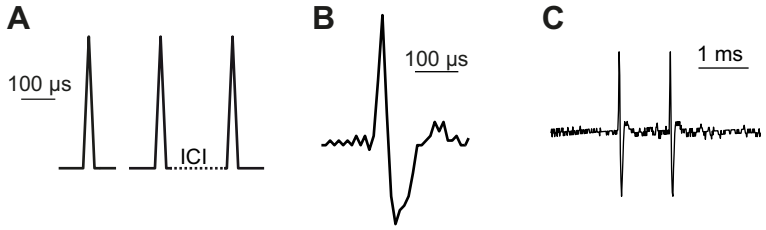

Figure 4.2: **Single click and click pair stimuli**. **A:** Triangular waveforms that were used to drive the loudspeaker. Each click had a total duration of 40 μs. The interclick interval (ICI) was systematically varied from 1-30 ms in click pairs. **B** and **C:** Air pressure fluctuations induced by a single click and a click pair, measured with a high precision microphone at the site of the animal's ear.

4.2.2 Data analysis

The linear regression fits to first-spike latencies were calculated in Excel 2013 (Microsoft Office). All other data analysis was carried out using Matlab (The MathWorks, Inc.). The data presented here stems from the following neuron types: 8 receptor neurons, 17 local neurons (LNs) and 15 ascending neurons (ANs). The receptor neurons were not divided into high- and low-frequency types (e.g., Michelsen 1971). The LNs can be divided into two subgroups: The primary-like LNs (TN1, N = 8; SN1, N = 1) which respond receptor-like, and the non-primary-like LNs (BSN1, N = 8). Ascending neurons can be grouped into direction-coding neurons (AN1, N = 7; AN2, N = 2) and pattern-coding neurons (AN10, N = 1; AN11, N = 2; AN12, N = 3). All ANs included in this study are excited by auditory input at specific intensities (Ronacher and Stumpner, 1993, see also chapter 2). Since not all neurons were tested with all click pair ICIs, the exact N per stimulus is given in the "Results" section.

Detection threshold. The detection threshold for single clicks and click pairs had to be determined in order to assess the integration time of the neurons.
The time window of stimulus-related activity was found by visual inspection of the post-stimulus time histograms of each neuron for each stimulus across all intensities. Thereby a time window ranging 5-60 ms after stimulus onset could be chosen. A sign test was conducted to compare the spontaneous spike count to the stimulus-induced spike count (the spontaneous activity was determined during a time window of the same duration before stimulus onset). One sign test per intensity per stimulus was conducted. The detection threshold of the neuron for a specific stimulus was defined as the lowest intensity at which post-stimulus activity significantly exceeded spontaneous activity with $p < 0.05$.

As in some recordings only 5 single click repetitions were presented, the detection threshold was determined as the lowest intensity at which the neuron responded in at least 4 out of 5 trials. Since many neurons responded with only one spike per stimulus at close-to-threshold intensities, "false positive" single spikes would strongly affect the results derived from a low number of stimulus repetitions. Therefore it was checked that no spontaneous activity occurred during 130 ms before stimulus onset in these cases, to only include neurons with a low probability of a spontaneous spike occurring just during the time window of expected stimulus-induced activity. This procedure was applied on the data of four LNs (2 TN1, 2 BSN1). See fig. 4.3A for examples of detection thresholds identified with 10 and 5 repetitions of the single click, respectively.

After this procedure, I had obtained the detection thresholds for the single click and for each click pair for every individual neuron. For further analysis, the data were pooled per neuron type. Therefore, the difference between the detection

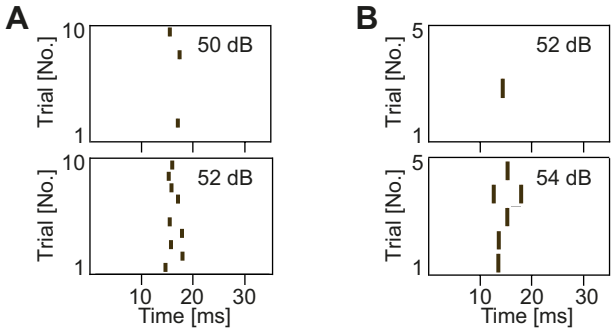

Figure 4.3: **Examples of detection threshold determination**. **A:** Spike raster plot of a neuron with 10 single click repetitions. Detection threshold at 52 dB, determined with the sign test ($p < 0.05$); the stimulus is subthreshold at 50 dB. **B:** Spike raster plot of a neuron with 5 single click repetitions. The detection threshold is 54 dB, the intensity at which it responded in 4 out of 5 trials. The click is subthreshold at 52 dB. Stimulus onset at 0 ms.

threshold for click pair stimuli ($tresh_{cp}$) and the single click ($tresh_{sc}$) was calculated by

$$\Delta threshold = tresh_{\mathrm{cp}} - tresh_{\mathrm{sc}}$$

Thus, a single measure of relative detection threshold shift (Δ*threshold*) per stimulus was derived. A $\Delta threshold < 0$ denotes a lower detection threshold for click pairs, and $\Delta threshold > 0$ a higher detection threshold for click pairs than for a single click. Accordingly, $\Delta threshold = 0$ reveals the same detection threshold for both the single click and the click pair. The Δ*threshold*-values were averaged across all specimens of one neuron type and plotted as a function of the click pair ICIs. The degree and time courses of temporal integration could then be inferred from these data plots.

As mentioned above, temporal integration has often been described by a leaky energy integration model (e.g., Plomp and Bouman 1959; Zwislocki 1960; Zwislocki et al. 1962). The data were fit to this model by fitting an exponential function with the least-squares-method, if two requirements for the model were met: Δ*threshold* should not considerably exceed -3 dB, and Δ*threshold* should decrease monotonically with ICI. The detection threshold shift Δ*threshold* according to the leaky integrator model is given by

$$\Delta threshold = -10 \log \left(e^{-\Delta t/\tau} + 1 \right),$$

with Δt as the click pair ICI and τ as the time constant of the integrator, at which Δ*threshold* reaches half of its maximal amplitude (see also Tougaard 1996).

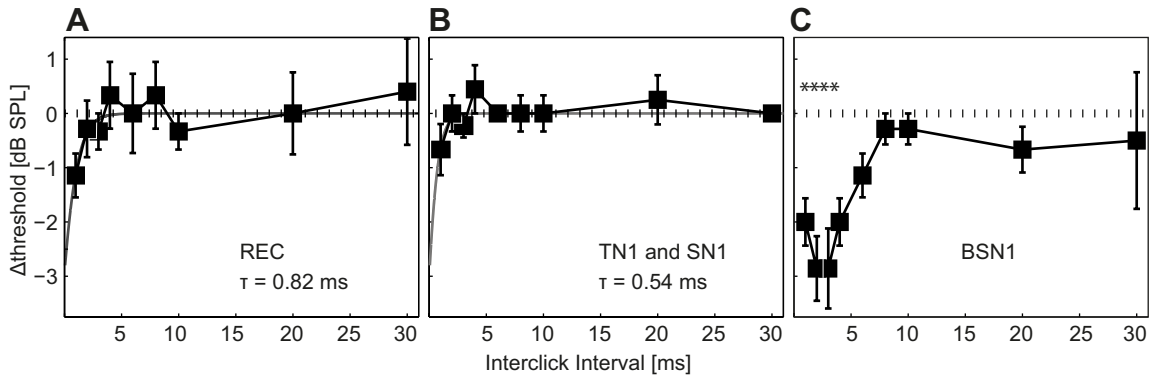

Figure 4.4: **Temporal integration in receptor neurons and local neurons.** At $\Delta threshold = 0$ (stippled lines), the detection thresholds for the click pairs were the same as for a single click. **A:** Temporal integration in receptor neurons (N = 8; ICI 2, 20 ms N = 7; 3, 4, 8 ms N = 6; 10, 30 ms N = 5) could be described with a leaky energy integrator model with a time constant of 0.82 ms (gray curve, $R^2 = 0.69$). **B:** Temporal integration in TN1 and SN1(N = 9; ICI 8, 10, 20 ms N = 8; 30 ms N = 1). Findings resemble receptor neurons; the time constant derived from leaky integrator model fit was 0.54 ms (gray curve, $R^2 = 0.58$). **C:** Temporal integration in the local neuron BSN1 (N = 7; ICI 30 ms N = 4). The threshold reduction was significant at 1-4 ms ICIs ($p < 0.05$, Wilcoxon signed rank-test). **A-C:** Values are means, error bars depict standard errors.

4.3 Results

Different time courses and detection threshold shifts were implemented in the neurons of the locust auditory pathway. The leaky energy integration model was applicable to the auditory receptor neurons and the primary-like local neurons (TN1 and SN1), because in these neurons the threshold shift decreased monotonically with the interclick interval (ICI), and the threshold shift did not exceed -3 dB. Higher order interneurons (the non-primary-like local neuron BSN1 and the ascending neurons) showed two distinct phenomena: Either, no temporal integration effects on threshold, or non-monotonic threshold shifts within a range of "optimal" interclick intervals clearly exceeding the extent of energy integration.

4.3.1 Leaky energy integration in receptors and primary-like local neurons

The differences between the thresholds found for a single click and for click pairs with increasing interclick intervals (ICIs) for the receptor neurons are shown in fig. 4.4A. A clear threshold reduction occurred at an ICI of 1 ms, but at larger click separations the two-click paradigm yielded similar thresholds as a single click ($\Delta threshold \approx 0$). The results were consistent with energy integration by a leaky integrator with a time constant of 0.82 ms ($R^2 = 0.69$). Similar results were found

for the primary-like LNs, TN1 and SN1 (fig. 4.4B); here the effect was weaker. The fit of the leaky energy integrator model revealed a time constant of 0.54 ms ($R^2 = 0.58$). However, the time constant estimates in both the receptors and primary-like local neurons could only be determined approximately, because the smallest ICI used in this study was 1 ms. But clearly the integration time constant was < 1 ms, and the primary-like local neurons did not exhibit any indication of temporal integration which exceeded the temporal integration in receptor neurons.

4.3.2 No clear indication of temporal integration in two ascending neuron types

In two types of ascending neurons, AN2 and AN11, no clear indication of temporal integration was found (fig. 4.5A, B). This result is puzzling, because temporal integration occurred in the receptors; accordingly, all higher order interneurons should show the same effects as the receptors (a threshold reduction at 1 ms ICI). I will address this issue in the discussion section.

4.3.3 Temporal integration at specific ICIs in non-primary-like local and ascending neurons

Some neuron types showed large threshold shifts, with maximal reductions at specific ICIs. This group comprises the local neuron BSN1, and the ascending neurons AN1, AN10 and AN12. Due to the non-monotonic shape of the temporal integration curves, a leaky integration model could be excluded for these neuron types.

The BSN1 exhibited a clear threshold reduction up to 6 ms ICI, as seen in fig. 4.4C. This effect was significant at 1-4 ms ICI with $p < 0.05$ (Wilcoxon signed rank-test), and a larger reduction in threshold occurred at 2-3 ms ICI than at 1 ms ICI. Looking at the single neuron data, 4 out of 7 specimens had a lower threshold at 2 and/or 3 ms than at 1 ms ICI, and in no specimen was the 1 ms threshold below the threshold at 2 and/or 3 ms ICI.

In the AN1 neurons, the maximal threshold shift was approximately -3 to -4 dB, as can be inferred from fig. 4.5C. The effect was strongest and significant with $p < 0.05$ (Wilcoxon signed rank-test) at 3-6 ms ICI. In 4 out of 7 recorded specimens, the threshold was lowest at ICIs between 3-6 ms, and in none was the threshold higher at 3-6 ms ICI than at 1 and/or 2 ms ICI. A threshold reduction occurred up to 8 ms ICI.

A third group of neurons comprising AN10 and AN12 displayed even larger threshold reductions, with threshold shifts of -6 dB and $\sim$ -7 dB, respectively, for click pairs (fig. 4.5D, E). As in BSN1 and AN1, the threshold did not increase monotonically with ICI, but occurred at an optimal time window, which were ICIs ≤ 4 ms in AN10, and in AN12 2-4 ms ICI. In AN12, the detection thresholds at 2-4 ms ICI were as low as or lower than at 1 ms ICI in all specimens, and lower in 2 out of 3 specimens. The threshold reduction was visible up to an ICI of 10 ms.

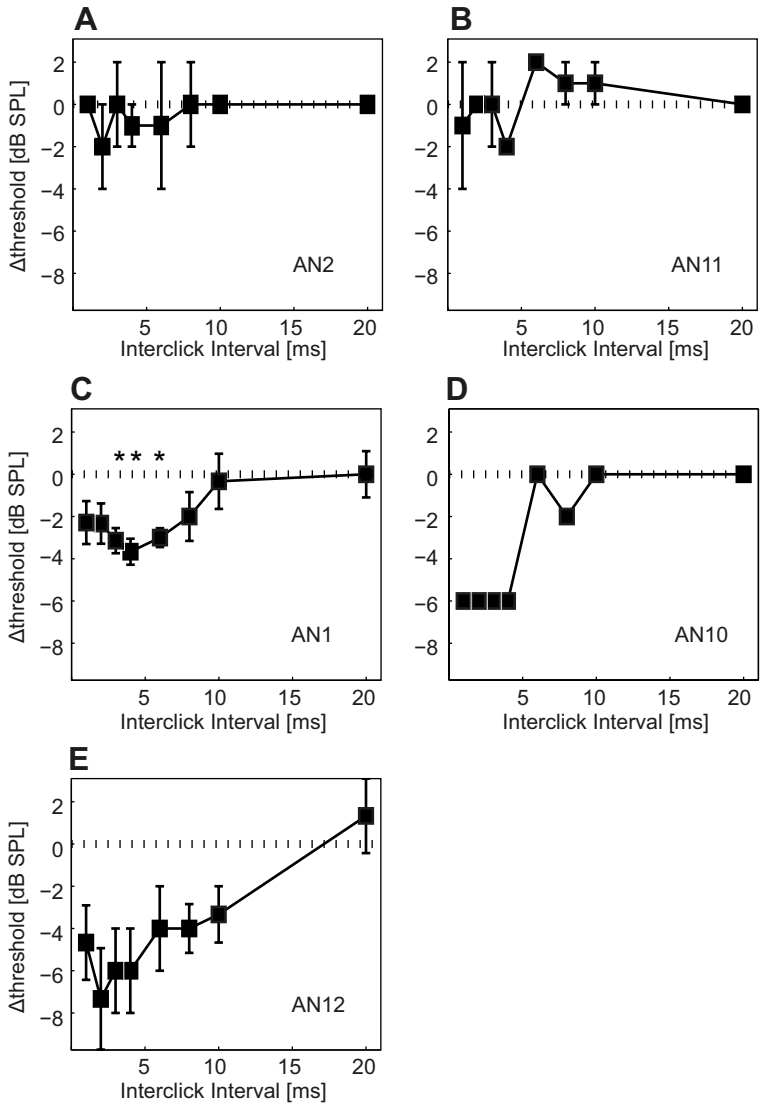

Figure 4.5: **Temporal integration in ascending neurons.** At $\Delta threshold = 0$ (stippled lines) the detection thresholds for the click pairs were the same as for a single click. **A-B:** In neurons AN2 (N = 2) and AN11 (N = 2), the threshold for click pairs was not systematically lower or higher than for single clicks. **C:** In AN1 (N = 7; ICI 2, 4-10 ms N = 6; 20 ms N = 5) a threshold reduction for click pairs occurred, with lowest thresholds at 3-6 ms ICIs, significant with $p < 0.05$ (Wilcoxon signed rank-test). **D-E:** In AN10 (N = 1) and AN12 (N = 3), strong threshold reductions occurred. **A-C, E:** All values are means, error bars depict standard errors.

Testing detection thresholds with a click pair paradigm poses certain difficulties, due to the fact that results can be influenced by "joint probability" (compare Tougaard 1996, 1998). That is, if no temporal integration occurred, the two clicks of a pair would be processed independently. Each click then has a certain detection probability, which sums up for two independent events. Hence, a doubling of inputs at close-to-threshold intensities yields a doubling of spiking probability. This could influence the detection threshold determination, which here is based on the total spike count elicited by a stimulus. If, however, a true integration of the two clicks occurred, the latency of the spike response would be time-locked to the second click in a pair. The first-spike latencies would then shift continuously with the ICI, and a linear regression fit to the first-spike latencies should accordingly reveal a slope around 1. To test for this effect, I analyzed the first-spike latencies of neurons; only neurons with negligible levels of spontaneous activity were included. Most spikes clearly occurred after the second click in BSN1, AN1, AN10 and AN12 (fig. 4.6), and the latencies increased significantly with ICI, commonly with $p < 0.01$ or $p < 0.001$. The 95 % confidence intervals of the slopes of regression fits to first-spike latencies in BSN1, AN10 and AN12 comprised the value 1 in most tests. In AN1, the slope tended to be < 1. However, the spike raster plots of single specimens (see fig. 4.7) show that a response was elicited by click pairs with a specific ICI, indicative of true temporal integration, and not "joint probability". If it was a joint probability effect, the spike response would: 1) Extend to click pairs with longer ICIs, and 2) the spikes would be distributed such that each click elicited 50 % of the spikes. Fig. 4.7 is also a good example for interindividual variability within one neuron type.

Thus, in all neuron types analyzed, the threshold shifts observed were based on temporal integration.

4.4 Discussion

4.4.1 Leaky energy integration in the periphery of the locust's auditory pathway

Only neurons in the very periphery of the locust auditory pathway responded in a way consistent with a leaky energy integrator model. These neuron types comprised the auditory receptors and the primary-like local neurons, TN1 and SN1.

The time constant τ of leaky integration, derived from the model fits, was 0.82 ms for the receptor neurons and 0.54 ms for the primary-like local neurons. For the receptors, this very short τ is in line with results of Gollisch and Herz (2005). According to their study, integration at an ICI of 1 ms is based on electrical integration at the neural membrane, because mechanic integration at the tympanum decays faster. In addition, Windmill et al. (2008) investigated tympanal mechanics with short (15 μs) sound pulses and found that the oscillation of the tympanic membrane outlasted their stimulus by a factor of 10 (see also Schiolten et al. 1981). Hence, even at 1 ms ICI, which was the smallest ICI used in this study, the oscillation of the tym-

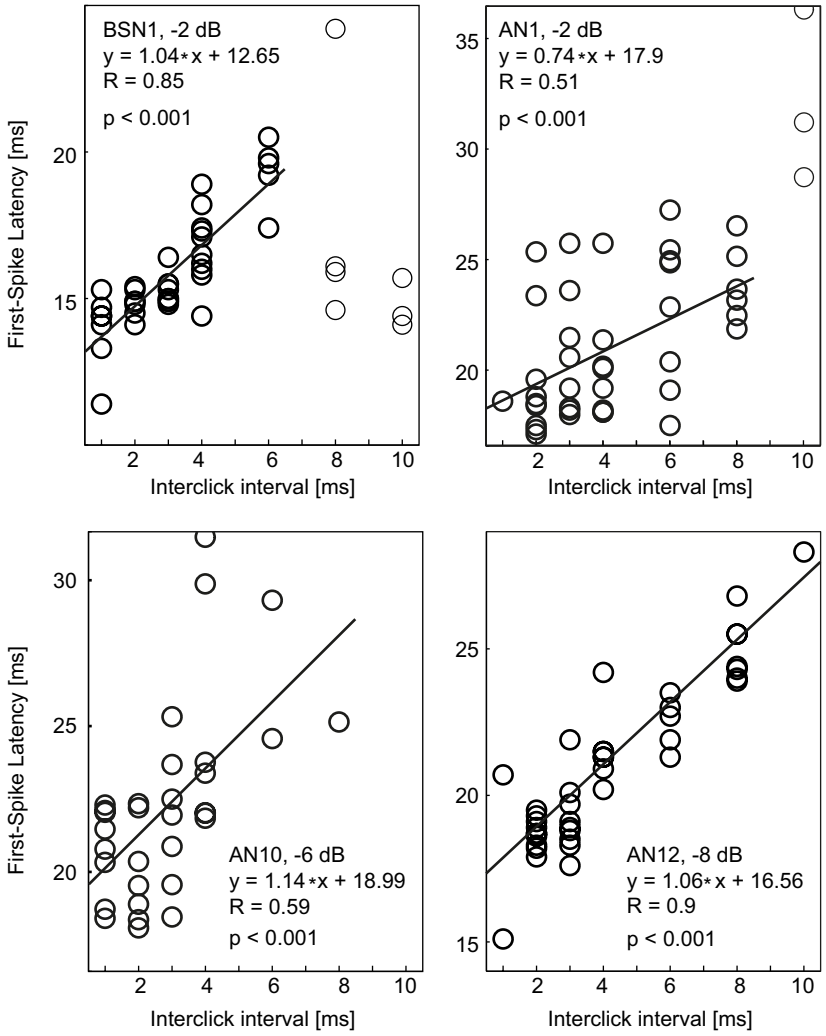

Figure 4.6: **Analysis of first-spike latencies of typical single neurons, to test for a "joint probability" effect on detection threshold measures.** Neurons were stimulated at intensities below single click detection threshold. Linear regression lines were fit to the first-spike latencies at all ICIs in which a threshold shift occurred at the group level in the neuron type (data points included for fit are printed in bold; compare fig. 4.4C, fig. 4.5C-E). The 95 % confidence interval of the regression fits enclose the value 1, though in AN1 the slope was < 1. A slope around 1 indicates a linear increase of the first-spike latency with the timing of the second click and thus temporal integration of the two clicks in a pair.

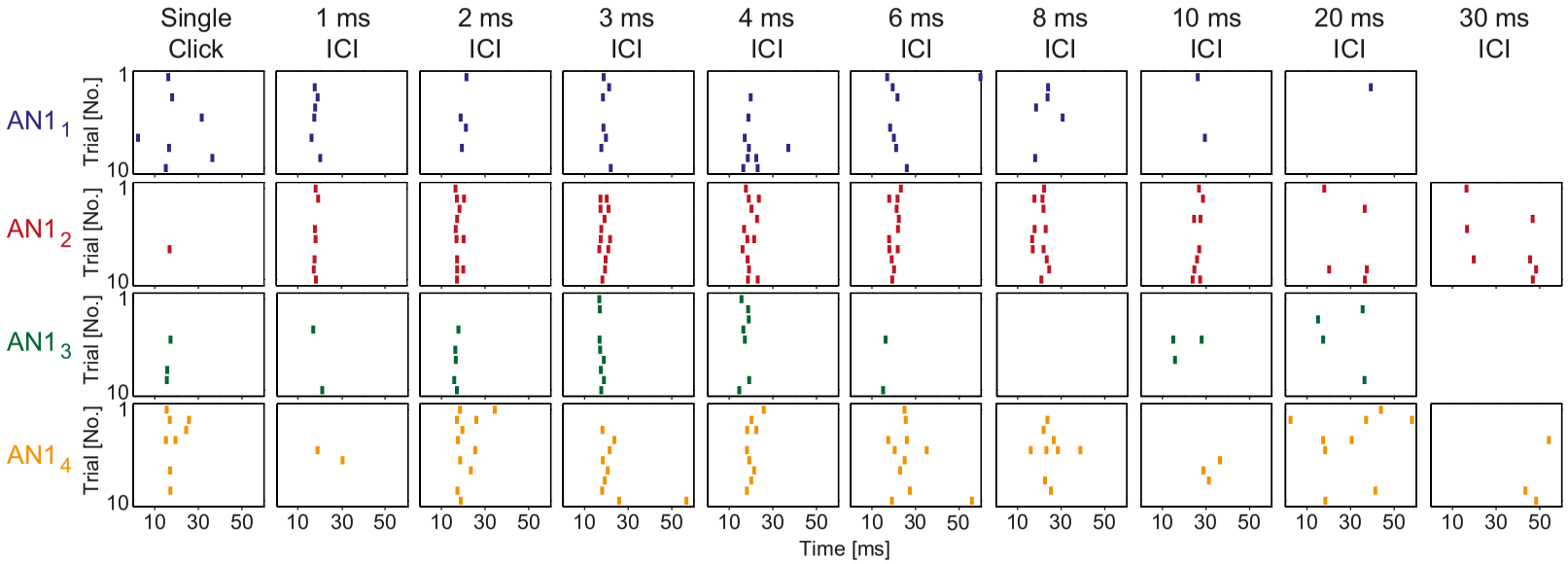

Figure 4.7: **The detection threshold in AN1 neurons is lower for click pairs with small and intermediate ICIs.** Spike raster plots of four specimens of the AN1 neuron type that showed low rates of spontaneous activity. Responses of the four individual specimens, labeled by color, to single clicks and click pairs. Though interindividual variability occurred, neurons tended to preferably respond to click pairs of small and intermediate ICIs, compared to single clicks or click pairs with longer ICIs, indicative of temporal integration. No effect of "joint probability" (see text) was found. Intensities of stimuli: -2 to -4 dB relative to single click detection threshold.

panic membrane elicited with the 40 μs clicks most probably had ceased before the second click reached the tympanum. It is therefore likely that temporal integration at the timescales reported in this thesis is based on neuronal integration, that is, the accumulation of electrical charges over the neuronal membranes. Interestingly, the integration time in locust receptors is clearly smaller than the 3.4 ms and 4.1 ms obtained with a click pair paradigm for the A1 receptor in moths (Tougaard, 1996), yielding a higher temporal resolution in the locust receptors.

Temporal integration in primary-like local neurons (TN1 and SN1) was generally weak and happened in the range of temporal integration in the receptors. A time constant of $\sim$ 0.5 ms was derived from the fit of the leaky integrator model. Apparently, these local neurons did not perform neuron-intrinsic summation of subthreshold input, since the effects did not exceed those of the receptor neurons.

The short time constants in receptor neurons and primary-like local neurons enable a precise coding and a high temporal resolution for the analysis of sound signals in the periphery of the locust's auditory system.

4.4.2 Temporal integration at higher processing stages

The threshold shifts indicative of temporal integration in the ascending and nonprimary-like local neurons (BSN1, AN1, AN10 and AN12) exceeded the time constants and shift amplitudes found in receptor neurons and primary-like local neurons by far. Thus, additional mechanisms must be postulated. Maximal threshold reductions occurred at neuron type-specific ICI windows (2-3 ms for BSN1, 3-6 ms for AN1, $<$ 6 ms for AN10, 2-4 ms for AN12). Further the maximal threshold reductions differed between neuron types ($\sim$ -3 dB for BSN1, $\sim$ -4 dB for AN1, -6 dB for AN10, $\sim$ -7 dB for AN12).

All higher order interneurons receive their input ultimately from the receptor neurons, either directly via monosynaptic connections, or indirectly via synaptic processing of receptor-driven first order interneurons (Boyan, 1992). Any effect exceeding the temporal integration in the receptor neurons must occur downstream of the receptor axons, namely earliest in the first synapse between the receptor and the respective LN. The processing within these synapses can be highly nonlinear, and affected by, e.g., spike-timing dependent plasticity and synaptic facilitation and depression (Baker and Carlson 2014; for reviews, see Zucker and Regehr 2002; Dan and Poo 2004). Interclick interval-dependent synaptic transmission efficacy could therefore strongly affect the integration time of the postsynaptic cell. Further, a temporal jitter of individual presynaptic inputs (because of, e.g., different synaptic delays or differences in axonal conductance speeds) could cause a broad compound EPSP which allows for longer temporal integration in the postsynaptic neuron than a narrow EPSP. Also active dendritic currents (Remme and Rinzel, 2011) and passive membrane properties of a neuron can influence integration time. With a slow EPSP decay due to slow membrane kinetics a second input can be in-

tegrated at longer interstimulus intervals. Further, the time courses of excitatory and inhibitory input shape the neuronal response of the auditory neurons (Stumpner and Ronacher, 1991; Oswald et al., 2006). With higher processing level and the number of synaptic connections and different membrane capacities involved, more mechanisms and their time courses can interact in a complex manner to produce the final temporal integration time of a higher order neuron. Generally, some of the mechanisms can be regarded as purely presynaptic to the respective neuron. Others necessarily require neuron-intrinsic computations on top of presynaptic processing, such as input summation. Due to the complexity of possible computations, it is difficult to disentangle the influence of different mechanisms of temporal integration capabilities of a single, particularly higher order neuron. I will now discuss the results in order to find hints for possible mechanisms underlying temporal integration in the different neuron types and try to disentangle the purely presynaptic from neuron-intrinsic effects at least roughly to some degree, before addressing some of these mechanisms in chapter 5 in detail.

The BSN1 neuron receives input from different receptor populations (Römer and Marquart, 1984). Thus, a temporal jitter of the input, induced by axonal conductance speed differences not only in individual receptor neurons but also in different receptor populations (Römer, 1976; Halex et al., 1988), could enable a neuron-intrinsic temporal summation of sub-threshold inputs. The BSN1 projects onto the AN1 (Marquart, 1985; Boyan, 1992), and could therefore mediate temporal integration within the range of its own time constant. The extent of the threshold reduction is similar in both neuron types. However, the optimal ICI window is longer in AN1. Additional effects therefore seem to contribute to the temporal integration properties of AN1.

A candidate mechanism to explain the occurrence of "optimal" ICIs for several higher order interneurons (BSN1, AN1, AN12) is neuronal facilitation. Two-tone facilitation has been described for subthreshold stimuli, e.g., in the cochlear nerve of gerbils (Henry, 1991) and in the cochlear nucleus of guinea pigs (Jiang et al., 1996), evident from a decrease in detection threshold for two consecutive tones. An exclusive tuning to specific ICIs, comparable e.g. to duration tuning known from the vertebrate midbrain and cortex (e.g., Ehrlich et al. 1997; He et al. 1997), was not found in the locusts' neurons: all cells in the present study responded to a single click when it was loud enough. The multiple-looks model proposed by Viemeister and Wakefield (1991) could be excluded, because it incorporates a long-term decrease in detection thresholds in the range of several hundred milliseconds. It is however possible that locust brain neurons act according to a multiple-looks strategy.

4.4.3 Relations between temporal integration and temporal filtering data

The very short integration times of receptors and primary-like neurons TN1 and SN1 are in line with results obtained in a modulation-transfer-function paradigm, where these neurons exhibited a high temporal resolution with mean corner frequencies of 172 $\pm$ 17 Hz, and 142 $\pm$ 43 Hz, respectively (data from Wohlgemuth et al. 2011, and Weschke and Ronacher 2008). Correspondingly, the best modulation frequencies were high (131 $\pm$ 28 Hz, and 103 $\pm$ 33 Hz).

In ascending neurons corner frequencies and best modulation frequencies were distinctly lower. The mean corner frequencies of AN1, AN2, AN11 and AN12 ranged between 40 and 78 Hz. The mean best modulation frequencies lay between 30 and 56 Hz (compare also Ronacher 2014). These ascending neuron data fits to a more integrative filter type, which leads to lower corner frequencies and lower best modulation frequencies (Nagel and Doupe, 2006). These results however do not explain the differences observed between AN2 and AN11 (no effect of temporal integration on detection threshold) on one hand (fig. 4.5A, B), and AN1 and AN12 with strong temporal integration effects (fig. 4.5C, E). BSN1 had a somewhat intermediate position between the primary-like local and the ascending neurons, with a corner frequency of 129 $\pm$ 45 Hz, and a best modulation frequency of 81 $\pm$ 41 Hz.

Clemens et al. (2012) reported results of a modeling study revealing two distinct neuron classes. These classes largely corresponded to local and ascending neurons: TN1 and SN1 belonged to the class of "derivative-like" neurons, whereas BSN1 (phasic subtype), AN1, and AN2 belonged to the "leading-suppressive" class. The neurons differed only marginally in the filter shapes derived from the spike-triggered averages but differed strongly in their spike-triggered covariance-filters. These data by Clemens et al. (2012) do however not explain the differences between AN1 and AN2 observed here.

The differences between the findings of Weschke and Ronacher (2008), Wohlgemuth et al. (2011) and Clemens et al. (2012) and the present study could be attributed to several differences in the experimental paradigms:

1. **Stimulus intensity.** Nagel and Doupe (2006) reported strong effects of stimulus intensity on filter shape. A possible mechanism could be the interactions between excitation and inhibition, and their respective timing. These might determine the shape of auditory filters (Clemens et al., 2012; Hennig et al., 2014; Ronacher, 2014), and their influence is intensity-dependent (Stumpner and Ronacher, 1991; Stumpner et al., 1991). The filters described by Clemens et al. (2012) were obtained at intensities 10-15 dB above the respective neuron's threshold, and the modulation transfer functions from Wohlgemuth et al. (2011) were measured with a stimulation at $\sim$ 20 dB above threshold.

2. **Temperature.** Neuronal activity in the nervous system of poikilothermic animals, including the processing of acoustic stimuli, is influenced by temper-

ature (Janssen, 1992; Franz and Ronacher, 2002; Fonseca and Correia, 2007), as is the shape of auditory filters (Slee et al., 2010). Clemens et al. (2012) performed experiments at room temperature (personal communication), which might account for some of the differences in neuronal filtering properties.

3. **Adaptation.** In the click pair paradigm, neuronal adaptation and refractoriness are reduced to a minimum, in contrast to the experiments in Weschke and Ronacher (2008), Wohlgemuth et al. (2011) and Clemens et al. (2012). Adaptation affects neuron types differently, by reducing the response to an auditory stimulus (Hildebrandt et al., 2009); this could influence temporal filtering capabilities of a neuron when it is adapted compared to a non-adapted state.

4.4.4 No temporal integration in several neuron types

Some cells did not show effects of temporal integration exceeding the integration in receptors, such as the primary-like local neurons TN1 and SN1, and others showed no threshold shifts at all (AN2 and AN11). This latter observation was unexpected: since the receptors integrate over short ICIs, at least this effect should be transmitted to later stages. A possible reason for the (apparent) loss of threshold reduction might be that the threshold reduction was rather small in the receptors and primary-like neurons. Thus the increasing variability at the next processing level (see Vogel et al. 2005) might have masked this small effect in a way that it could not be determined with the 2 dB-steps applied here. However, a so small effect may not be biologically relevant.

4.4.5 Relation to long-term temporal integration

For the auditory periphery of vertebrates it has been proposed that true energy integration occurs only with a short time constant, and long term integration is based on the accumulation of independent synaptic sub-events eventually leading to spike generation in an auditory receptor with a time delay (Heil and Neubauer, 2001, 2003). Other authors have also refuted the idea of long integration time constants in the auditory periphery, and argue instead that long-term temporal integration is centrally generated (e.g., Viemeister and Wakefield 1991; Viemeister et al. 1992; Lütkenhöner 2011; Saija et al. 2014). Also for insects, Tougaard (1998) proposes a distinction between two temporal integration time constants: An intrinsic one for the peripheral auditory neurons, and a behavioral time constant, generated in the central nervous system. Previous experiments have in fact shown that grasshoppers have "behavioral time constants", substantially longer than the neuronal ones presented here: male grasshoppers (*Chorthippus biguttulus*) for instance respond to female songs lasting only 250 ms as precisely as to songs of the natural duration of 1000 ms (Ronacher and Krahe, 1998, 2000), which suggests an upper limit for a behavioral integration time constant of around 250 ms.

4.4.6 Conclusion

To summarize, in the locust's auditory pathway temporal integration properties differ remarkably between neuron types. Only the responses of neurons at the very periphery could be described by a leaky integrator model. In contrast, several neurons at the next processing stages exhibited a stronger threshold reduction at "optimal" interclick intervals, longer than 1 ms. I will address the specific mechanisms contributing to these observations in the following chapter.

5 Neurophysiological Mechanisms Underlying Temporal Integration

In chapter 4, I described temporal integration at the three processing stages of the locust auditory pathway in the metathoracic ganglion. The time courses and extent of temporal integration differed remarkably between neuron types. I further mentioned possible cellular mechanisms underlying temporal integration. These could be divided into two main groups: 1) Neuron-intrinsic computations, and 2) presynaptic effects. In this chapter, I aimed at revealing the type of mechanism realized in the neurons of the auditory pathway of the migratory locust. To this end, I studied excitatory postsynaptic potentials evoked by single clicks and click pairs in dendritic recordings. Individual parts of this chapter were included in Wirtssohn and Ronacher (2015).

5.1 Introduction

There are two main mechanisms by which an interneuron can integrate excitatory dendritic input: 1) By spatial summation, and 2) by temporal summation (Spruston et al., 2007). For spatial summation, a neuron integrates simultaneous input over several postsynaptic sites; this could, e.g., occur when several synchronously firing presynaptic neurons project onto the same interneuron (Spruston, 2009). During temporal summation, the interneuron sums postsynaptic input arriving with a delay, which can in principle be evoked at one postsynaptic site only (Magee, 2000; Spruston et al., 2007). Here it is necessary that the membrane potential depolarization evoked by the first input has not decayed yet (London and Häusser, 2005). The changes in membrane potential and particularly the shape of the resulting excitatory postsynaptic potential (EPSP) depend on the underlying mechanism of summation: During spatial summation, the EPSP amplitude is larger than for a single input, while during temporal summation several peaks occur, which ultimately add up to larger depolarizations than induced by a single input (fig. 5.1).

In the previous chapter, temporal integration time constants of neurons in the locust auditory pathway were quantified using a click pair paradigm. Most neuron types exhibited a threshold shift for a double click stimulus compared to a single click stimulus up to a certain delay between the two clicks. This phenomenon might be explained by neuron-intrinsic temporal integration: The EPSPs evoked by the first and second click could be temporally summated, such that, eventually, the membrane potential depolarization reaches the spiking threshold. The time course

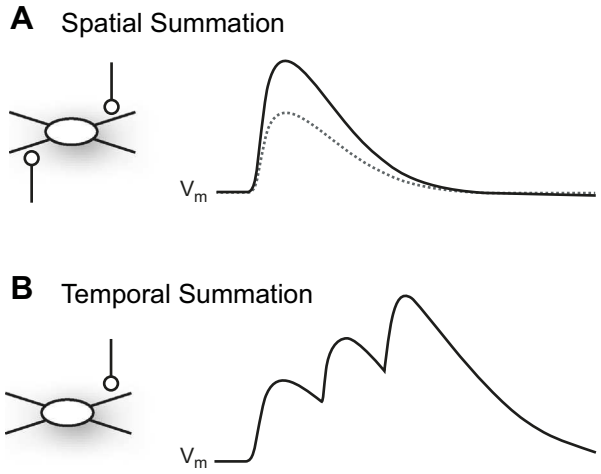

Figure 5.1: **Spatial versus temporal summation. A:** Spatial summation (black line) occurs when two synapses are activated simultaneously, leading to a higher EPSP than evoked by one synapse alone (gray dotted line). **B:** Temporal summation occurs due to repeated activation of a synapse, when the EPSP decay time exceeds the delay between successive synaptic input. In both cases, summation is sublinear, that is, the total depolarization of the membrane voltage (V_{m}) is smaller than the linear sum of the single inputs. Modified from Spruston (2009).

of the EPSP evoked by the first click or a single click would thus limit the temporal integration time of the neuron.

In addition to interneuron-intrinsic summation, another mechanism could explain a detection threshold shift to a click pair compared to a single click in an auditory neuron: The nonlinearities of synaptic transmission. It is well-known that the efficacy of synaptic transmission can be influenced by the history of synaptic activity. In addition to long-term effects like long-term potentiation and depression (for reviews, see Ito, 1989; Madison et al., 1991; Bear and Malenka, 1994), synaptic activity can also alter transmission within a synapse rapidly. These mechanisms are known as spike time-dependent plasticity, and can affect the efficacy of subsequent synaptic transmission in the millisecond range (for review, see Zucker and Regehr, 2002), and can be of presynaptic or postsynaptic origin, purely as well as combined (Abbott and Regehr, 2004).

As briefly mentioned in chapter 4.4, particularly synaptic short-term facilitation could account for a threshold shift in an interneuron to the second click in a click pair. Through facilitation of an excitatory synapse, the second (or more) activation of a synapse leads to a larger membrane depolarization in the postsynaptic neuron; this results in a comparably larger second EPSP, eventually eliciting a spike (Bower and Haberly, 1986; Fortune and Rose, 2001; Silberberg et al., 2004). Applied to the click pair paradigm, the second click would thus evoke a larger EPSP at an excitatory synapse than the first click or a single click alone, and such enable a spike

response at a lower intensity. Possible mechanisms for facilitation include the increase of transmitter release probability from residual Ca^{2+}-levels in the presynapse upon arrival of a second action potential with a brief delay (Katz and Miledi, 1968; Dittman et al., 2000; Zucker and Regehr, 2002), retrograde cues (Davis and Murphey, 1993; Reyes et al., 1998; Branco and Staras, 2009), rapidly adapting inhibition (proposed by Nelson and Young, 2010) and selective disinhibition (Klyachko and Stevens, 2006). Short-term synaptic plasticity can act as a temporal filter, since it aids to enhance or suppress the response to stimuli at specific repetition frequencies (for review, see Fortune and Rose, 2001). Of course, neuron-intrinsic and synaptic mechanisms are not mutually exclusive, and can interact within one neuron type.

Further, a threshold reduction could also be purely inherited from the presynaptic network. Here, the presynaptic neuron could deliver integrated input and thereby evoke a response at a lower intensity. In this case, one could expect an EPSP (eliciting a spike) time-locked to the second click, and not to a single or the first click.

To summarize, the shape and time course of an EPSP could reveal the mechanism(s) underlying temporal integration times. Since different neuron types exhibited specific integration time constants, it is particularly interesting how this phenomenon arises, and whether it is based on neuron-specific mechanisms. To address this question, I studied the shapes and time courses of EPSPs in dendritic recordings of several higher order interneurons.

5.2 Material and methods

5.2.1 Stimulus protocols and experimental procedure

The setup for acoustic stimulation, the stimulus protocols, experimental procedures and detection threshold determination methods were identical with chapter 4.2. Single clicks and click pairs with varying interclick interval (ICI) were presented.

5.2.2 Analysis of postsynaptic potentials

The shapes of excitatory postsynaptic potentials (EPSPs) of single specimens of the nonprimary-like local neuron BSN1 and the ascending neurons AN1, AN10 and AN12 were analyzed (that is, N = 1 each). To this end, the membrane voltage traces in subthreshold stimulus trials (trials in which the stimulus was presented at intensities below detection threshold and no spike response occurred) were smoothed with a moving average window of 62.5 μs and averaged, if at least 3 out of 10 trials were subthreshold. The baseline potential of the neuron was then calculated by averaging across 130 ms before stimulus onset; singular spontaneous spikes were excluded to not bias the baseline measure. The standard deviation (SD) of the baseline potential was calculated as the SD of membrane voltage during the same time

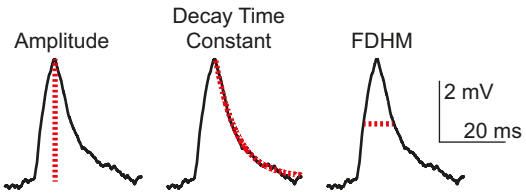

Figure 5.2: **EPSP parametrization.** Three parameters were obtained from each EPSP. Left: EPSP amplitude (red), relative to membrane potential baseline. Middle: Exponential fit (red) to the decaying phase of the EPSP to determine decay time constant. Right: Full-duration-at-half-maximum (FDHM, red) of the EPSP.

window. The maximum amplitude of the averaged potential after stimulus onset was compared to the baseline. If this amplitude exceeded the baseline potential + 3 $\times$ SD, an EPSP was registered. The following measures were calculated to parametrize the EPSPs: The EPSP amplitude, the EPSP decay time constant, and the EPSP full-duration-at-half-maximum (fig. 5.2). EPSP amplitudes were determined as the difference between the baseline voltage and the maximum voltage peak. A single exponential function was fitted either to the decaying phase of the EPSP, or to the decaying phase after the last peak in a compound EPSP, to derive the decay time constant. Results were only included into further analysis, when the fit described the data with sufficient quality ($R^2 \geq 0.75$). The full-duration-at-half-maximum (FDHM) was calculated to quantify the duration of the excited state.

Note that by this procedure, an EPSP was composed of the averaged membrane voltage traces from ≥ 3 single trials in which the stimulus was subthreshold. For each neuron, one value for the EPSP amplitude, the decay time constant and the FDHM were obtained per click pair ICI per intensity, provided that an EPSP occurred at the respective stimulus condition.

5.3 Results

5.3.1 Effect of stimulus intensity, stimulus type and click pair ICI on EPSPs

BSN1 neuron. In BSN1, EPSP amplitudes were larger at higher sound pressure levels, but decay time constants and FDHM values were not significantly different for increasing sound pressure levels (fig. 5.3A). An EPSP was elicited by a single click presented with subthreshold intensity starting from -4 dB below single click detection threshold. EPSP amplitudes and the full-duration-at-half-maximum (FDHM) tended to increase up to $\sim$ 6 ms and 4 ms ICI, respectively (fig. 5.4A); there was no consistent relationship found between ICI and EPSP decay time constant (mean 4.2 ms, SD: 1.5 ms, including single click).

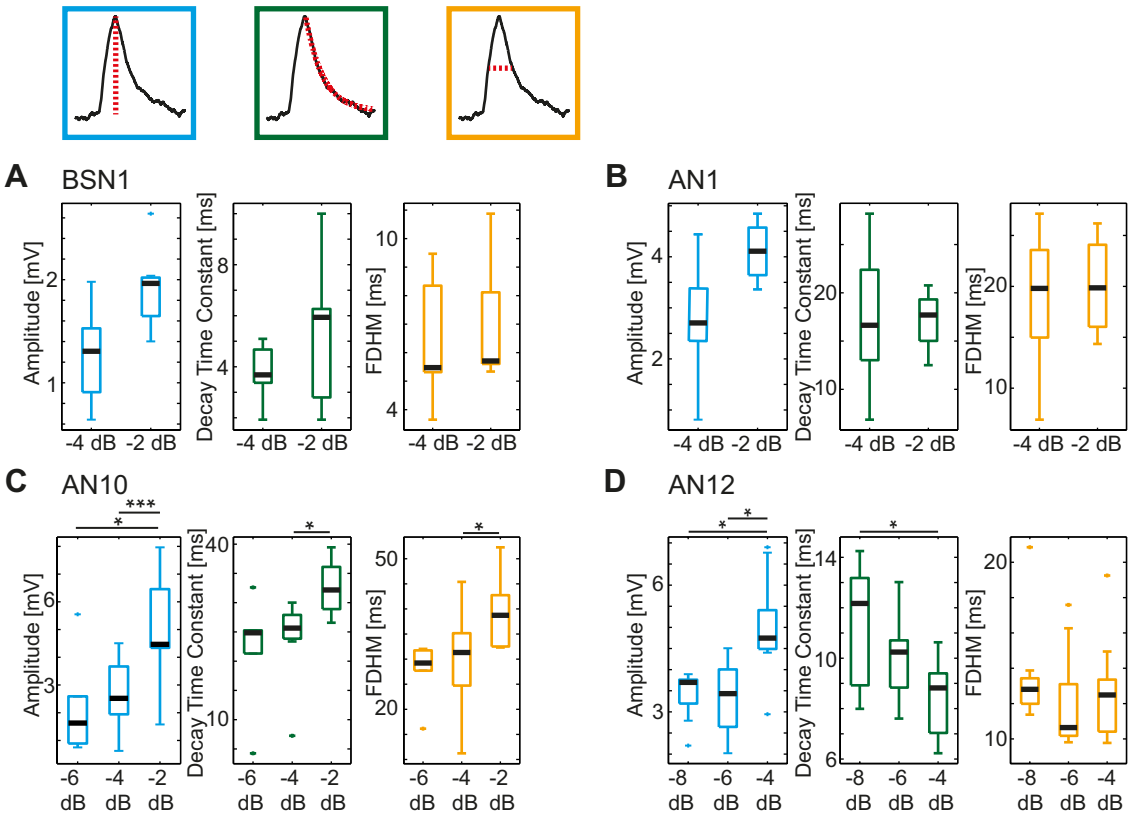

Figure 5.3: **Intensity-dependence of EPSP parameters.** Color code: Amplitude in blue, decay time constant in green, FDHM in yellow. **A:** The EPSP amplitude of BSN1 increased with sound intensity ($p = 0.052$, paired t-test calculated for interclick interval values when paired comparison was available). Decay time constants and FDHM were intensity-invariant. These findings resemble those for the AN1 neuron EPSP in **B. C:** In the AN10 EPSP, amplitude, decay time constants and FDHM increased with intensity, partly significantly (repeated measures-ANOVA). **D:** The EPSP amplitude of the AN12 increased with amplitude, and decay time constants decreased, partly significantly (repeated measures-ANOVA). The FDHM was intensity-invariant. **A-D:** Data were included in the plots, when more than 3 data points (that is, values for more than 3 ICIs) were obtained at the respective intensity. Intensities are given relative to single click detection threshold.

AN1 neuron. In AN1, the decay time constants and FDHM values appeared intensity-invariant, the EPSP amplitudes increased with sound intensity (fig. 5.3B). No test on significance was calculated, because values for a pair-wise comparison were too few. A significant EPSP in response to single click stimulation occurred at -4 dB relative to detection threshold intensity. For click pairs, EPSP amplitudes seemed to increase with ICI up to $\sim$ 6 ms; however, only at one intensity could these parameters be obtained for each ICI step (fig. 5.4B). No consistent effect of ICI on EPSP decay time constant (mean 17.1 ms including single click, SD: 5.9 ms) or FDHM was found (fig. 5.4B).

AN10 neuron. In AN10, an EPSP evoked by a single click occurred starting from -4 dB below detection threshold. Generally, amplitudes, decay time constants and FDHM increased with intensity (fig. 5.3C). The EPSP amplitudes in response to click pairs were largest for click pairs with ICIs $\leq$ 4 ms, while FDHM constantly increased with ICI; decay time constants (mean 27.1 ms, SD: 8.9 ms) were relatively constant for all stimuli, including single clicks (fig. 5.4C).

AN12 neuron. AN12 exhibited a clear EPSP as a response to single clicks presented at subthreshold intensities, starting at least -8 dB below detection threshold (which was the lowest intensity presented during this recording). The EPSP amplitudes tended to increase with intensity, while decay time constants decreased, and FDHM was intensity-invariant (fig. 5.3D). For click pair stimuli, the EPSP amplitude was highest up to ICIs of $\sim$ 4-8 ms. At the same time the FDHM was lowest at ICIs 2-4 ms, and then increased up to 10 ms ICI (fig. 5.4D). On the group level, the time window $\leq$ 10 ms ICI corresponds to the range of temporal integration described in chapter 4 (fig. 4.5E). Decay time constants were relatively unaffected by stimulus type (single click vs. click pair) and ICI (mean 9.7 ms, SD: 1.9 ms; fig. 5.4D).

5.3.2 Temporal summation reflected by EPSP shapes

All four neuron types displayed an EPSP in response to an auditory input with an intensity too low to evoke a spike response (BSN1: fig. 5.5A, AN1: fig. 5.5C, AN10: fig. 5.5D, and AN12: fig. 5.5E). The second click of a click pair stimulus, arriving at a specific delay, could thus principally be integrated neuron-intrinsically, as long as the EPSP evoked by the first click had not decayed.

BSN1 neuron. The shape of the EPSP of BSN1 (fig. 5.5B) revealed temporal summation at small ICIs, which ceased at longer ICIs ($\geq$ 6 ms), such that two distinct peaks of similar amplitude occurred (fig. 5.5B). Neuron-intrinsic temporal summation based on a summation of electric charges across the neuronal membrane could thus occur up to $\sim$ 4 ms ICI at this recording site. Further, the first peak in click pair EPSPs did not yield a higher amplitude than a single click EPSP (compare fig. 5.5A

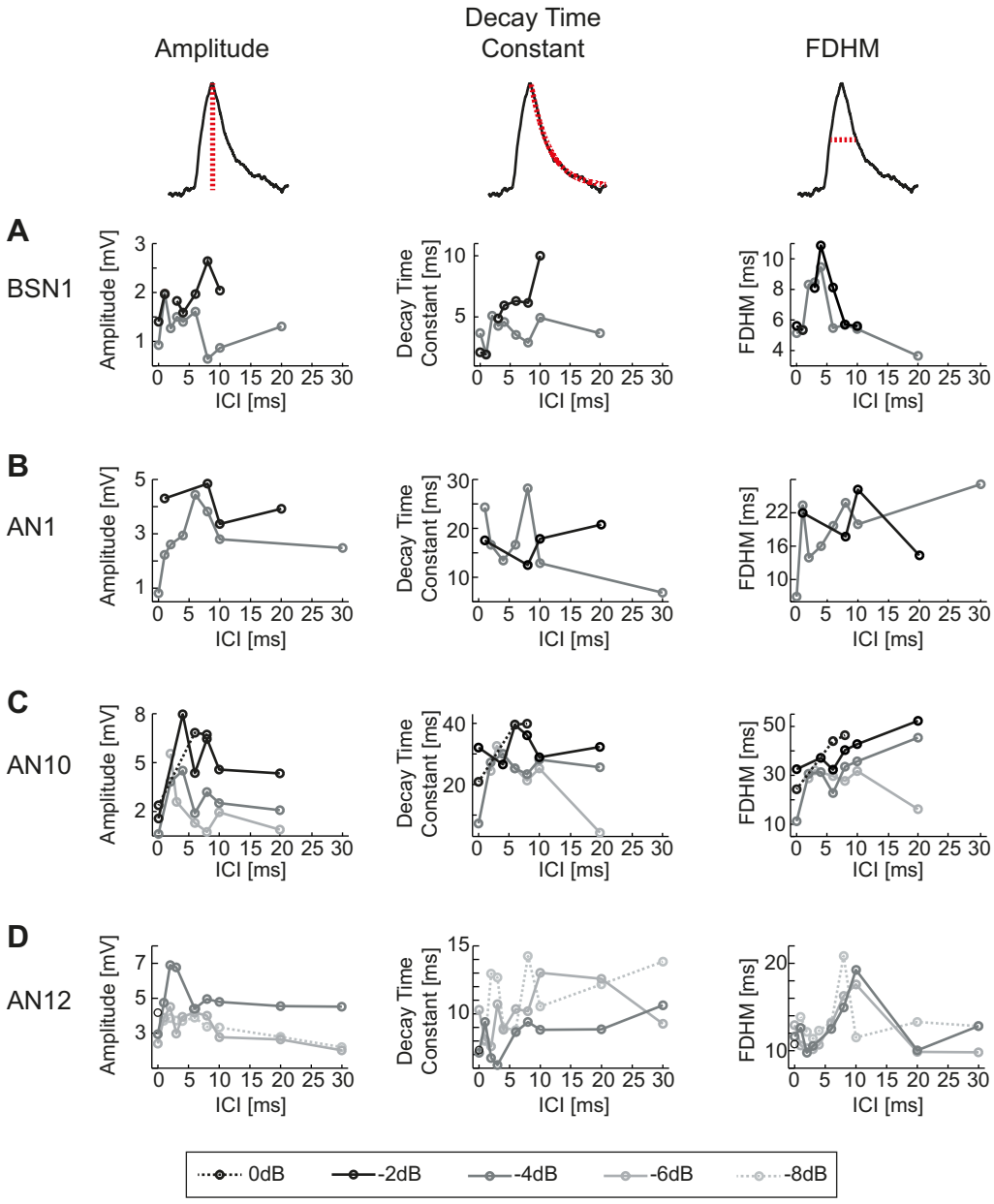

Figure 5.4: **EPSP parameters as a function of the interclick interval.** Amplitude, decay time constant and FDHM (full-duration-at-half-maximum) of the EPSP of **A:** the BSN1 neuron, **B:** the AN1 neuron, **C:** the AN10 neuron, and **D:** the AN12 neuron. Values at 0 ms ICI denote results for single clicks. Intensities are given relative to single click detection threshold. See text for description of these results.

and B, the bump in the rising flank of the 4 ms ICI EPSP, and the first peak of the 8 ms ICI EPSP). Presynaptic integration, leading to an increase in synaptic inputs and thus a higher first EPSP peak at small ICIs, appeared negligible to temporal integration in BSN1 at this recording site.

AN1 neuron. Neuron-intrinsic temporal summation occurred up to long ICIs in the AN1 neuron, which is reflected by the increase of the FDHM for click pairs compared to single clicks (fig. 5.4B), and the shapes of the click pair EPSPs at short and longer ICIs (fig. 5.5C). At $\sim$ 1-6 ms ICIs, the first peak (visible as small bump in rising flank of the average EPSP in fig. 5.5C) in click pair trials elicited a higher EPSP than a single click alone, indicating that the AN1 received integrated and therefore stronger input from the presynaptic network. At larger ICIs temporal summation still occurred, but the first peak of the compound EPSP approximated the height of a single click EPSP (fig. 5.5C).

AN10 neuron. The increase of the FDHM with ICIs up to 20 ms in AN10 shows that input was summed over long time scales. However, this increase in FDHM did not come along with a steady increase in EPSP amplitude; EPSP amplitudes were highest at small ICIs in click pairs, but stayed elevated compared to a single click over the whole range of ICIs. Interestingly, the EPSP displayed two peaks in a compound EPSP only at relatively long ICIs ($\geq$ 8 ms, fig. 5.5D).

AN12 neuron. In AN12, prominent EPSPs clearly visible even in single trials occurred at very low intensities (fig. 5.5E). The shapes of the single trial EPSPs reveal that the underlying mechanism for integration in the AN12 was neuron-intrinsic temporal summation (fig. 5.5F). However, at 1-4 ms ICIs, the first EPSP peak was much larger than at longer ICIs; this implies that at small ICIs, the neuron very likely receives already integrated input from the presynaptic network.

5.4 Discussion

All neurons analyzed in this chapter displayed a shift in detection threshold in response to a click pair compared to a single click on the group level, as described in chapter 4. The extent in threshold reduction and its time range were neuron type-specific. Therefore in this chapter, I targeted the underlying mechanisms in different neurons by analyzing dendritic recordings to find evidence for presynaptic and/or neuron-intrinsic mechanisms explaining these findings. I could show that all neurons included in this analysis (the nonprimary-like local neuron BSN1 and the ascending neurons AN1, AN10 and AN12) exhibited excitatory postsynaptic potentials in response to auditory stimulation at subthreshold intensities, which is a prerequisite for neuron-intrinsic temporal summation or integration. In all neu-

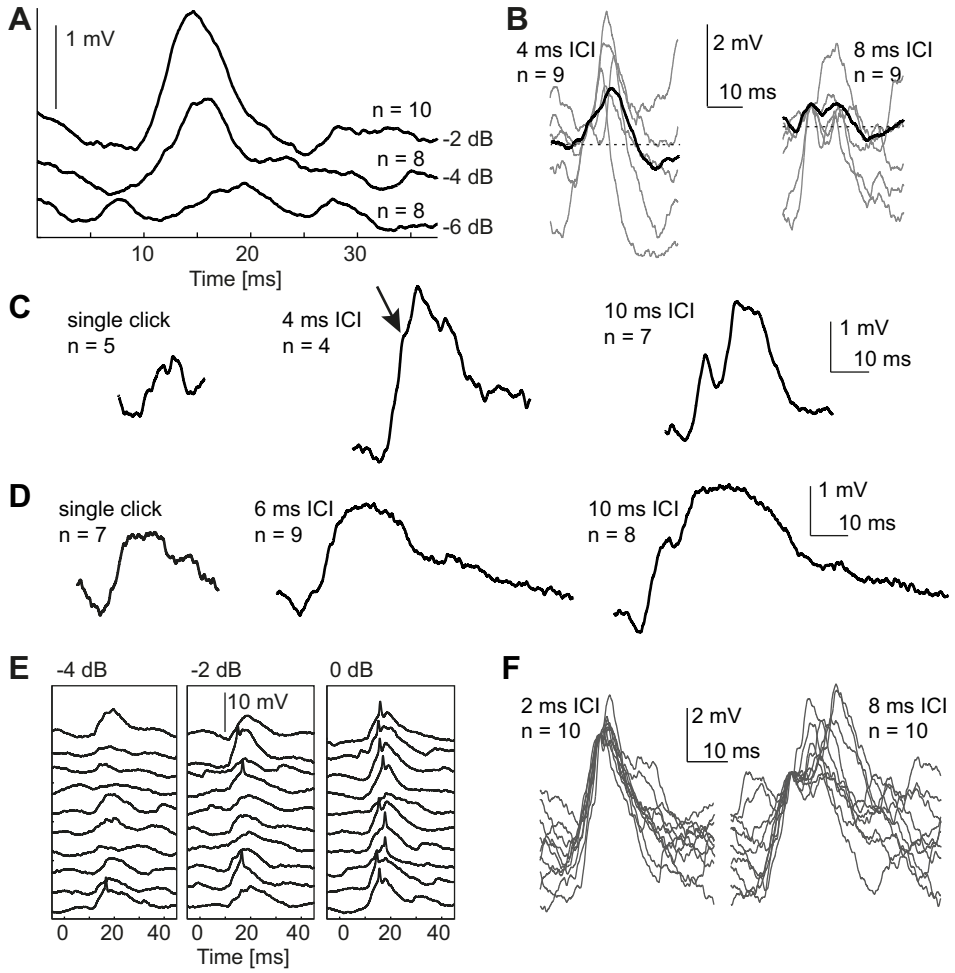

Figure 5.5: **EPSP shapes.** Intensities given relative to single click detection threshold. **A:** BSN1 membrane potential after a single click; a clear EPSP was elicited starting from -4 dB. **B:** Mean EPSP (black) of BSN1 evoked by click pairs with 4 and 8 ms ICI, at -4 dB. Stippled line: baseline value before stimulus onset. Gray: example single trial traces, aligned to the first peak. The second peak was higher than the first in all single trials at 4 ms ICI, but at 8 ms ICI in only 4 out of 9 trials. **C:** EPSP of AN1 in response to a single click, and to exemplary click pairs, at -4 dB. Temporal summation occurred at small (here: 4 ms) and intermediate ICIs (here: 10 ms). The first peak of the response to 4 ms ICI, barely visible as a slight bump in the rising phase of the EPSP (arrow), was higher than for the single click or the first click at 10 ms ICI. **D:** EPSP of AN10 in response to a single click and to exemplary click pairs at -4 dB. A clear second peak occurred at longer ICIs only. **E:** Single trial EPSPs in the AN12 neuron. 10 single clicks presented at -4 dB (left panel), at -2 dB (middle panel), and at detection threshold intensity (right panel). **F:** Single trial EPSPs aligned to the first peak show that the second peak in the EPSP tended to be higher at short (here: 2 ms) and longer (here: 10 ms) ICIs. Intensity shown -6 dB; trials aligned to first peak.

ron types, temporal summation of two clicks occurred, revealed by the analysis of the EPSP shapes. However, the change of EPSP parameters with interclick interval (ICI) and the intensity-dependence of these parameters are, again, different across neuron types. The only consistent finding was the increase of EPSP amplitude with intensity, thereby leading to an increase in spiking probability with increasing intensity.

The time window of temporal summation was longer in the ascending neurons (ANs) than in the BSN1. This qualitatively correlated to the findings in chapter 4, that is, BSN1 temporally integrated only up to 6 ms ICI, but AN1 and AN10 up to $\sim$ 8 ms and AN12 up to at least 10 ms ICIs. In BSN1 and AN12, the time course of temporal summation (visible in the EPSP shapes) and the resulting increase of the FDHM up to $\sim$ 4 and 10 ms, respectively, corresponded well to the range of temporal integration properties of these neurons on a group level (compare fig. 4.4C, fig. 4.5E). Presynaptic integration modulated the response in AN12 for stimuli with small ICIs, while evidence for this mechanism was not found in BSN1.

In AN1, I found evidence for both presynaptic and neuron-intrinsic temporal integration. However, no single EPSP value corresponded to the time course of temporal integration on the group level (compare fig. 4.5C). In AN10, neuron-intrinsic temporal summation could only definitely be shown for ICIs $\geq$ 8 ms. Interestingly, this time range exceeds the temporal integration determined by a spike count measure clearly (compare fig. 4.5D). While FDHM steadily increased with ICI, this only lead to a consistent increase in amplitude at small ICIs for which a detection threshold reduction was found. It is therefore not clear which mechanisms contributed to the temporal integration on a functional level in AN10.

The amplitude, decay time and FDHM strongly depend on synaptic location, that is, also on recording site (Magee, 2000; Magee and Cook, 2000). This can account for discrepancies between the temporal integration times on a functional level (compare chapter 4) and the temporal summation described here. Evidence for presynaptic facilitation (compare, for instance, Clark et al. 1994), mediated e.g. by presynaptic Ca^{2+} and transmitter release levels (Zucker and Regehr, 2002) or electric coupling between axons (Clarac et al., 1992), was not found. However, facilitation effects on EPSP amplitude could be rather small in magnitude (Thomson et al., 1993; Debanne et al., 1996). Hence more experiments with higher numbers of stimulus repetitions and individual neurons are necessary to address this mechanism.

To summarize, evidence for both presynaptic and neuron-intrinsic contributions to the temporal integration properties of neurons was found. Presynaptic temporal integration could be shown for neurons on the third processing level of the metathoracic ganglion, the ascending neurons AN1 and AN12, but neuron-intrinsic temporal summation was found also in the local neuron BSN1. Considering that receptors and primary-like local neurons (compare chapter 4) did not integrate over

longer ICIs than 1 ms, temporal integration on longer time scales could originate in neuron-intrinsic computations at a higher order processing level, that is, in the BSN1 neuron.

5.4.1 Limitations of the current experimental approach

The experiments and their analysis as presented here have some limitations. First, dendritic recordings are relatively unstable. Therefore data could only be obtained from single specimens, and interindividual variability could not be addressed. However, finding EPSPs as a response to subthreshold acoustic stimulation proves that temporal integration cannot be purely presynaptic in these specific neuron types, but must — at least partially — be based on neuron-intrinsic computations. Therefore these results should be regarded as examples of possible integration mechanisms and their time courses, clearly showing that temporal integration is not purely presynaptic to specific neuron types. Thus I could show fundamental principles that can be used as target mechanisms in future experiments.

Second, as mentioned above, the shapes and time courses of EPSPs can depend on synaptic location relative to the recording site. Unfortunately, this could generally confound comparing interindividual variability, because differences between neurons of one type could be attributed both to variability among individuals and among different recording sites.

Third, it is impossible to record all synaptic inputs simultaneously. Thus it remains unclear what the total input into one neuron looks like and which mechanisms are implemented at different synaptic locations.

Pharmacological interventions, patch clamp recording techniques and the application of current injections, as well as paired recordings from the pre- and postsynaptic neuron could further help to disentangle, e.g., passive membrane capacities from nonlinear synaptic processing.

6 Response Recovery in the Locust Auditory Pathway

In the previous two chapters, I described the temporal integration characteristics of the neurons in the locust auditory pathway. In this chapter, I will now address the temporal resolution of these very neurons. To investigate temporal integration, *sub-threshold* stimulation was applied, while here for the temporal resolution measurements, *above-threshold* stimulation was utilized in a "response recovery"-paradigm. Large parts of this chapter were submitted in a manuscript (see "Publikationen").

6.1 Introduction

Sensory systems commonly display adaptation, a reduction of neuronal firing in response to repeated or prolonged stimulation. This is especially crucial for the auditory system, because auditory signals are fast and transient by nature. Thus, the recovery of response from adaptation induced by a preceding stimulus is an important determinant of temporal resolution of auditory neurons.

Grasshoppers are suitable model organisms for exploring questions of temporal resolution and response recovery, because many species use acoustic signaling before mating (see chapter 2 for details). As mentioned in chapter 4, a number of studies have focused on the temporal resolution abilities of the neurons in the auditory pathway of grasshoppers. Temporal resolution has been studied with different paradigms, such as gap detection, modulation transfer functions, and stimulus reconstruction methods (Ronacher and Stumpner, 1988; Machens et al., 2001; Prinz and Ronacher, 2002; Franz and Ronacher, 2002; Ronacher et al., 2008; Wohlgemuth et al., 2011). Shapes and time courses of auditory filters in this system were investigated by applying randomly amplitude-modulated noise stimuli (Clemens et al. 2012). All these studies have two aspects in common: 1) They used long stimuli that induced strong adaptation, thus neuronal properties were captured in the adapted state; 2) the time courses of excitatory and inhibitory inputs as well as the influences of adaptation processes and refractoriness could not be disentangled.

To uncover the basic temporal resolution abilities of auditory neurons, I applied a paradigm in which pre-stimulus adaptation was reduced to a minimum. I used a click pair-paradigm while recording intracellularly, and measured the response recovery to the second click in comparison to a single click. By similar methods, the temporal resolution of the auditory system was investigated in, e.g., cats (Parham et al., 1996), humans (Ohashi et al., 2005), odontocetes (Supin et al., 2007), and songbirds (Henry et al., 2011). Schrode and Bee (2015) demonstrated that temporal resolution determined with click pairs in the auditory brainstem corresponded

to the amplitude modulation rates of the species-specific song of two frog species; the species with the faster amplitude modulations of the song envelope exhibited higher temporal resolution in the brainstem.

In many of those studies, the amplitude recovery of compound potentials was analyzed. The same basic idea was here transferred to intracellular data obtained from single neurons, and the relative spike count elicited by single clicks and click pairs was examined. If a neuron encodes the second click of a pair with as many spikes as a single click, its response has fully recovered. By determining the necessary interclick interval (ICI) leading to 100 % response recovery, I quantified the extent and time course of recovery from acute adaptation. Generally, the spike duration and the refractory period likely determine the upper limits of temporal resolution. However, a first input can affect the processing of a second successive input not only in terms of spike count, but also in terms of spike timing precision (see, e.g., Grinnell and Hagiwara, 1972; Pollak et al., 1977; Pollak, 1980; Young, 1989).

To summarize, the main questions explored in this chapter are: 1) How fast does the response of a neuron recover in terms of spike count and spike timing from a short preceding stimulus? 2) What is the maximal temporal resolution of different neuron types, when pre-stimulus adaptation is reduced to a minimum? 3) What are the time courses of recovery from adaptation in different neuron types belonging to different processing stages? 4) Which phenomena characterize the response recovery in different neuron types?

6.2 Material and methods

6.2.1 Stimulus protocols and experimental procedure

After establishing a stable recording, the neuron was tested with 100 ms noise pulses (5-40 kHz, applied in 8 dB-steps from 32 to 88 dB SPL, yielding a rate-intensity function) whether sound from the left or right speaker elicited a spike response at a lower intensity. The click stimuli were, except for a few rare cases, delivered from the speaker located on the more effective side. Similar to the acoustic stimulation in chapters 4 and 5, single clicks and click pairs were presented. Each single click had a total duration of 40 μs. The delay between two clicks in a pair (interclick interval, ICI) was systematically varied. ICIs used were 1, 2, 3, 4, 6, 8, 10, 20 and 30 ms, with an interstimulus interval of 260 ms. Each stimulus was repeated 10 times; for a detailed description of the stimuli, see fig. 4.2. In contrast to chapters 4 and 5, stimulus intensity was adjusted to $\sim$ 5-20 dB above the neuron's respective threshold on a cell-to-cell basis, such that the stimulation intensity was within the dynamic range of the neuron's rate-intensity function (compare Stumpner, 1988; Stumpner and Ronacher, 1991). Most specimens of one neuron type (AN3) were strongly spontaneously active, which is typical of this neuron type. However, this

rendered an estimation of the threshold rather difficult for the adjustment of stimulus intensity.

6.2.2 Data analysis

Data analysis was carried out using Matlab (The MathWorks, Inc). A total of 46 neurons was included in this study: 10 receptor neurons, 20 local neurons (LNs) and 16 ascending neurons (ANs). See chapter 2 for a detailed description of the neuronal network.

Data from four receptor neurons stem from recordings in the auditory nerve from one individual. The LNs were TN1 (N = 7), BSN1 (N = 8), a group of non-primary-like LNs with phasic response characteristics (LN_{phas}, N = 3), and a second group of LNs with tonic response characteristics (LN_{ton}, N = 2). The neurons of the BSN1 type were divided into two groups based on their response to a single click: Five BSN1 neurons responded with a burst of spikes, and are therefore referred to as $BSN1_b$ (BSN1, *bursting type*; fig. 6.1B). Three BSN1 neurons responded commonly with one spike or sometimes two spikes to a single click and are therefore called $BSN1_{nb}$ (BSN1, *non-bursting type*; fig. 6.1C). These two BSN1 subtypes likely correspond to the "tonic" and "phasic" subtype, described by Stumpner (1989). For the LN_{phas} and LN_{ton} neurons, staining results were insufficient for unambiguous identification by morphology. However, based on their rate-intensity functions these neurons could be clearly distinguished from the receptors, the TN1 and the BSN1. The neurons were grouped according to their physiological properties as described in table 6.1. Because the physiology of the two LN_{ton} neurons was highly similar, they very likely belonged to the same neuron type. Probably the the LN_{phas} were SN4 neurons (Stumpner, 1988).

The ANs recorded for this study were: AN1 (N = 5), AN3 (N = 4), AN10 (N = 1), AN11 (N = 2) and AN12 (N = 4). Because not all cells were tested at all click pair ICIs, the exact N for each stimulus is denoted in the "Results" section. Some specimens of the AN3 neuron type exhibited high levels of spontaneous activity. Here only spikes going along with an excitatory postsynaptic potential (EPSP) were counted as stimulus-induced; spiking activity could, in a few cases, occur due to a post-inhibitory rebound. These spikes were only counted as stimulus-induced when the current level of spontaneous activity was negligible.

Response recovery

To assess the response recovery, the spike counts elicited by each stimulus were determined. The mean spike count elicited across 10 single clicks was defined as 100 %. To assess the response recovery of a neuron for the second click in a pair, the mean single click-induced spike count was subtracted from the mean spike count induced by a click pair. The remaining spike count was then normalized by the single click spike count. If the neuron responded to a click pair with the same number of spikes as to a single click, there was no response recovery (0 %). If the neuron

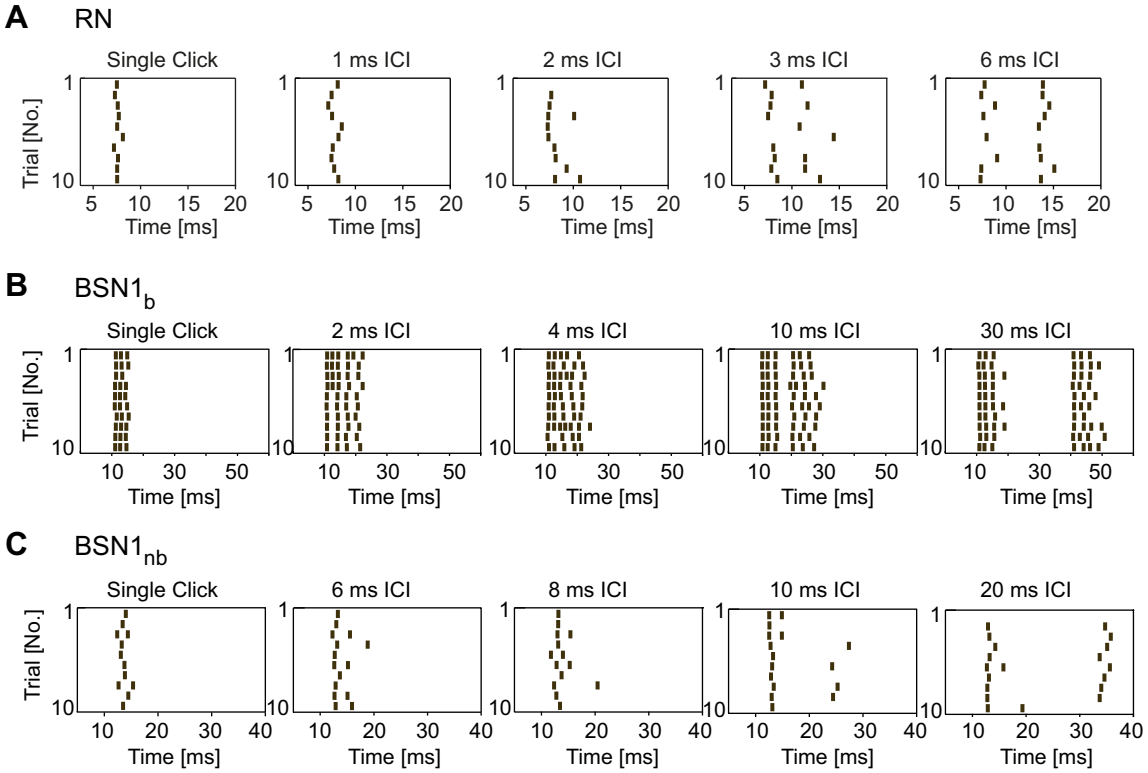

Figure 6.1: **Spike raster plot of an example receptor neuron and the two BSN1 subtypes, with responses to single clicks and click pairs. A:** The receptor neuron responded with one spike per single click. For a click pair with 1 ms ICI, the neuron did not respond to the second click (response recovery = 0 %). With increasing ICI the response gradually recovered, and at 3 and 6 ms ICI the neuron responded to both clicks (response recovery = 70 % and 90 %, respectively). Here the spikes could also be clearly attributed to one of the two clicks. **B:** Spike raster plot of an example $BSN1_b$ neuron. Neurons of this type responded with a spike burst to single clicks; response recovery was slower than in receptor neurons. **C:** Suppression of the second click in an example $BSN1_{nb}$. This neuron type responded with one or at maximum two spikes to a single click. The response to the second click was largely masked up to intermediate and long ICIs.

Table 6.1: The LNs that could not be identified based on their morphology due to insufficient staining results were grouped based on their physiological properties, derived from the rate-intensity function measurements with a 100 ms noise pulse.

LN group	**N**	**Physiological Properties**
LN_{phas}	3	first-spike latencies $\sim$ 10 ms phasic onset response low detection threshold bell-shaped intensity-response function maximal firing rate $\sim$ 120 Hz depolarized membrane potential during acoustic stimulation
LN_{ton}	2	first spike-latencies $\sim$ 10 ms tonic response detection threshold for noise $\sim$ 40 dB reduction of firing rate at high intensity maximal firing rate between 140 and 180 Hz direction-selective

displayed twice the spike count for a click pair stimulus, the neuron's response had fully recovered (100 %). See fig. 6.1A for examples of responses of a receptor neuron to different stimuli. The response recovery was plotted as a function of ICI to infer the response recovery profile of the respective neuron type (fig. 6.2, fig. 6.4). The responses of the neurons to the click stimuli were also partly compared to their onset responses to the 100 ms-stimuli, presented for the rate-intensity function measurements.

Spike timing precision

It was further tested whether the processing of the first click modulated the response to the second click in terms of spike timing precision. To this end, the standard deviation (SD) of spike times was calculated for the first spike to each click in a pair. Neurons had to fulfill two criteria to be included into this analysis: 1) Only stimuli to which the neuron responded to both clicks in at least 8 out of 10 trials were included, and spike timing precision was only calculated across these trials; 2) the responses to each click had to be clearly separated in time, such that two distinct distributions of spikes occurred (see fig. 6.1A, 3 and 6 ms ICI). In this case, each spike could be clearly attributed to one of the two clicks. These criteria excluded click pairs with short ICIs in most neuron types, as well as most neurons that responded with spike bursts. For this reason, among the ascending neuron types only the data of the AN1 neuron could be used.

Spike waveform analysis

Waveforms of single click-induced spikes were obtained by aligning the single trial traces to their maxima and calculating the median across trials. The median spike

waveforms were correlated to response recovery times. Recordings of neurons in which a spike afterhyperpolarization (AHP) was visible in the median spike waveform were included into further analysis: Here, the membrane potential baseline was calculated across a time window with a duration of 37.5 ms, up to 12.5 ms before the spike. The standard deviation (SD) of the membrane potential fluctuations was calculated across the same time window. An exponential function was fitted from the minimum of the median spike waveform until the end of the AHP; this point was determined when the membrane potential reached the baseline again and stayed within two SDs around baseline for at least 1 ms. The width of the AHP was measured as full-duration-at-half-minimum (FDHMin).

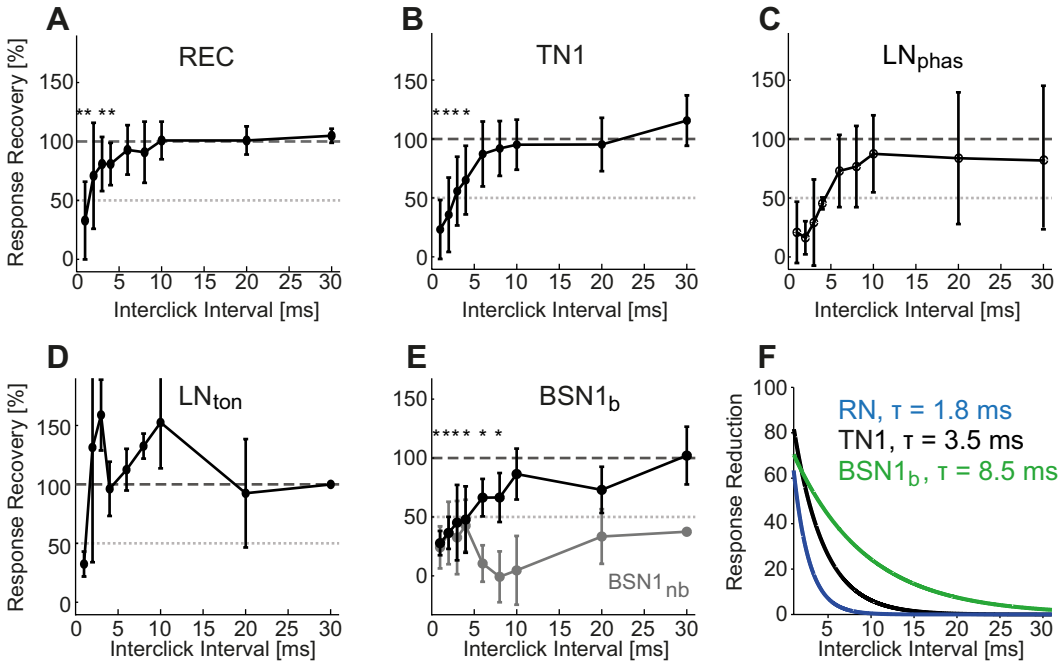

Figure 6.2: **Response recovery in receptors and local neurons.** Response recovery of **A:** Receptor neurons (N = 10; ICI 3, 4, 10 ms N = 9; 8, 20 ms N = 8; 30 ms N = 4), **B:** TN1 (N = 7; ICI 20 ms N = 6; 30 ms N = 3), **C:** LN_{phas} (N = 3; ICI 30 ms N = 2), **D:** LN_{ton} (N = 2; ICI 30 ms N = 1), and **E:** $BSN1_b$ (black line, N = 5; ICI 30 ms N = 3) and $BSN1_{nb}$ (gray line, N = 3; ICI 30 ms N = 1). **A-E:** Values are means, error bars depict SD. Gray dotted lines correspond to a response recovery of 50 %, gray stippled line to 100 %. $**$ = $p < 0.01$, $*$ = $p < 0.05$ (signed rank test). **F:** Recovery from response reduction for neurons with primary-like profiles (see "Results"). Exponential fits ($R^2 \geq 0.87$) to spike count reduction in receptor neurons, TN1 and $BSN1_b$. Time constants τ can be interpreted as the decay of adaptation.

6.3 Results

6.3.1 Primary-like response recovery in receptors and most local neurons

In receptor neurons the response to the second click was markedly reduced only at the shortest ICIs, and the response recovered to 100 % at an ICI of $\sim$ 6 ms; the reduction was significant with $p < 0.01$ at 1 ms ICI, and with $p < 0.05$ at 3 and 4 ms ICI (signed rank test; fig. 6.2A). This steady, monotonic response recovery profile is further referred to as "primary-like". The local neuron TN1 showed a similar response recovery profile, with a significant response reduction at 1-4 ms ICI ($p < 0.05$, signed rank test) and full recovery reached at $\sim$ 6-8 ms ICI (fig. 6.2B). So did neurons of the $BSN1_b$ type (fig. 6.2E, black curve), with a somewhat slower response recovery (significant reduction at 1-8 ms ICI, $p < 0.05$, signed-rank test). The burst of spikes to a single click in the responses of $BSN1_b$ had durations up to 8.2 ± 1 ms (maximal durations $\pm$ standard error). Though the shape of the response recovery function of the LN_{phas} neuron was primary-like, the interindividual variability was high particularly at 20 and 30 ms ICIs (fig. 6.2C).

A primary-like response reduction indicates moderate adaptation. To quantify the adaptation of receptor neurons, TN1 and $BSN1_b$, single exponential functions were fit to the average response reduction (fig. 6.2F, $R^2 \geq 0.87$). Double exponential fits did not significantly improve fit quality. The amplitude of the initial fit at 1 ms ICI represents the strength of initial response reduction. The time constant derived from the fit functions describes the time courses of the decay of adaptation. The receptor neurons were least affected, $\sim$ 60 % reduction, and the adaptation decayed fastest (τ = 1.8 ms). The adaptation in TN1 was stronger ($\sim$ 80 % reduction) and lasted longer (τ = 3.5 ms). $BSN1_b$ exhibited the longest adaptation effects with a decay time constant of τ = 8.5 ms, while its initial adaptation magnitude was between receptors and the TN1 neuron, with $\sim$ 70 % response reduction.

6.3.2 Nonlinear response recovery in higher order neurons

Several interneuron types, comprising some LNs (LN_{ton}, $BSN1_{nb}$) and the ANs, showed a "nonlinear" response recovery: Either the response to the second click was reduced at specific ICIs and did not recover steadily, or an initial response recovery was followed by a delayed moderate response reduction. In a third response type, a click pair elicited more spikes than could be expected from two independent single clicks, corresponding to a response gain. One neuron type displayed a balanced ICI-dependent response gain and suppression.

In the LN type $BSN1_{nb}$, the response to the second click was strongly suppressed up to 20-30 ms ICI (fig. 6.2E, gray curve). To the onset of the longer stimuli presented for the rate-intensity function measurements, this neuron type typically responded with 1-2 spikes at intermediate intensities; at high intensities, this onset

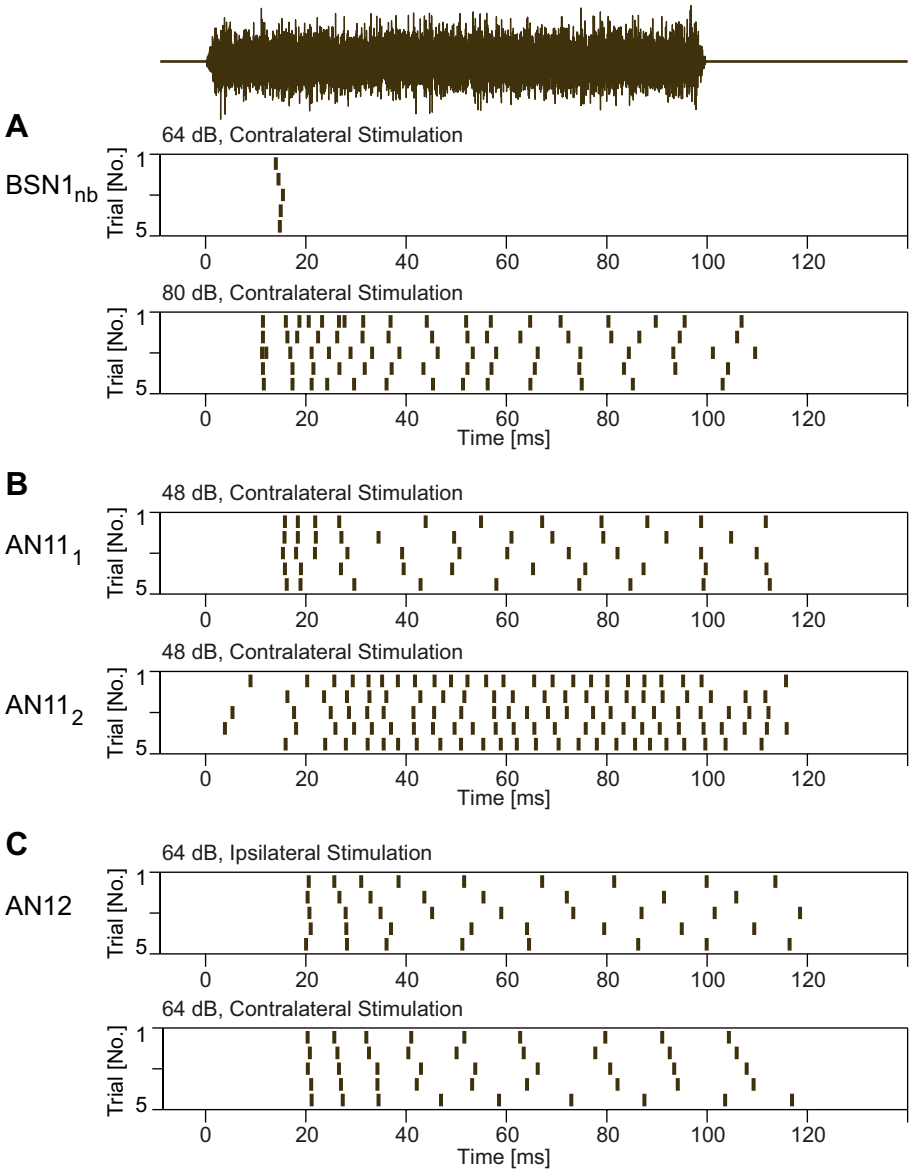

Figure 6.3: **Spike raster plots from example neurons showing the firing response to noise pulses.** This stimulus (upper row; duration: 100 ms, onset at 0 ms) was used for rate-intensity function measurements. Intensities shown lie in the range of click stimulus intensities. "Contra-" and "ipsilateral" refer to the neuron's soma position relative to the side of acoustic stimulation. **A:** At intermediate intensities (close to click stimulus intensity; here: 64 dB), this representative $BSN1_{nb}$ neuron fired at stimulus onset. At high intensities (here: 80 dB), the phasic onset response was followed by a short "quiet" interval and rather tonic firing. **B:** While the $AN11_1$ neuron responded phasically to stimulus onset, the $AN11_2$ exhibited a tonic response (spikes before ~ 20 ms were spontaneous activity). **C:** This representative AN12 neuron responded with several precise spikes to stimulus onset, followed by an adaptation of the firing rate during the stimulus.

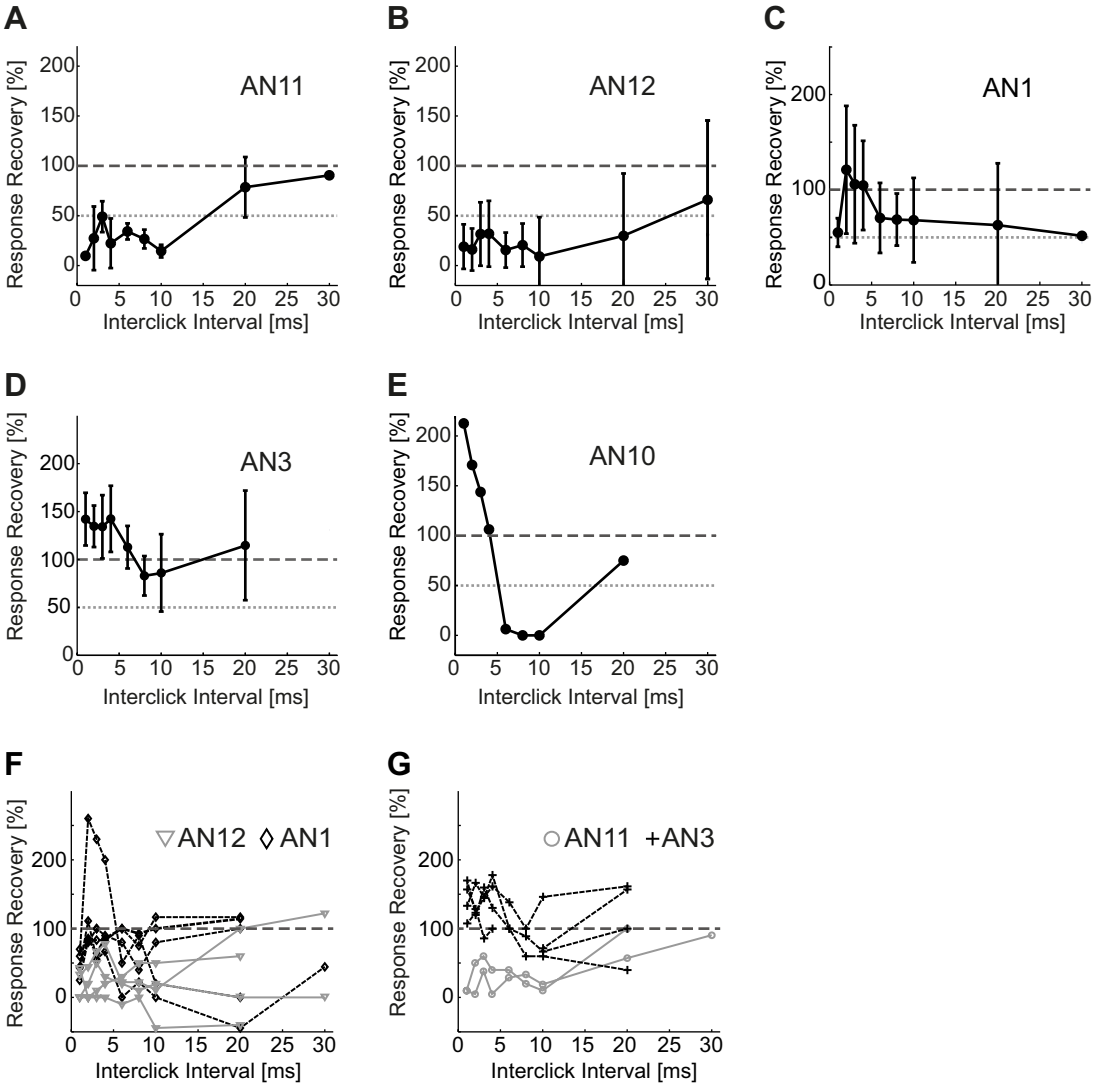

Figure 6.4: **Response recovery in ascending neurons.** Response recovery in **A:** AN11 (N = 2; ICI 30 ms N = 1), **B:** AN12 (N = 4; ICI 30 ms N = 2), **C:** AN1 (N = 5; ICI 30 ms N = 1), **D:** AN3 (N = 4; ICI 6, 8 ms N = 3), and **E:** AN10 (N = 1). **F-G:** Response recovery of single ascending neurons. **A-D:** Values are means, error bars depict standard deviation.

response was typically followed by a "quiet" period, followed then by a more or less tonic firing (for an example, see fig. 6.3 A; see also Stumpner, 1989; Stumpner and Ronacher, 1991). Similar response recovery functions were found in the ascending neurons AN11 and AN12 (fig. 6.4A, B). Here, the decrement of the response to the second click was comparable to the findings in $BSN1_{nb}$, with response recovery values distinctly below 50 %. The AN11 neurons did not respond consistently to the 100 ms-noise pulses (phasic onset responses as well as tonic responses occurred; see fig. 6.3B for examples). The AN12 neurons typically fired several spikes, which were synchronous across trials, at stimulus onset during the rate-intensity function measurements. The firing rate then adapted clearly during the stimulus (fig. 6.3C; see also Stumpner and Ronacher, 1991; Eberhard et al., 2015).

In contrast to these neuron types, in the AN1 neurons the response recovered very fast, within $\sim$ 2-3 ms, and was then followed by a delayed moderate response reduction up to 10 ms or more. Though the effect was not significant due to large interindividual variation, the average response recovery did not reach 100 % at 6-30 ms ICIs (fig. 6.4C). It is possible that either some mechanism (e.g., facilitation) boosted the response at small ICIs, or that AN1 predominantly received inputs from presynaptic neurons that recovered fast or integrated over those very small ICIs, as described in chapter 4.

In the LN_{ton} and the AN3 neuron type, an ICI-dependent response gain occurred. In LN_{ton} click pairs evoked a strong response at small ICIs and again at intermediate ICIs (fig. 6.2D), whereas AN3 yielded a response gain at ICIs < 8 ms (fig. 6.4D).

The AN10 neuron finally represented a further response recovery profile: A mix of response gain at ICIs < 4 ms, and delayed suppression, until almost full recovery at 20 ms ICI (fig. 6.4E); unfortunately, only one recording could be obtained from this neuron type.

In fig. 6.4F and G, the response recovery of the single ascending neurons is plotted to show interindividual variability. Fig. 6.5A shows example spike rasterplots of neurons with distinct response recovery profiles, one with a "quasi-linear" response recovery (AN1; two clicks elicited twice as many spikes as a single click), and one with an almost complete suppression of the response to the second click (AN12). As shown in fig. 6.5B, the AN3 neuron could respond well to a single click ($AN3_1$), but also exhibit spikes only in some trials ($AN3_2$) at the intensities presented in this experiment.

To compare the time course of response recovery in all neuron types, the response recovery functions were interpolated as the first intersection of the response recovery plots with the 50 % response recovery line (gray lines in fig. 6.2A-E, fig. 6.4A-E), to reveal the ICI necessary for 50 % response recovery. The results are summarized in table 6.2.

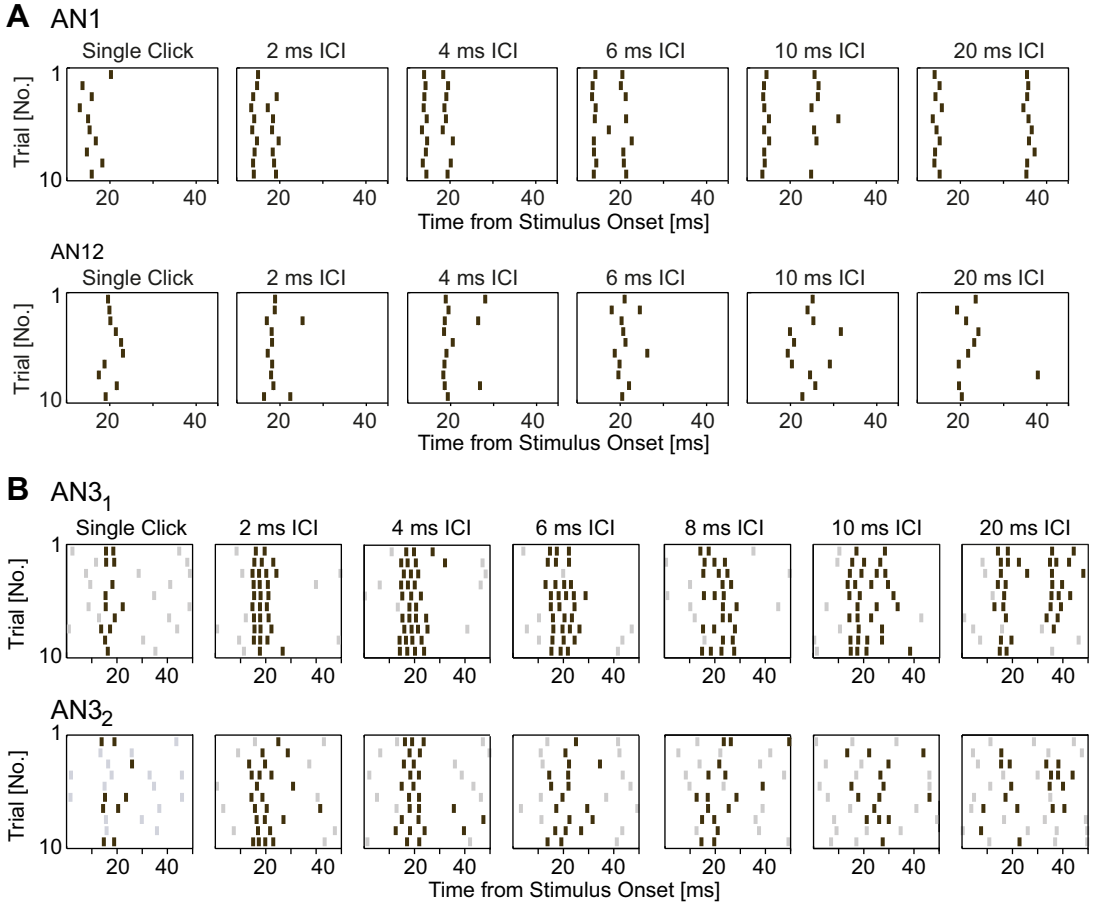

Figure 6.5: **Example rasterplots of different response types of ANs.** Responses of example single neurons to single clicks and click pairs with different ICIs. **A:** A neuron that responded with two spikes to a click pair starting from 2-3 ms ICIs (AN1), and a neuron with an almost complete suppression of the response to the second click up to 20 ms ICI (AN12). **B:** A neuron type exhibiting a response gain for click pairs at short and intermediate ICIs. Spikes marked in gray were spontaneous activity, only spikes marked in brown were counted as stimulus-induced spikes (that is, were accompanied by an EPSP). $AN3_1$ commonly responded to a single click, whereas $AN3_2$ did not respond well to a single click stimulus.

Table 6.2: Interclick interval at 50 % response recovery, interpolated from the first intersection of the response recovery functions with the 50 % response recovery line (fig. 6.2, fig. 6.4); ICI = interclick interval.

Neuron Type	**ICI at 50 % Response Recovery**
Receptor	1.5 ms
TN1	2.8 ms
LN_{phas}	4.3 ms
LN_{ton}	1.2 ms
$BSN1_{b}$	4.2 ms
$BSN1_{nb}$	> 30 ms
AN1	< 1 ms
AN3	< 1 ms
AN10	< 1 ms
AN11	15.5 ms
AN12	25.5 ms

6.3.3 Can neuron-specific spike waveforms explain response reduction or gain?

The analysis of the spike waveforms of the different neuron types might reveal mechanisms underlying the time courses of response recovery, for example a gain or a suppression of the response to the second click. The overshoot of a spike is commonly followed by an afterhyperpolarization (AHP) of the membrane potential, induced by an efflux of cations through slow voltage-gated potassium channels (Hodgkin and Huxley, 1952). During the AHP – see fig. 6.6A for an example spike waveform induced by a single click in a receptor neuron – the excitability of the neuron is reduced. AHPs could be analyzed in three neuron types (receptors, $BSN1_{nb}$, AN12); no clear AHPs were visible in the recordings of other neurons, which could, e.g., depend on recording site and quality.

To test whether the moderate reduction in spike count in response to the second click observed in the receptor neurons could be based on the time course of the AHP, the time constants of the AHP decay were compared to the time constants of response recovery of the individual receptors. The AHP decay time constants clearly exceeded the time required for response recovery in most receptor neurons, and so did full-duration-at-half-minimum (FDHMin) of the AHP (fig. 6.6B; table 6.3). In $BSN1_{nb}$ neurons an AHP was visible in the spike waveforms, but exponential fits gave poor results due to the jagged appearances of the spike waveform traces. Consistent with Hildebrandt et al. (2009), AHPs of the BSN1 neurons tended to be rather subtle in amplitude. With ~ 6.2 ms, FDHMin was longer than in the receptor neurons in $BSN1_{nb}$ (table 6.3); refractoriness could be the cause for the response reduction only within this time range. In AN12, the spike AHP decayed with $\tau \sim 2$ ms, and had a similar FDHMin (table 6.3). Therefore, refractoriness

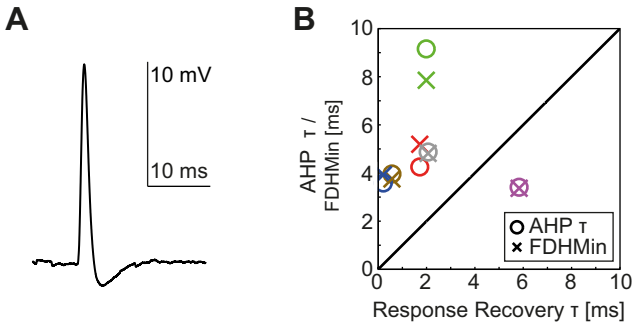

Figure 6.6: **Spike waveform analysis of receptor neurons. A:** Spike waveform of an example receptor neuron (spikes from 8 trials averaged). **B:** Response recovery time constants of individual receptor neurons, compared to afterhyperpolarization (AHP) decay times and FDHMin, respectively. Data from the same receptor are indicated in the same color, averages in gray; τ = time constant.

Table 6.3: Spike afterhyperpolarization (AHP) parameters for three neuron types. Values are means, ± standard errors.

Neuron Type	N	FDHMin	AHP Decay τ	Response Recovery τ
Receptor	5	4.8 ± 0.8 ms	4.9 ± 1.1 ms	2.1 ± 1 ms
$BSN1_{nb}$	3	6.2 ± 2.6 ms	-	-
AN12	3	2.4 ± 0.6 ms	2 ± 0.6 ms	-

could not be causal for response reduction up to high ICIs. No delayed inhibitory inputs (as, e.g., proposed by Creutzig et al., 2010) following the stimulation with a single click were visible in the membrane potential of $BSN1_{nb}$ or AN12. In contrast, in many specimens excitatory inputs occurred time-locked to the second click, which did not evoke a spike (fig. 6.7).

Two neuron types, LN_{ton} and AN3, exhibited a response gain to the second click at specific ICIs (compare fig. 6.2D and fig. 6.4D). The spikes elicited by a single click were followed by a depolarization, followed by a rather slow repolarization in both neuron types (fig. 6.8A, B). Interestingly, in all specimens a sustained depolarization compared to the membrane potential before stimulus presentation was typical of the response to a single click. This is in contrast to the neurons which did not show a response gain, and might enable an enhanced response to a second click succeeding with a short ICI.

To summarize, the spike AHP did not fully explain response reduction in any neuron type. However, the refractory period certainly contributed to response reduction at small ICIs. In LN_{ton} and AN3, a sustained membrane potential depolarization occurred after single clicks.

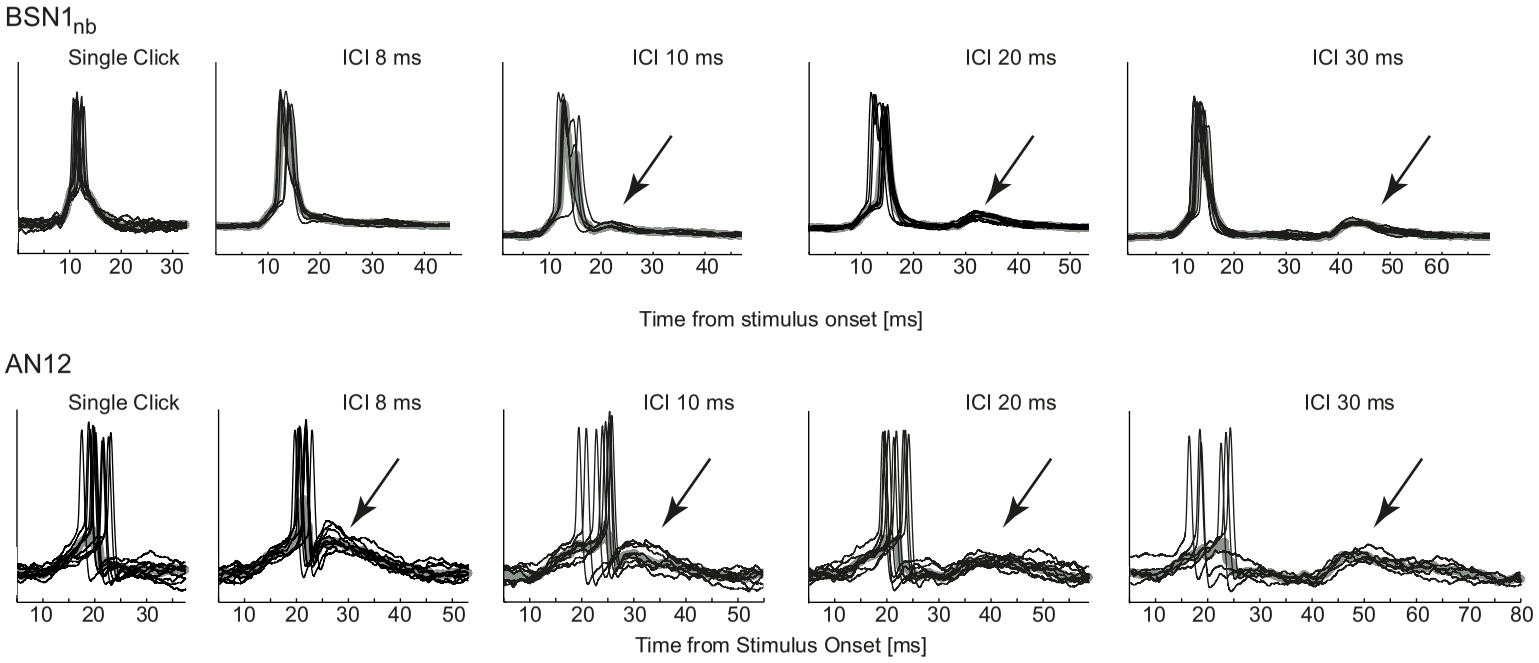

Figure 6.7: **Spike waveforms and membrane potential of a BSN1 and an AN12 neuron.** Single trial membrane potential traces of a $BSN1_{nb}$ (upper panel) and an AN12 (lower panel) neuron in response to single clicks and click pairs with increasing ICIs. In both neurons, an EPSP occurred time-locked to the second click, but no spike was elicited (arrows; only trials with no spikes to second stimulus shown). Gray traces: Median across single trial traces, not aligned to spike. Note that the AHP was very subtle in $BSN1_{nb}$, it is barely visible when trials are not aligned to peak and the median is calculated.

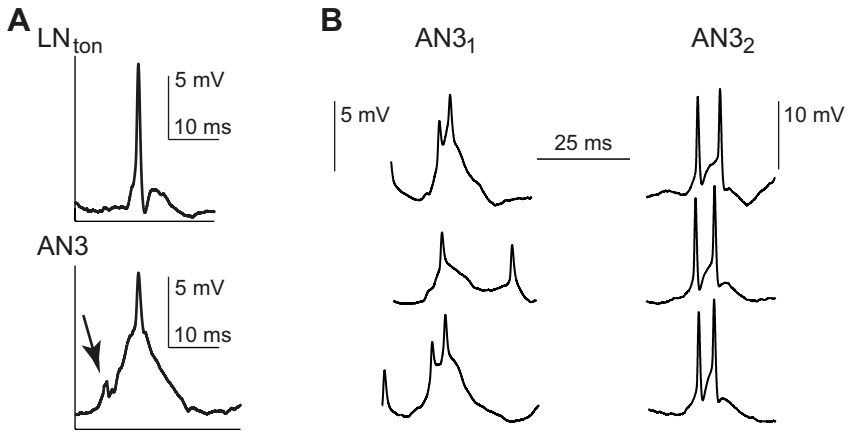

Figure 6.8: **Spike waveforms of neuron types which exhibited a response gain. A:** Median spike waveforms of an exemplary LN_{ton} and an AN3 neuron, evoked by a single click. Single trial traces were aligned to peak before calculating the median. A sustained membrane potential depolarization was common in neurons of these types. Jagged appearance in AN3 waveform (arrow) was induced by spontaneous spikes, which occurred in single trials. **B:** Single trial traces obtained from AN3 neurons (the same cells as shown in fig. 6.5B). Spikes shown occurred in response to a single click and were followed by a sustained membrane potential depolarization.

6.3.4 Recovery of spike timing precision

A preceding stimulus (the first click in a pair) might modulate the response to a later stimulus (the second click in a pair) not only in terms of spike count, but also in terms of temporal precision. To test this, I compared spike timing precision for the two clicks. Results are shown for neuron types in which at least three specimens met inclusion criteria (see "Material and Methods"-section). In receptor neurons and the primary-like local neuron TN1, the response to the first click tended to be equally or more precise across trials than the response to the second click up to an ICI of $\sim$ 10 ms (fig. 6.9A, B). The trend disappeared at 20 and 30 ms ICIs. Results were similar for $BSN1_b$ and AN1 (fig. 6.9C, D). An independent processing of the second click at 20 ms ICI in terms of spike timing precision was therefore indicated in these neuron types.

6.4 Discussion

Many studies have measured how quickly neurons adapt. The emphasis of the present study lay on the recovery from acute adaptation, which is an important determinant of temporal resolution. In summary, five response profiles were found: I) Primary-like response recovery at early processing stages (receptors, local interneu-

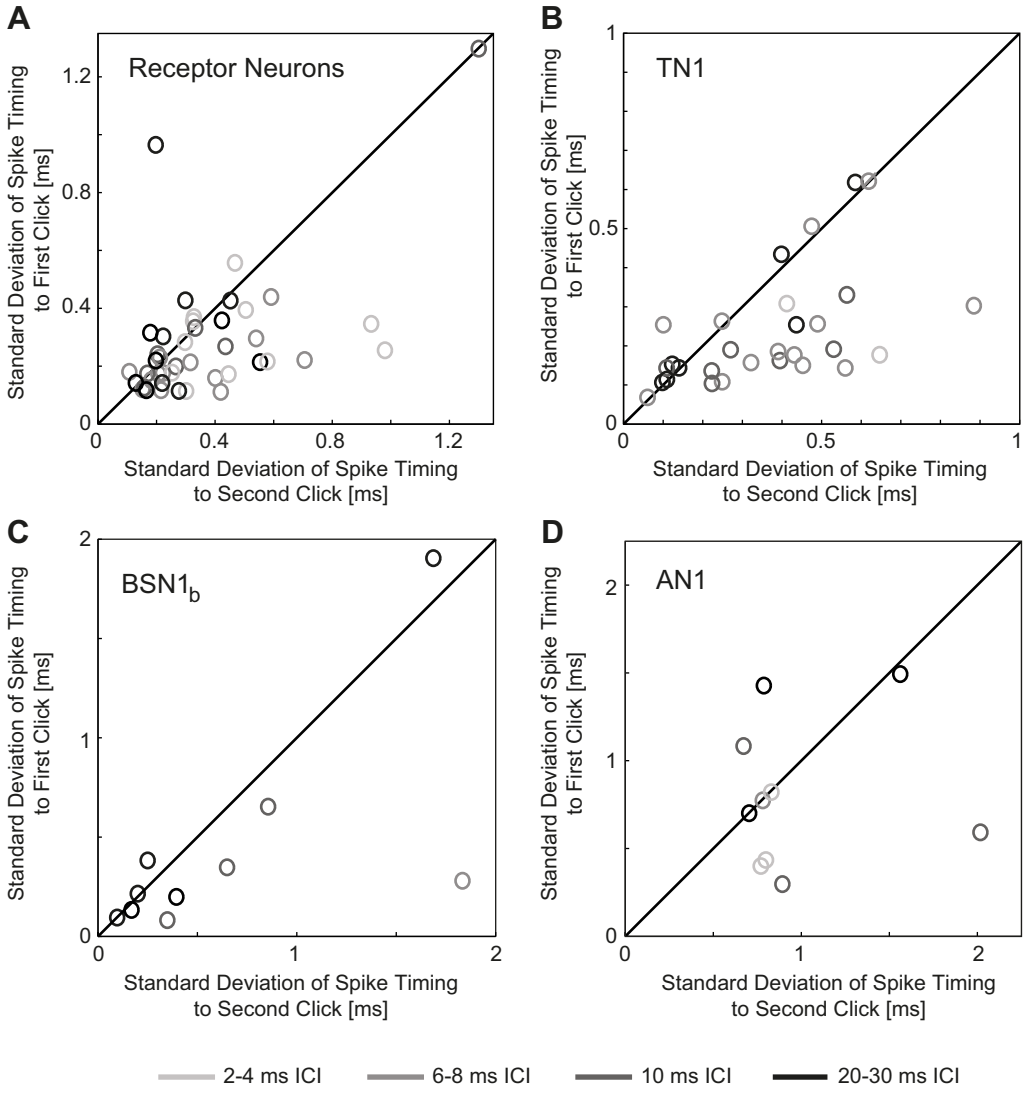

Figure 6.9: **Spike timing precision of the response to the first and the second click.** Standard deviation of spike timing of **A:** Receptor neurons (N = 7), **B:** TN1 (N = 7), **C:** $BSN1_b$ (N = 4), and **D:** AN1 (N = 3). Values below bisectrices indicate a higher spike timing precision for the response to the first click. Darker colors indicate longer interclick intervals (ICIs).

rons TN1, LN_{phas} and $BSN1_b$). II) Strong response reduction up to a long lasting complete suppression of the response to the second click ($BSN1_{nb}$, AN11, AN12). III) Fast recovery with a delayed moderate response reduction (AN1). IV) Interclick interval-dependent response gain (LN_{ton}, AN3). V) Both a gain and a suppression of the response, depending on interclick interval (AN10). The response suppression and response gain phenomena were restricted to LNs and ANs, which are second- or third-order interneurons. See also table 6.2 for a summary of the results.

Adaptation in receptor neurons can be based on input-driven mechanisms, operating, e.g., within the transduction process, or on output-driven mechanism like the spike afterhyperpolarization (AHP), or slow calcium- or voltage-dependent currents (Hudspeth et al., 2000; Benda and Herz, 2003; Gollisch and Herz, 2004). In downstream neurons, adaptation can in addition be inherited from the presynaptic network and be affected by presynaptic neurons, synaptic depression, inhibitory inputs, and neuron-intrinsic spike-triggered adaptation currents with various time constants (Brown and Adams, 1980; Madison and Nicoll, 1984; Stumpner, 1989; Finlayson and Cynader, 1995; Fleidervish et al., 1996; Chance et al., 1998; Benda and Herz, 2003; Hildebrandt et al., 2009). That is, adaptation can be of presynaptic as well as neuron-intrinsic origin. For the interneurons I thus could not disentangle intrinsic from presynaptic effects, though the analysis of spike waveforms may provide some helpful insights into possible mechanisms yielding the response profiles. However, on a functional level, the temporal resolution of interneurons *in vivo* is strongly dependent on synaptic input; therefore, the term "response recovery" will be used also for the interneurons throughout the "Discussion" section, irrespective of the underlying process.

The response recovery of a neuron from acute adaptation limits its temporal resolution, and therefore may reflect the implemented temporal filtering: Neurons that recover quickly can faithfully encode fast modulations of the signal envelope or signals succeeding at high rates. In contrast, neurons with strong reduction of the response to the second click can be interpreted as low-pass filters, since only information about stimuli succeeding with long interstimulus delays will be resolved. Neurons with a response gain can be selective for a specific delay between stimuli. I will now discuss the different temporal filtering properties of the neurons in the grasshopper's auditory pathway in more detail, and relate these to possible underlying mechanisms.

6.4.1 Moderate adaptation, reflected by a primary-like response recovery

In this study, I showed that previously unadapted receptor neurons recovered from a preceding stimulus within a few milliseconds, reaching almost full recovery ~ 6 ms after the first stimulus, which corresponds to a theoretical repetition rate of the stimulus of more than 150 Hz. This ability is fundamental for the high temporal resolution of receptor neurons, though adaptation induced by prolonged continu-

ous stimulation very likely further reduces temporal resolution. Interestingly, the refractory period, manifesting itself e.g. in the duration of the spike AHP, clearly exceeded the time constants of response recovery of individual receptor neurons (fig. 6.6B). On average, the time constants of the AHP decay ranged around 4 ms, and thus were longer than the ICIs during which the response was reduced most strongly (fig. 6.2A, table 6.3). Hence, the refractory period could partly be "overridden" by a new stimulus.

The time constants of recovery from acute adaptation increased with processing level among the neurons with a primary-like response recovery (table 6.2; fig. 6.2F); this possibly corresponds to the observed reduction in temporal resolution of grasshopper auditory neurons at higher processing stages (Wohlgemuth and Ronacher, 2007; Ronacher et al., 2008; Ronacher, 2014).

Effects of presynaptic inhibition shaping the primary-like response recovery in higher order interneurons were not found. TN1 neuron receives only monosynaptic excitatory input from the receptors (Römer and Marquart, 1984; Stumpner and Ronacher, 1991), and inhibition cannot contribute to adaptation in this neuron type. For the $BSN1_b$ neurons, the recovery of response to the second click was slowest. The duration of the $BSN1_b$ spike burst elicited by the first click could prevent or limit the processing of stimuli succeeding within short ICIs, thus resulting in low-pass filtering properties of $BSN1_b$ (fig. 6.1B and 6.2E, table 6.2; see also Wohlgemuth et al., 2011). However, all downstream neurons from the afferent receptors will very likely inherit a reduced excitation – at least at short ICIs. Thus, neuron-intrinsic and presynaptic effects cannot be clearly disentangled.

6.4.2 Response suppression

The high temporal accuracy of peripheral neurons was lost in most neurons at higher processing stages. A response suppression to the second click may result in low-pass filtering, and occurred in several neuron types which are known to receive excitatory and inhibitory presynaptic input. However at least in $BSN1_{nb}$ and AN12, there was no indication that the first click triggered a delayed inhibitory synaptic input (fig. 6.7). Furthermore, the AHP duration of these neurons was distinctly shorter than the time window of response suppression (table 6.3), and could therefore not satisfactorily explain the response recovery profiles. In some specimens of both neuron types the second click did evoke a clear EPSP, but not a spike. Why did this EPSP not trigger a spike? Possibly the second EPSP was subthreshold due to spike time dependent depression (a presynaptic mechanism; Tsodyks and Markram, 1997; Fortune and Rose, 2001; Baker and Carlson, 2014), or refractory Na^+-channels (a neuron-intrinsic mechanism; Kim and Rieke, 2003).

The correlation between response suppression to the second click and the phasic onset responses to the longer stimuli of the rate-intensity function in $BSN1_{nb}$ (fig. 6.2E, fig. 6.3A) supports the notion that a neuron-intrisic mechanism might reduce

firing probability after an onset response or a first click by inducing short-term, acute adaptation (but see Hildebrandt et al., 2009). This could be the ionic conductance of the neuronal membrane, for instance due to the kinetics of a potassium current (for a review, see Wicher et al., 2001). In contrast, in AN12 strong intrinsic adaptation could clearly not be responsible for preventing the neuron from firing more spikes within a certain time window, since it could also fire spike bursts at stimulus onset (Stumpner and Ronacher, 1991; Eberhard et al., 2015, see also fig. 6.3C). Possibly, presynaptic effects played a stronger role in the AN12 response recovery behavior.

In the AN11 neurons, the spike AHP could not be directly compared to response recovery, because no clear AHPs were visible in any recording obtained here. Since clear inhibitory postsynaptic potentials (IPSPs) occurred at higher intensities (data not shown), the shape of the response recovery function might potentially be influenced by a delayed inhibition. No correlation was found between the sustained response suppression to the second click, compared to the onset response to longer stimuli (fig. 6.3B, fig. 6.4A). Thus, at present there is no evidence for a strong intrinsic adaptation current triggered by the first click of the click pairs.

6.4.3 Response gain

A response gain at specific ICIs might enable high-pass filtering, because the respective neuron may be selective for stimuli succeeding at high repetition frequencies. Possibly, a response gain at small ICIs also reflects the tuning to a pause delay. In the grasshopper pathway, two interneurons (LN_{ton}, AN3) exhibited more spikes to the second click than to a single click, indicated by a response recovery exceeding 100 % (fig. 6.2D, fig. 6.4D). This process can be compared to a paired-pulse facilitation, possibly of presynaptic origin (Del Castillo and Katz, 1954; Clark et al., 1994; Mennerick and Zorumski, 1995). Interestingly, Palombi et al. (1994) also found facilitation in some higher order interneurons in the vertebrate dorsal cochlear nucleus, in contrast to a response depression to the second stimulus in the periphery, namely the auditory nerve fibres. Another possibility, supported by the spike shapes of LN_{ton} and AN3 (fig. 6.8), would be predominantly intrinsic processes, such as a prolonged excitation of the cell due to, e.g., a slow membrane time constant. The response gain could also be influenced by temporal integration, at least in those AN3 specimens that did not respond well to a single click (fig. 6.5B). A single click might here have been close to threshold, such that two clicks in a pair were temporally integrated.

6.4.4 Conclusion

In conclusion, I could reveal the adaptation recovery time courses at three processing stages in the grasshopper auditory pathway. These were partly characterized

by different non-linear phenomena, indicative of neuron-specific temporal filtering capabilities, which may form the basis for extracting species-specific features of a grasshopper song.

7 The Effect of Temperature on Temporal Filtering

After addressing the *stimulus-dependence* of temporal filtering in the locust auditory pathway in the previous chapters, I will now turn to the *context-dependence* of temporal filtering. To this end, the body temperature of the animals was experimentally manipulated. Such neuronal processing under different environmental conditions could be simulated, namely at cold and warm temperatures.

The work presented in this chapter originates from a collaboration with Dipl.-Phys. Frederic Roemschied and Prof. Susanne Schreiber from the "Computational Neurophysiology Group" of the Humboldt-Universität zu Berlin. The contributions are as follows:

- Conception of research: Susanne Schreiber, Bernhard Ronacher
- Design of experiments: Sarah Wirtssohn, Frederic Roemschied (equal contribution)
- Data acquisition: Sarah Wirtssohn
- Data analysis and development of analytic tools: Frederic Roemschied
- Figure drafts: Frederic Roemschied
- Figure finalization: Sarah Wirtssohn
- Discussion and interpretation of results: Sarah Wirtssohn, Frederic Roemschied, Susanne Schreiber, Bernhard Ronacher

7.1 Introduction

The body temperature of poikilothermic animals is tightly coupled to the ambient temperature, and these animals face the challenge to maintain their body functions and generate appropriate behaviors under a potentially wide temperature range. These tasks are confounded by the fact that temperature influences neuronal processing (Sanborn, 2006; Robertson and Money, 2012), e.g. by affecting the dynamics of synaptic potentials (Thompson et al., 1985), ion channel kinetics (Pusch et al., 1997; Motomura and Narahashi, 2000), response latency (Warzecha et al., 1999; Franz and Ronacher, 2002), neuronal firing rate (Smolders and Klinke, 1984; Spavieri Jr et al., 2010) and trial-to-trial variability (Eberhard et al., 2015). In poikilothermic animals temperature thus affects both sensory processing (Stiebler and

Narins, 1990; van Dijk et al., 1997; Franz and Ronacher, 2002; Fonseca and Correia, 2007) as well as neuromuscular functions involved in the generation of a behavior, e.g., sound vocalization (Gerhardt, 1978; Doherty, 1985; Pires and Hoy, 1992).

Many poikilothermic animals, invertebrates as well as vertebrates, use acoustic communication. Among these, maybe most prominent, are many frog and insect species (for review, see Gerhardt and Huber, 2002). For acoustic communication systems temperature plays a decisive role, since the spectral and the temporal characteristics of a signal can be temperature-dependent (Martin et al., 2000; Ritchie et al., 2001; Gerhardt and Huber, 2002; Ladich and Schleinzer, 2015). In addition, the sender and receiver may not have the same body temperature due to temperature gradients in the habitat (Römer, 2001). For instance, consider grasshoppers in a meadow: a male grasshopper, stridulating above the ground on a blade of grass on a sunny day, may have a significantly higher body temperature than the female, hiding in the shadow on the ground listening to the male's song.

As described in chapter 2, a female grasshopper has to recognize and evaluate the male's calling song. In order to accomplish this task, the incoming song has to be appropriately filtered for species-specific temporal features (Clemens and Ronacher, 2013; Ronacher et al., 2015). Female grasshoppers of several species prefer songs produced by a male at the matching body temperature (von Helversen, 1972; von Helversen and von Helversen, 1981; Bauer and von Helversen, 1987), which has been taken as an indication for a temperature coupling between the sender and the receiver; that is, male song production and female preference functions possibly underlie a matching temperature dependence. Bauer and von Helversen (1987) showed that the neuronal structures for song production and song recognition are separated: The rate of the song pattern is determined by the temperature of the thorax, in which the central pattern generators driving stridulation movements are localized. The preference of a specific song pattern however depends on the brain temperature.

Temperature thus clearly induces a shift of song preferences also in grasshoppers. How does temperature then affect signal processing within the auditory pathway? Could temperature-dependent temporal filtering within auditory neurons explain the behavioral findings? To tackle this question, temporal filtering implemented in interneurons in the metathoracic auditory pathway of the migratory locust (*Locusta migratoria*, an acridid grasshopper species) was determined at temperatures ranging between $\sim$ 20-32 °C. The axons of these neurons ascend to the brain and are therefore referred to as ascending neurons or ANs (see chapter 2 for a detailed description of the neuronal network). The ANs perform some signal preprocessing by encoding specific temporal features of a sound (Stumpner et al., 1991; Ronacher et al., 2004). As demonstrated in chapters 4 and 6, these neuron types possess different integration and response recovery times, which may enable neuron-specific temporal filtering. The neuronal structure in the metathoracic auditory pathway is

evolutionarily highly conserved among grasshopper species (Ronacher and Stumpner, 1988; Neuhofer et al., 2008). Hence their filtering capabilities likely provide the subset of temporal information extracted from an acoustic signal the brains of different grasshopper species use in order to detect and recognize their own species-specific song.

In the present study, temporal filtering was described by a single unit's linear spike triggered average filter and a nonlinear gain function translating the filter output into a firing rate (e.g., Schwartz et al., 2006; Clemens et al., 2012). A Q_{10} model was fit to the temporal filtering parameters. The temperature coefficient, Q_{10}, is a common measure of temperature dependence, and indicates the effect of a 10 °C temperature increase on a parameter (reviewed in, e.g., Cossins and Bowler, 1987; Davenport, 2012). A Q_{10} = 1 describes a temperature-invariant parameter, while a Q_{10} = 2 reveals a doubling of a parameter (e.g., a neuron's firing rate) with a 10 °C temperature increase. A decrease of a parameter with temperature, for instance the pulse duration in an insect calling song, results in a $Q_{10} < 1$.

7.2 Material and methods

7.2.1 Spike-triggered averages and nonlinear gain functions

I will first explain the basic idea of a spike triggered average-filter of a sensory neuron, as applied in this study. The spike triggered average (STA) is calculated across all segments of a long stimulus which evoke a spike in a neuron. These different stimulus segments, starting a certain time before a spike (in this study: 64 ms), are averaged. The mean of the total stimulus is subtracted. This procedure reveals a linear STA filter, corresponding to the temporal feature the neuron responds to. The convolution of the STA filter with each segment of the stimulus yields a projection value, and the firing rate at this projection value can be derived from the data to calculate the nonlinear gain function of the neuron. That is, this nonlinearity translates the filter output into the neuron's firing rate, and can be used to predict the neuron's response to any given stimulus.

In the present study, the nonlinearity was always high at positive filter values. A positive lobe in the STA filter shape thus indicates a neuron's preference to an increase in stimulus intensity in the corresponding time window. Accordingly, a negative lobe in the STA filter shape indicates a neuron's preference for a stimulus with a decrease in stimulus intensity in the corresponding time window. The "optimal" stimulus evoking the highest firing rates has an amplitude modulation of the stimulus envelope (relative to the mean stimulus intensity) with a time course corresponding exactly to the STA filter.

7.2.2 Stimulus protocols and experimental procedure

The acoustic stimulation consisted of a broadband carrier (5-40 kHz), with a signal envelope that was amplitude-modulated with low-pass Gaussian noise with a cutoff frequency of 200 Hz. The mean intensity was set to 60 dB, and the intensity modulations had a standard deviation of 6 dB. This intensity was chosen in order to cover the dynamic range of most ascending neurons (compare Stumpner and Ronacher, 1991). To estimate the STA filters, the amplitude-modulated stimulus was presented for 6-17.7 min. To evaluate the performance of the STA model, a 6 s-segment was repeated at least 18 times. This protocol was applied at 1-3 constant temperatures (ranging from ~ 20 °C to ~ 32 °C) within the same animal (see chapter 3.2 for details on temperature control and monitoring). The order of temperatures (from cold to warm or vice versa) was randomized to rule out a serial effect. During the experimental manipulation of the animal's body temperature, 50 ms-noise pulses were presented at an intensity of 50 dB, to enable a tracking of single unit spike waveforms which gradually changed with temperature. By this procedure, data from 9 units were obtained at several temperatures. The data from all units, including those for which the STA filter was determined at one temperature only, were pooled for population analysis, rendering a total of ~ 150 units[1]. Data from a total of 12 animals were included in this study; of these, one animal was recorded from at a single temperature, from two animals at three temperatures, and the other animals at two temperatures with 5 °C $\leq \Delta T \leq$ 10 °C.

7.2.3 Data analysis

Details on data analysis can be inferred from Frederic Roemschied's PhD thesis ("Computational Neurophysiology Group", Humboldt-Universität zu Berlin). For the sake of completeness, I will here give a rough overview of the analysis methods and the according references.

All data analysis was carried out using Matlab (The MathWorks, Inc.). To extract the spikes fired by a single unit from the extracellular signal, the "initial sorting" algorithm described in Franke et al. (2010) was applied. All waveforms recorded at a constant temperature were sorted together. During temperature manipulation, the waveforms in response to the 50 ms-noise stimuli were sorted together when ΔT did not exceed 2 °C. Thus, the waveforms were sorted in overlapping chunks, such that a unit's spiking could be traced across a gradual change of the spike waveform, induced by changing temperature.

[1]Note that this does not correspond to 150 individual neurons. Units could also be, e.g., non-auditory neurons or singular artifacts, or spikes from a single neuron might be divided into two units. However, weighting the STA filter data according to their significance (see chapter 7.2.3) minimized the influence of these units on the results.

The STA filters were obtained by the procedures outlined in Clemens et al. (2012). The nonlinearity which translates the filter output into a neuron's firing rate was computed according to the "ratio of Gaussians" described in Pillow and Simoncelli (2006). The model quality was estimated by comparing the firing response predicted by the model to the firing rates evoked by the 6 s-stimuli, which yielded good results: The model predictions did not significantly differ from the empirical neuronal responses (corrected p calculated after Petersen et al. 2008: 0.61 ± 0.24; compare Clemens et al., 2012).

To estimate the significance of the STA filter, "mock STAs" were created by randomly shifting the spike train of the neuron along the stimulus. An STA sample was considered significant when it did not fall in the [1,99]th percentile of the "mock STA" distribution across the same sample. The larger the fraction of significant samples in an STA, the higher the overall significance of the STA filter.

Because the raw STA filters were noisy (fig. 7.1), a mixture of two Gaussians (one positive, one negative) was fit to the STAs with:

$$f(t, \mu_1, \mu_2, \sigma_1, \sigma_2, m) = (1 - m) \cdot N(t, \mu_1, \sigma_1) - m \cdot N(t, \mu_2, \sigma_2)$$

Here, μ_1 and σ_1 are the mean and the standard deviation of the positive Gaussian (describing the positive filter lobe), and μ_2 and σ_2 of the negative Gaussian (describing the negative filter lobe). The mixing parameter m describes the combination of the two Gaussians, and in the above formula corresponds to m_{neg}, that is, the weight of the negative lobe relative to the weight of the positive lobe. The amplitude of the fitted filters was normalized with

$$G(t, \mu_1, \mu_2, \sigma_1, \sigma_2, m) = f(t, \mu_1, \mu_2, \sigma_1, \sigma_2, m)/norm(f)$$

All further analysis was carried out on the fitted STA filters, referred to as $\text{STA}_{\text{Gauss}}$ filters. The weight of the positive lobe was calculated by

$$m_{\text{pos}} = 1 - m_{\text{neg}}$$

with $m_{\text{pos}} = 1$ corresponding to a purely positive filter, and $m_{\text{pos}} = 0$ to a purely negative filter (see also fig. 7.2). Note that almost all filters found in the data set had both negative and positive parts.

To test the temperature effect on the $\text{STA}_{\text{Gauss}}$ filters, several measures were compared across temperatures. These were: The latencies of the negative and positive peaks, full-width-at-half-minimum (FWHMin) and -maximum (FWHM), total filter width (delay between the negative and positive peak) and m_{pos}. Note that due to the normalization of the $\text{STA}_{\text{Gauss}}$ filters, the negative and positive peak amplitudes cannot be compared across temperatures. A Q_{10} model was fit to the data, with

$$f(T_0 + \Delta T) = f(T_0) \cdot {Q_{10}}^{(\Delta T/10)}$$

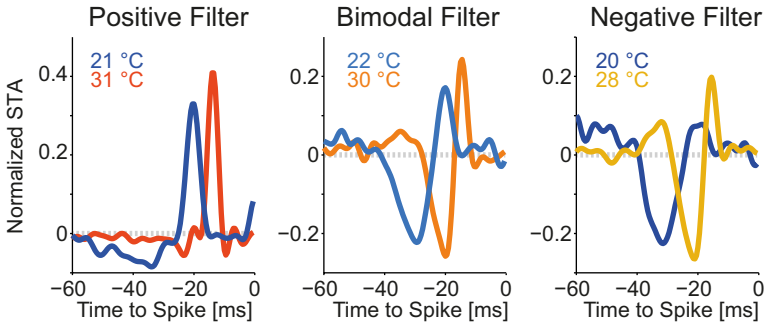

Figure 7.1: **All STA filter types were affected by temperature.** Exemplary raw STA filters of single units, obtained at two temperatures, of the three major filter types found. Positive filters (left) had a predominantly positive lobe with little or no negative proportions, bimodal filters (middle) had a positive and negative lobe, and negative filters (right) were characterized by a predominant negative proportion.

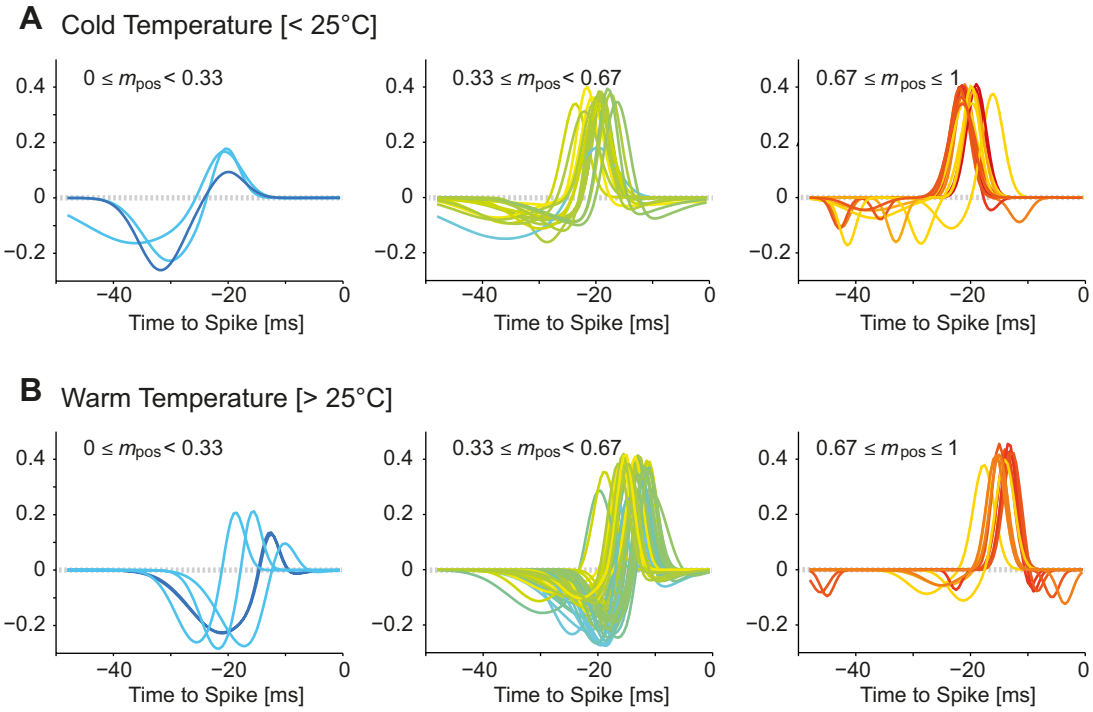

Figure 7.2: **Gaussian fits to STA filters.** Gaussian fits to STA filters with $R^2 \geq 0.75$ at cold (**A**) and warm (**B**) temperatures, grouped into predominantly positive, bimodal and predominantly negative filter types according to the weight of the positive filter lobe, m_{pos}. Color codes correspond to STA_{Gauss} filter datapoints in fig. 7.5.

The temperature T_0 was chosen such that most data points were available at this temperature. For the fit, the data points were weighted according to the significance of the respective STA filter. In fig. 7.3, the darkness of the symbol represents the STA filter significance; the darker the symbol, the more significant the fraction of negative (fig. 7.3A, C) or positive (fig. 7.3B, D) STA filter samples. For filter width, both the negative and positive filter fractions were evaluated, and to obtain a conservative measure and reduce noise in the data set, darkness indicates the lower fraction of significant STA samples of either the positive or the negative lobe in fig. 7.3E. In fig. 7.3F, darkness indicates the square root of the R^2 of the Gaussian fits to the raw filters multiplied by the total of significant samples.

To test for the temperature dependence of the nonlinear gain functions, the exponential model

$$r = e^{(x\text{-}x_0)/\tilde{c}},$$

was fit to the rising phase of the nonlinearity, with x_0 indicating a function value of 1, and with the growth constant $\tilde{c}$. A linear regression was calculated between temperature and each of the fit parameters.

7.3 Results

7.3.1 Temperature-dependence of linear STA filters

Three general types of STA filter sets were found in the present data set: Unimodal filters with either a dominant positive or negative lobe, and bimodal filters exhibiting a negative lobe followed by a positive lobe or vice versa. As fig. 7.1 shows, all of these types were affected by temperature. All STA filters derived from the fit of the two Gaussians to the raw STA filters (further referred to as STA_{Gauss} filters) with $R^2 \geq 0.75$ are shown in fig. 7.2.

The Q_{10}-fits revealed a significant temperature dependence of the STA_{Gauss} filter parameters: peak latencies, FWHMin and FWHM as well as filter width and m_{pos} (the weight of the positive lobe) decreased with temperature, with Q_{10} values of 0.61-0.75 (fig. 7.3). These results obtained from the population data were supported by the single unit data available for several temperatures: Data from single units tended to follow the population trend. Only for m_{pos}, the population and single unit data were less consistent than for the other features, because m_{pos} did not systematically decrease across single units (fig. 7.3F). Generally, no significant difference was found between the Q_{10} model predictions and the single unit results (signed rank test), both when all data from single units were tested, and those data from single units with $\Delta T \geq 5$ °C (fig. 7.4).

Note that all STA_{Gauss} filter parameters, except for m_{pos}, describe the temporal compression of the feature preference. In contrast, a temperature-dependent change

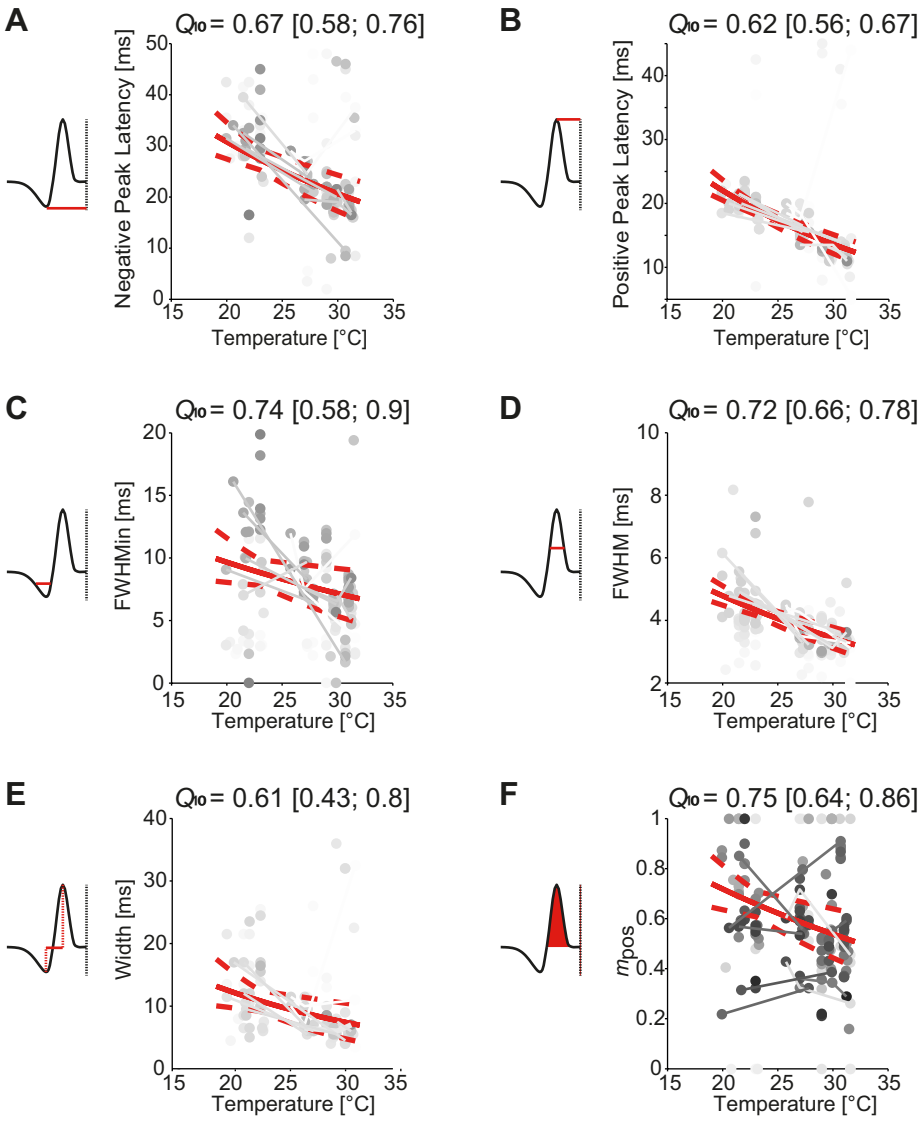

Figure 7.3: **Q_{10}-fits to $\text{STA}_{\text{Gauss}}$ filter parameters revealed a significant temperature effect.** All examined $\text{STA}_{\text{Gauss}}$ filter parameters were temperature dependent: **A:** the negative peak latency, **B:** the positive peak latency, **C:** full-width-at-half-minimum (FWHMin), **D:** full-width-at-half-maximum (FWHM), **E:** filter width, and **F:** the weight of the positive lobe (m_{pos}). Red solid and stippled lines: Q_{10} fit, with 95 %-confidence intervals. Numbers in squared brackets: lower and upper limits of the 95 %-confidence intervals; Q_{10} values were significantly $<$ 1. Dots connected by lines: data from single units at multiple temperatures. Symbol color generally indicates STA filter significance with increasing darkness (see chapter 7.2.3 for details).

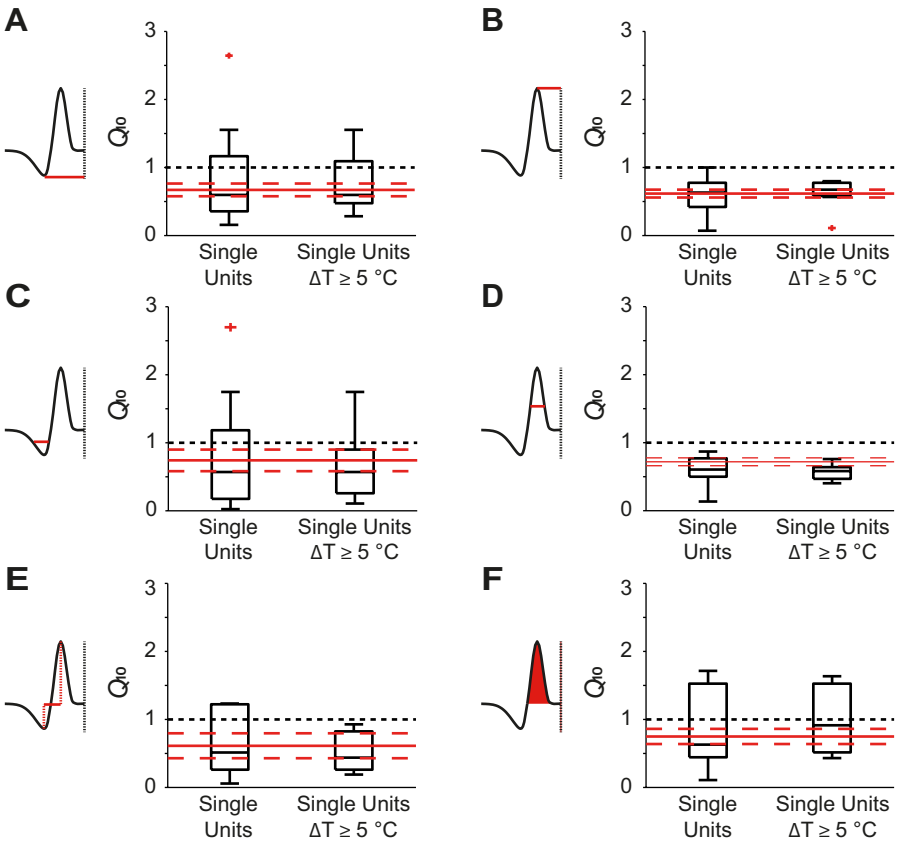

Figure 7.4: **Temperature dependence of $\mathbf{STA_{Gauss}}$ filters: Comparison of $\boldsymbol{Q_{10}}$ model results with the data from single units which could be recorded at several temperatures.** The Q_{10} model results are not significantly different (signed rank test) from the single unit data (N = 15) and the single unit data with $\Delta T \geq 5$ °C (N = 7) for **A:** the negative peak latency, **B:** the positive peak latency, **C:** FWHMin, **D:** FWHM, **E:** filter width, and **F:** m_{pos}. Red lines show results of Q_{10} fits, solid lines indicating the mean and stippled lines the 95 %-confidence intervals.

in m_{pos} (the relative contribution of the positive compared to the negative lobe of the STA filter) influences the basic filter shape, such that the preferred temporal feature could be fundamentally altered. Therefore, a temperature-dependence of m_{pos} is particularly interesting.

To further reduce noise in the data and unravel temperature effects on m_{pos}, the distribution of m_{pos} was analyzed along STA_{Gauss} filters with fit results of $R^2 \geq 0.75$ to the raw STA filters (fig. 7.5). A clear shift occurred from predominantly positive filters to more bimodal filters, showing that the weight of the negative lobe increased with temperature (fig. 7.5A, B). A linear regression indicated a significant, though small, decrease in m_{pos} with temperature ($p < 0.001$; fig. 7.5C).

7.3.2 No evidence for a temperature dependent nonlinearity

Not only the linear filter time course and shape might be affected by temperature, but also the nonlinear gain function which translates the filter output to the neuron's firing rate. No clear temperature effect was revealed by the direct comparison of single unit nonlinearities, recorded at several temperatures; though the nonlinearities could exhibit differences between temperatures, the changes were not consistent across units. The nonlinearity could be shifted to more positive or more negative projection values at higher temperatures, and the firing rate did not consistently increase with temperature (see fig. 7.6A for example single unit nonlinearities).

The exponential fits to the rising phase of the nonlinearity (with the two fit parameters x_0 giving the function value 1, and the growth constant $\tilde{c}$) yielded good results with $R^2 \geq 0.94$. A linear regression to each of the two fit parameters showed no significant correlation with temperature (p = 0.34 and 0.6; fig. 7.6B).

7.4 Discussion

To summarize, the time course and the shape of the linear STA_{Gauss} filters were temperature-dependent. There was no evidence for a general temperature effect on the nonlinear gain function. The findings on the population level were in large parts consistent with the single unit data. These findings demonstrate that temperature influences temporal filtering parameters in the interneurons in the locust's auditory pathway.

7.4.1 Temperature effects on temporal filtering

The STA filters became narrower, and the peak widths and the peak latencies decreased with temperature with a Q_{10} ranging between 0.62-0.74 (fig. 7.3). That is, the neuronal preference changed to a temporally compressed feature compared to

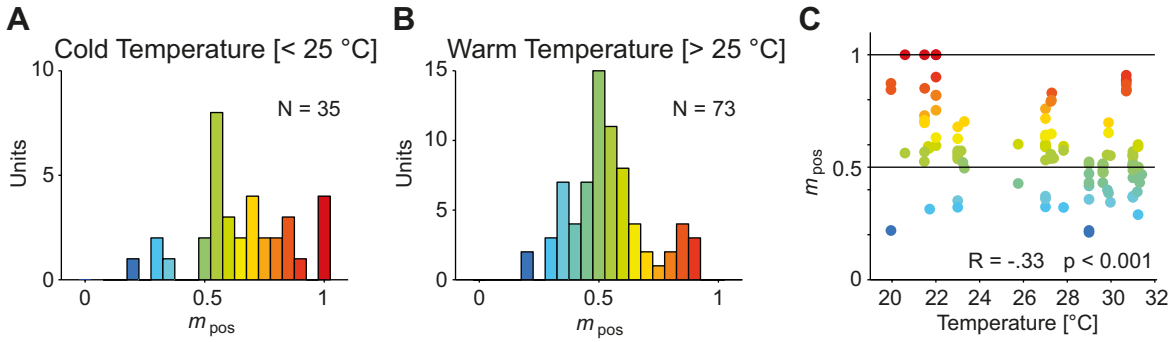

Figure 7.5: **The negative lobe of the STA_{Gauss} filters became more prominent at higher temperatures.** The distribution of m_{pos} among STA_{Gauss} filters at cold (**A**) and warm (**B**) temperatures showed a shift from more positive to more negative filter shapes at higher temperatures. **C:** A linear regression indicated that this shift was small, but significant. Only STA_{Gauss} filters with $R^2 \geq 0.75$ to the raw STA filters were included. Color codes correspond to STA_{Gauss} filters in fig. 7.2.

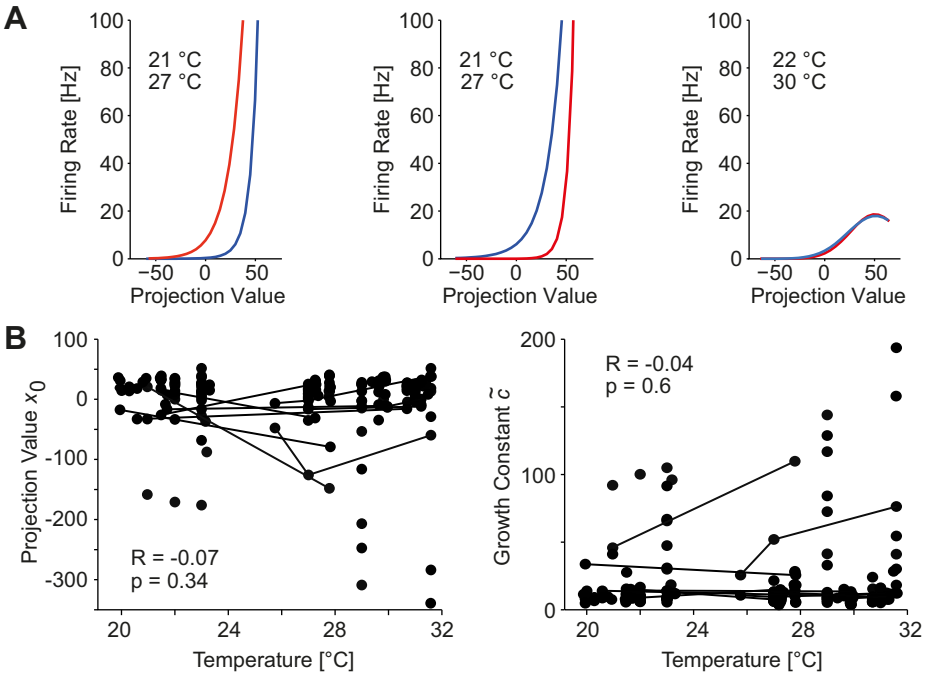

Figure 7.6: **Temperature dependence of nonlinear gain functions. A:** Examples of nonlinear gain functions for three units, recorded at several temperatures. The gain functions could be shifted to more negative or positive projection values, or not be affected at all. Red indicates higher, blue colder temperature. **B:** A linear regression showed no significant temperature effect on x_0 and $\tilde{c}$.

the preferred feature at a lower temperature. A decrease in peak latency, particularly of the positive peak, is well in line with previous findings that firing latencies to acoustic stimuli decrease with temperature in grasshoppers and other poikilothermic animals (Wolf, 1986; Stiebler and Narins, 1990; Coro et al., 1994; Franz and Ronacher, 2002; Preuss and Faber, 2003; Fonseca and Correia, 2007; Eberhard et al., 2015). The shorter the latency of the positive peak, the faster the neuron responded to an intensity increase in the stimulus. Prinz and Ronacher (2002) reported an improvement of temporal resolution in receptor neurons with increasing temperature. This effect may well be transferred to the higher order interneurons, which could induce the narrower STA filter peaks and the decrease of general filter widths.

In addition, the filters became more negative with temperature, that is, the weight of the positive peak (m_{pos}) decreased and the negative lobe of the filters became larger in comparison to the positive lobe. As a result of this, with a temperature increase the distribution of filter types tended to shift to more bimodal and negative filters (fig. 7.5). This effect could potentially influence the feature selectivity of the respective neurons. How this actually affects signal recognition is not clear at this moment. Possibly, an increase in filter negativity could sharpen filter tuning for pause durations in a grasshopper song. However, the effect is small (though highly significant), and does not occur consistently within single units; therefore, behavioral or biological implications following this shift remain unclear for the time being.

7.4.2 Temporal compression of feature preference: A sign of temperature compensation?

However, a Q_{10} value of 0.6-0.7 is relatively small, since it indicates a change of a parameter by only $\sim$ 30-40 %. In comparison, biochemical reactions tend to have Q_{10} values > 2.5 (Wolfenden et al., 1999; Sanborn, 2006), and many biological functions increase by a factor of 2 or more with a 10 °C temperature increase (e.g., French and Kuster, 1982; Bennett, 1985; Robertson and Money, 2012), which indicates a parameter change of more than 100 %. This suggests that temporal filtering in locust auditory interneurons is partly temperature-compensated, as has been shown for several functions and processing stages in locusts (Robertson and Money, 2012; Eberhard et al., 2014; Roemschied et al., 2014). Possible mechanisms could be a temperature-invariant transduction mechanism, network effects – for instance the balance of excitation and inhibition –, as well as neuron-intrinsic effects, as Roemschied et al. (2014) have demonstrated for locust auditory receptors. Generally, the present study shows that the effects of auditory receptors quantitatively extend to higher processing stages.

7.4.3 Temperature compensation in nonlinear gain functions through presynaptic adaptative coding?

It was surprising, however, that the nonlinearity which translates the linear filter output to a firing rate did not show indications of a consistent temperature effect. Previous studies demonstrated a maximum firing rate increase and an intensity threshold decrease in the ANs also recorded from in the present study, measured with noise pulses with durations of 10 ms and 100 ms, respectively (Wolf, 1986; Franz and Ronacher, 2002; Eberhard et al., 2015). Hence, a shift of the nonlinearity to lower projection values and higher firing rates could have been expected.

However, it has recently been demonstrated that peripheral auditory neurons adapt under prolonged stimulation of more than ~ 50 ms to the mean stimulus intensity, and then encode mainly the relative intensity fluctuations in an amplitude-modulated signal (Hildebrandt et al. 2015; compare also Dahmen et al. 2010). This adaptive coding occurs before the AN stage, and might thus presynaptically adjust firing rate and threshold in the ANs within 50 ms from stimulus onset. By this mechanism, a temperature-induced threshold shift and thus a shift of the nonlinearity to lower projection values would likely be canceled out quickly after stimulus onset.

7.4.4 Temperature dependence of temporal filters: A possible mechanism for temperature coupling?

It is well-documented that the temporal structure of the calling and courtship songs of poikilothermic animals is temperature-dependent. Syllable periods (Bauer and von Helversen, 1987) and pause and syllable durations (von Helversen, 1972) decrease with temperature in grasshoppers. To compare the Q_{10} values obtained from the STA filter parameters to this published data, the Q_{10} model fit was calculated to the data extracted from fig. 6 in Bauer and von Helversen (1987) and fig. 6 and 7 in von Helversen (1972). For T_0, the lowest temperature was chosen. This procedure revealed a Q_{10} of 0.63 for the syllable period of female grasshoppers of the species *Chorthippus parallelus* and 0.54 for *Chorthippus montanus* females; Bauer and von Helversen (1987) reported that this corresponded exactly to the temperature dependence of the male songs. *Chorthippus biguttulus* males change their song's pause durations with a Q_{10} of 0.59, and the syllable durations with 0.55, 0.61, and 0.56 (four, six, and eight pulses, respectively). These Q_{10}s correspond well in trend with the Q_{10}s of the STA filters, though the latter tend to be slightly higher. A matching temporal compression thus occurs both in the songs as well as the STA filters.

Since the neurons in the auditory pathway of grasshoppers are morphologically and physiologically largely conserved across species, this finding can very likely be generalized to other acridid grasshoppers. However, calling songs differ remark-

ably between species; thus, it is difficult to link the absolute filter parameters measured in these peripheral interneurons to the song parameters of different grasshoppers. A general trend, however, is a temporal compression of both the song and the sound features auditory neurons respond to. It is thus more likely that the changes in the STA filters reflect rather general aspects of temperature dependence of neuronal processing, and constitute the boundaries within which signals and signal processing structures have evolved.

7.4.5 Conclusion

Temporal filtering in neurons in the auditory pathway of locusts is temperature-dependent, which manifests itself firstly in a temporal compression of the feature preference, and secondly in a change in general feature selectivity. The temporal compression of the feature preference corresponds quantitatively to reported changes in grasshopper calling songs, and might thus potentially contribute to temperature coupling of the sender and the receiver at an early stage of auditory processing. How exactly the temperature effect on the preferred feature shape affects sound processing and recognition is not clear at the moment and poses an interesting question for further investigations.

No evidence was found for a general temperature-dependence of the nonlinear gain function, which translates the filter output into the neuronal firing rate. By this, the intensity-dependence of the auditory system, which has been previously demonstrated for short stimuli, might be canceled out in order to enable adaptive coding irrespective of temperature.

8 Conclusion

This thesis addressed the stimulus- and context-dependence of temporal filtering in the auditory pathway of the migratory locust, *Locusta migratoria*. To this end, temporal integration and response recovery from acute adaptation of single neurons were quantified by acoustic stimulation with short clicks and click pairs at subthreshold and above-threshold sound pressure levels, and the temporal feature selectivity of these neurons in a highly adapted state was investigated at several temperatures.

The general conclusion that can be drawn from this thesis is, that temporal filtering in the locust auditory pathway depends both on stimulus as well as on context. The subthreshold integration time of a neuron cannot be directly translated into the response properties to above-threshold stimulation. The distinction becomes clearest at the stage of the ascending neurons. An ascending neuron, in case of the AN12 for instance, may integrate subthreshold input over comparably long time windows of 10 ms or more. But once a single stimulus is loud enough to elicit a spike, the response to a succeeding stimulus can be suppressed for intervals exceeding 30 ms. In both cases, the AN12 exhibits low-pass filtering. Another example however, from the AN11 neuron, shows that a neuron's response to a second stimulus can be suppressed for long interstimulus intervals (enabling low-pass filtering), whereas the same neuron type does not perform clear subthreshold stimulus integration, which points more to high-pass or all-pass filtering properties. Hence, temporal filtering implemented in a certain neuron clearly depends on the specific stimulus at hand. Most likely, the short-term adaptations a neuron realizes in response to a specific stimulus are neuron-specific, which enables dynamic stimulus coding in this small, size-constrained system. Note that in case of subthreshold integration, the neuron is not in an adapted state, while once a spike is evoked by an above-threshold stimulus, (short-term) adaptation is triggered. This can be a mechanism contributing to dynamic temporal filtering.

Not only the stimulus at hand influences temporal filtering, but also the context of acoustic stimulation. This was investigated in the present thesis by determining temporal feature selectivity in auditory neurons at cold and warm temperatures. The main effect here was a temporal compression of the feature preference with a temperature increase, with an additional, though subtle, effect on the preferred feature shape. These effects, quantified by a Q_{10} model, match reported temperature effects on grasshopper song production, and hence might constitute a neuronal correlate for a temperature coupling of the sender and the receiver in this communication system, established early in the sensory periphery.

To conclude, the response properties of a specific auditory neuron are shaped by several temporal processing features, as integration time constants and adaptation time courses, arising from both neuron-intrinsic as well as network computations. Peripheral filtering extracts the information available for the brain in order to detect, localize and evaluate a signal, and, maybe most importantly, to generate an appropriate response behavior. Particularly in a size-constrained sensory system – like the grasshopper's auditory pathway – dynamic peripheral temporal filtering allows an organism to adapt to the current stimulus and ambience at hand. The basic mechanisms implemented in this relatively "simple" sensory system may resemble coding in more complex neuronal networks, since they constitute fundamental requirements for adequate signal processing.

8.1 Outlook

My work may inspire future research to further elucidate the cellular and molecular mechanisms which yield neuron-specific temporal filtering, e.g., the composition of ion channels in the neuronal membrane. Patch clamp recording techniques and simultaneous intracellular recordings from neuron pairs could further disentangle neuron-intrinsic from presynaptic network effects.

On a functional level, it would be interesting to test temporal integration of clicks in the presence of a constant background noise. This could reveal how adaptation influences the integration time, in that case of the relative changes in stimulus mean. Temporal integration as well as response recovery could be tested for temperature-dependence to compare qualitative and quantitative changes to the temperature effects on the STA filters. Thus, the temperature-dependencies of different neuronal computations and processes might be disentangled and compared.

From a broader perspective, it would be interesting to test the influence of stimulus- and context-dependent changes in temporal filtering on behavior. However, grasshoppers integrate a song over hundreds of milliseconds and more before responding – this probably masks temporal filtering on a short time scale or in the previously unadapted system, respectively. A possible target for behavioral testing could be the flight reflex, which might be acoustically triggered by very short sounds.

Bibliography

L. Abbott and W. G. Regehr. Synaptic computation. *Nature*, 431(7010):796–803, 2004.

C. A. Baker and B. A. Carlson. Short-term depression, temporal summation, and onset inhibition shape interval tuning in midbrain neurons. *The Journal of Neuroscience*, 34(43):14272–14287, 2014.

M. Bauer and O. von Helversen. Separate localization of sound recognizing and sound producing neural mechanisms in a grasshopper. *Journal of Comparative Physiology A*, 161(1):95–101, 1987.

M. F. Bear and R. C. Malenka. Synaptic plasticity: LTP and LTD. *Current Opinion in Neurobiology*, 4(3):389–399, 1994.

J. Benda and A. V. M. Herz. A universal model for spike-frequency adaptation. *Neural Computation*, 15(11):2523–2564, 2003.

A. F. Bennett. Temperature and muscle. *The Journal of Experimental Biology*, 115(1): 333–344, 1985.

J. M. Bower and L. B. Haberly. Facilitating and nonfacilitating synapses on pyramidal cells: A correlation between physiology and morphology. *Proceedings of the National Academy of Sciences*, 83(4):1115–1119, 1986.

G. Boyan. Common synaptic drive to segmentally homologous interneurons in the locust. *Journal of Comparative Neurology*, 321(4):544–554, 1992.

T. Branco and K. Staras. The probability of neurotransmitter release: Variability and feedback control at single synapses. *Nature Reviews Neuroscience*, 10(5):373–383, 2009.

D. A. Brown and P. R. Adams. Muscarinic suppression of a novel voltage-sensitive K^+ current in a vertebrate neurone. *Nature*, 283(5748):673–676, 1980.

F. S. Chance, S. B. Nelson, and L. F. Abbott. Synaptic depression and the temporal response characteristics of V1 cells. *The Journal of Neuroscience*, 18(12):4785–4799, 1998.

F. Clarac, A. El Manira, and D. Cattaert. Presynaptic control as a mechanism of sensory-motor integration. *Current Opinion in Neurobiology*, 2(6):764–769, 1992.

K. A. Clark, A. D. Randall, and G. L. Collingridge. A comparison of paired-pulsed facilitation of AMPA and NMDA receptor-mediated excitatory postsynaptic currents in the hippocampus. *Experimental Brain Research*, 101(2):272–278, 1994.

J. Clemens and B. Ronacher. Feature extraction and integration underlying perceptual decision making during courtship behavior. *The Journal of Neuroscience*, 33 (29):12136–12145, 2013.

J. Clemens, O. Kutzki, B. Ronacher, S. Schreiber, and S. Wohlgemuth. Efficient transformation of an auditory population code in a small sensory system. *Proceedings of the National Academy of Sciences*, 108(33):13812–13817, 2011.

J. Clemens, S. Wohlgemuth, and B. Ronacher. Nonlinear computations underlying temporal and population sparseness in the auditory system of the grasshopper. *The Journal of Neuroscience*, 32(29):10053–10062, 2012.

F. Coro, M. Perez, and A. Machado. Effects of temperature on a moth auditory receptor. *Journal of Comparative Physiology A*, 174(4):517–525, 1994.

A. R. Cossins and K. Bowler. *Temperature biology of animals*. Springer Science & Business Media, 1987.

F. Creutzig, J. Benda, S. Wohlgemuth, A. Stumpner, B. Ronacher, and A. V. M. Herz. Timescale-invariant pattern recognition by feedforward inhibition and parallel signal processing. *Neural Computation*, 22(6):1493–1510, 2010.

J. C. Dahmen, P. Keating, F. R. Nodal, A. L. Schulz, and A. J. King. Adaptation to stimulus statistics in the perception and neural representation of auditory space. *Neuron*, 66(6):937–948, 2010.

Y. Dan and M.-M. Poo. Spike timing-dependent plasticity of neural circuits. *Neuron*, 44(1):23–30, 2004.

J. Davenport. *Animal life at low temperature*. Springer Science & Business Media, 2012.

G. W. Davis and R. Murphey. A role for postsynaptic neurons in determining presynaptic release properties in the cricket CNS: Evidence for retrograde control of facilitation. *The Journal of Neuroscience*, 13(9):3827–3838, 1993.

E. De Boer. Auditory time constants: A paradox? In *Time resolution in auditory systems*, pages 141–158. Springer Berlin Heidelberg, 1985.

D. Debanne, N. C. Guérineau, B. H. Gähwiler, and S. M. Thompson. Paired-pulse facilitation and depression at unitary synapses in rat hippocampus: Quantal fluctuation affects subsequent release. *The Journal of Physiology*, 491(1):163–176, 1996.

J. Del Castillo and B. Katz. Statistical factors involved in neuromuscular facilitation and depression. *The Journal of Physiology*, 124(3):574–585, 1954.

J. S. Dittman, A. C. Kreitzer, and W. G. Regehr. Interplay between facilitation, depression, and residual calcium at three presynaptic terminals. *The Journal of Neuroscience*, 20(4):1374–1385, 2000.

J. A. Doherty. Temperature coupling and "trade-off" phenomena in the acoustic communication system of the cricket, *Gryllus bimaculatus* De Geer (Gryllidae). *The Journal of Experimental Biology*, 114(1):17–35, 1985.

M. J. B. Eberhard, S. D. Gordon, J. F. C. Windmill, and B. Ronacher. Temperature effects on the tympanal membrane and auditory receptor neurons in the locust. *Journal of Comparative Physiology A*, 200(9):837–847, 2014.

M. J. B. Eberhard, J.-H. Schleimer, S. Schreiber, and B. Ronacher. A temperature rise reduces trial-to-trial variability of locust auditory neuron responses. *Journal of Neurophysiology*, 114:1424–1437, 2015.

D. Ehrlich, J. H. Casseday, and E. Covey. Neural tuning to sound duration in the inferior colliculus of the big brown bat, *Eptesicus fuscus*. *Journal of Neurophysiology*, 77(5):2360–2372, 1997.

N. Elsner. Neuroethology of sound production in gomphocerine grasshoppers (Orthoptera: Acrididae). *Journal of Comparative Physiology*, 88(1):67–102, 1974.

P. A. Faure and R. R. Hoy. Neuroethology of the katydid T-cell. I. Tuning and responses to pure tones. *The Journal of Experimental Biology*, 203(21):3225–3242, 2000.

P. G. Finlayson and M. S. Cynader. Synaptic depression in visual cortex tissue slices: An in vitro model for cortical neuron adaptation. *Experimental Brain Research*, 106 (1):145–155, 1995.

I. A. Fleidervish, A. Friedman, and M. J. Gutnick. Slow inactivation of Na^+ current and slow cumulative spike adaptation in mouse and guinea-pig neocortical neurones in slices. *The Journal of Physiology*, 493(1):83–97, 1996.

P. Fonseca and T. Correia. Effects of temperature on tuning of the auditory pathway in the cicada *Tettigetta josei* (Hemiptera, Tibicinidae). *The Journal of Experimental Biology*, 210(10):1834–1845, 2007.

E. S. Fortune and G. J. Rose. Short-term synaptic plasticity as a temporal filter. *Trends in Neurosciences*, 24(7):381–385, 2001.

F. Franke, M. Natora, C. Boucsein, M. H. Munk, and K. Obermayer. An online spike detection and spike classification algorithm capable of instantaneous resolution of overlapping spikes. *Journal of Computational Neuroscience*, 29(1-2):127–148, 2010.

A. Franz and B. Ronacher. Temperature dependence of temporal resolution in an insect nervous system. *Journal of Comparative Physiology A*, 188(4):261–271, 2002.

A. French and J. Kuster. The effects of temperature on mechanotransduction in the cockroach tactile spine. *Journal of Comparative Physiology*, 147(2):251–258, 1982.

W. Garner. The effect of frequency spectrum on temporal integration of energy in the ear. *The Journal of the Acoustical Society of America*, 19:808–815, 1947.

H. Gerhardt and F. Huber. Acoustic communication in insects and anurans. *Chicago University Press, Chicago*, 2002.

H. C. Gerhardt. Temperature coupling in the vocal communication system of the gray tree frog, *Hyla versicolor*. *Science*, 199(4332):992–994, 1978.

T. Gollisch and A. V. M. Herz. Input-driven components of spike-frequency adaptation can be unmasked in vivo. *The Journal of Neuroscience*, 24(34):7435–7444, 2004.

T. Gollisch and A. V. M. Herz. Disentangling sub-millisecond processes within an auditory transduction chain. *PLoS Biology*, 3(1):e8, 2005.

T. Gollisch, H. Schütze, J. Benda, and A. V. M. Herz. Energy integration describes sound-intensity coding in an insect auditory system. *The Journal of Neuroscience*, 22(23):10434–10448, 2002.

D. M. Green. Temporal factors in psychoacoustics. In *Time resolution in auditory systems*, pages 122–140. Springer Berlin Heidelberg, 1985.

A. D. Grinnell and S. Hagiwara. Studies of auditory neurophysiology in non-echolocating bats, and adaptations for echolocation in one genus, *Rousettus*. *Zeitschrift für vergleichende Physiologie*, 76(1):82–96, 1972.

H. Halex, W. Kaiser, and K. Kalmring. Projection areas and branching patterns of the tympanal receptor cells in migratory locusts, *Locusta migratoria* and *Schistocerca gregaria*. *Cell and Tissue Research*, 253(3):517–528, 1988.

J. He, T. Hashikawa, H. Ojima, and Y. Kinouchi. Temporal integration and duration tuning in the dorsal zone of cat auditory cortex. *The Journal of Neuroscience*, 17(7): 2615–2625, 1997.

P. Heil. First-spike latency of auditory neurons revisited. *Current Opinion in Neurobiology*, 14(4):461–467, 2004.

P. Heil and H. Neubauer. Temporal integration of sound pressure determines thresholds of auditory-nerve fibers. *The Journal of Neuroscience*, 21(18):7404–7415, 2001.

P. Heil and H. Neubauer. A unifying basis of auditory thresholds based on temporal summation. *Proceedings of the National Academy of Sciences*, 100(10):6151–6156, 2003.

P. Heil, H. Neubauer, M. Brown, and D. R. Irvine. Towards a unifying basis of auditory thresholds: Distributions of the first-spike latencies of auditory-nerve fibers. *Hearing Research*, 238(1):25–38, 2008.

P. Heil, J. L. Verhey, and B. Zoefel. Modelling detection thresholds for sounds repeated at different delays. *Hearing Research*, 296:83–95, 2013.

R. M. Hennig, A. Franz, and A. Stumpner. Processing of auditory information in insects. *Microscopy Research and Technique*, 63(6):351–374, 2004.

R. M. Hennig, K.-G. Heller, and J. Clemens. Time and timing in the acoustic recognition system of crickets. *Frontiers in Physiology*, 5, 2014.

K. R. Henry. Enhancement of the cochlear nerve compound action potential: Sharply defined frequency-intensity domains bordering the tuning curve. *Hearing Research*, 56(1):239–245, 1991.

K. S. Henry, M. D. Gall, G. M. Bidelman, and J. R. Lucas. Songbirds tradeoff auditory frequency resolution and temporal resolution. *Journal of Comparative Physiology A*, 197(4):351–359, 2011.

K. J. Hildebrandt. Neural maps in insect versus vertebrate auditory systems. *Current Opinion in Neurobiology*, 24(1):82–87, 2014.

K. J. Hildebrandt, J. Benda, and R. M. Hennig. The origin of adaptation in the auditory pathway of locusts is specific to cell type and function. *The Journal of Neuroscience*, 29(8):2626–2636, 2009.

K. J. Hildebrandt, B. Ronacher, R. M. Hennig, and J. Benda. A neural mechanism for time-window separation resolves ambiguity of adaptive coding. *PLoS Biology*, 13 (3):e1002096–e1002096, 2015.

A. L. Hodgkin and A. F. Huxley. Currents carried by sodium and potassium ions through the membrane of the giant axon of *Loligo*. *The Journal of Physiology*, 116 (4):449–472, 1952.

A. Hudspeth, Y. Choe, A. Mehta, and P. Martin. Putting ion channels to work: Mechanoelectrical transduction, adaptation, and amplification by hair cells. *Proceedings of the National Academy of Sciences*, 97(22):11765–11772, 2000.

M. Ito. Long-term depression. *Annual Review of Neuroscience*, 12(1):85–102, 1989.

K. Jacobs, B. Otte, and R. Lakes-Harlan. Tympanal receptor cells of *Schistocerca gregaria*: Correlation of soma positions and dendrite attachment sites, central projections and physiologies. *Journal of Experimental Zoology*, 283(3):270–285, 1999.

R. Janssen. Thermal influences on nervous system function. *Neuroscience & Biobehavioral Reviews*, 16(3):399–413, 1992.

D. Jiang, A. R. Palmer, and I. Winter. Frequency extent of two-tone facilitation in onset units in the ventral cochlear nucleus. *Journal of Neurophysiology*, 75(1):380–395, 1996.

R. A. Kastelein, L. Hoek, C. A. F. de Jong, and P. J. Wensveen. The effect of signal duration on the underwater detection thresholds of a harbor porpoise (*Phocoena phocoena*) for single frequency-modulated tonal signals between 0.25 and 160 kHz. *The Journal of the Acoustical Society of America*, 128(5):3211–3222, 2010.

B. Katz and R. Miledi. The role of calcium in neuromuscular facilitation. *The Journal of Physiology*, 195(2):481–492, 1968.

K. J. Kim and F. Rieke. Slow Na^+ inactivation and variance adaptation in salamander retinal ganglion cells. *The Journal of Neuroscience*, 23(4):1506–1516, 2003.

V. A. Klyachko and C. F. Stevens. Excitatory and feed-forward inhibitory hippocampal synapses work synergistically as an adaptive filter of natural spike trains. *PLoS Biology*, 4(7):e207, 2006.

R. Krahe. *Verarbeitung verhaltensrelevanter Lautattrappen durch die aufsteigenden auditorischen Interneurone von Feldheuschrecken*. PhD thesis, Humboldt-Universität zu Berlin, 1997.

O. Kutzki. *Kodierung verhaltensrelevanter Gesangsparameter bei Chorthippus biguttulus*. PhD thesis, Humboldt-Universität zu Berlin, 2012.

F. Ladich and G. Schleinzer. Effect of temperature on acoustic communication: Sound production in the croaking gourami (labyrinth fishes). *Comparative Biochemistry and Physiology Part A: Molecular & Integrative Physiology*, 182:8–13, 2015.

M. London and M. Häusser. Dendritic computation. *Annual Review of Neuroscience*, 28:503–532, 2005.

B. Lütkenhöner. Auditory signal detection appears to depend on temporal integration of subthreshold activity in auditory cortex. *Brain Research*, 1385:206–216, 2011.

C. K. Machens, M. B. Stemmler, P. Prinz, R. Krahe, B. Ronacher, and A. V. M. Herz. Representation of acoustic communication signals by insect auditory receptor neurons. *The Journal of Neuroscience*, 21(9):3215–3227, 2001.

D. V. Madison and R. A. Nicoll. Control of the repetitive discharge of rat CA1 pyramidal neurones in vitro. *The Journal of Physiology*, 354:319–331, 1984.

D. V. Madison, R. C. Malenka, and R. A. Nicoll. Mechanisms underlying long-term potentiation of synaptic transmission. *Annual Review of Neuroscience*, 14(1):379–397, 1991.

J. C. Magee. Dendritic integration of excitatory synaptic input. *Nature Reviews Neuroscience*, 1(3):181–190, 2000.

J. C. Magee and E. P. Cook. Somatic EPSP amplitude is independent of synapse location in hippocampal pyramidal neurons. *Nature Neuroscience*, 3(9):895–903, 2000.

V. Marquart. Local interneurons mediating excitation and inhibition onto ascending neurons in the auditory pathway of the grasshopper. *Naturwissenschaften*, 72:42–44, 1985.

S. D. Martin, D. A. Gray, and W. H. Cade. Fine-scale temperature effects on cricket calling song. *Canadian Journal of Zoology*, 78(5):706–712, 2000.

G. Meckenhäuser, S. Krämer, F. Farkhooi, B. Ronacher, and M. P. Nawrot. Neural representation of calling songs and their behavioral relevance in the grasshopper auditory system. *Frontiers in Systems Neuroscience*, 8:183, 2014.

S. Mennerick and C. F. Zorumski. Paired-pulse modulation of fast excitatory synaptic currents in microcultures of rat hippocampal neurons. *The Journal of Physiology*, 488(1):85–101, 1995.

J. Meyer and N. Elsner. How well are frequency sensitivities of grasshopper ears tuned to species-specific song spectra? *The Journal of Experimental Biology*, 199(7): 1631–1642, 1996.

A. Michelsen. The physiology of the locust ear. I. Frequency sensitivity of single cells in the isolated ear. *Zeitschrift für vergleichende Physiologie*, 71(1):49–62, 1971.

H. Motomura and T. Narahashi. Temperature dependence of pyrethroid modification of single sodium channels in rat hippocampal neurons. *The Journal of Membrane Biology*, 177(1):23–39, 2000.

K. I. Nagel and A. J. Doupe. Temporal processing and adaptation in the songbird auditory forebrain. *Neuron*, 51(6):845–859, 2006.

P. C. Nelson and E. D. Young. Neural correlates of context-dependent perceptual enhancement in the inferior colliculus. *The Journal of Neuroscience*, 30(19):6577–6587, 2010.

D. Neuhofer, S. Wohlgemuth, A. Stumpner, and B. Ronacher. Evolutionarily conserved coding properties of auditory neurons across grasshopper species. *Proceedings of the Royal Society of London B*, 275(1646):1965–1974, 2008.

T. Ohashi, K. Ochi, H. Nishino, M. Kenmochi, and K. Yoshida. Recovery of human compound action potential using a paired-click stimulation paradigm. *Hearing Research*, 203(1):192–200, 2005.

K. Okanoya and R. J. Dooling. Temporal integration in zebra finches (*Poephila guttata*). *The Journal of the Acoustical Society of America*, 87(6):2782–2784, 1990.

A.-M. M. Oswald, M. L. Schiff, and A. D. Reyes. Synaptic mechanisms underlying auditory processing. *Current Opinion in Neurobiology*, 16(4):371–376, 2006.

P. S. Palombi, P. M. Backoff, and D. M. Caspary. Paired tone facilitation in dorsal cochlear nucleus neurons: A short-term potentiation model testable in vivo. *Hearing Research*, 75(1-2):175–183, 1994.

K. Parham, H. Zhao, and D. Kim. Responses of auditory nerve fibers of the unanesthetized decerebrate cat to click pairs as simulated echoes. *Journal of Neurophysiology*, 76(1):17–29, 1996.

K. Pearson and R. Robertson. Interneurons coactivating hindleg flexor and extensor motoneurons in the locust. *Journal of Comparative Physiology*, 144(3):391–400, 1981.

R. S. Petersen, M. Brambilla, M. R. Bale, A. Alenda, S. Panzeri, M. A. Montemurro, and M. Maravall. Diverse and temporally precise kinetic feature selectivity in the VPm thalamic nucleus. *Neuron*, 60(5):890–903, 2008.

J. W. Pillow and E. P. Simoncelli. Dimensionality reduction in neural models: An information-theoretic generalization of spike-triggered average and covariance analysis. *Journal of Vision*, 6(4):9, 2006.

A. Pires and R. Hoy. Temperature coupling in cricket acoustic communication. I. Field and laboratory studies of temperature effects on calling song production and recognition in *Gryllus firmus*. *Journal of Comparative Physiology A*, 171(1):69–78, 1992.

R. Plomp and M. Bouman. Relation between hearing threshold and duration for tone pulses. *The Journal of the Acoustical Society of America*, 31:749–758, 1959.

G. D. Pollak. Organizational and encoding features of single neurons in the inferior colliculus of bats. In *Animal Sonar Systems*, pages 549–587. Springer US, 1980.

G. D. Pollak, D. S. Marsh, R. Bodenhamer, and A. Souther. Characteristics of phasic on neurons in inferior colliculus of unanesthetized bats with observations relating to mechanisms for echo ranging. *Journal of Neurophysiology*, 40(4):926–942, 1977.

T. Preuss and D. S. Faber. Central cellular mechanisms underlying temperature-dependent changes in the goldfish startle-escape behavior. *The Journal of Neuroscience*, 23(13):5617–5626, 2003.

P. Prinz and B. Ronacher. Temporal modulation transfer functions in auditory receptor fibres of the locust (*Locusta migratoria* L.). *Journal of Comparative Physiology A*, 188(7):577–587, 2002.

M. Pusch, U. Ludewig, and T. J. Jentsch. Temperature dependence of fast and slow gating relaxations of ClC-0 chloride channels. *The Journal of General Physiology*, 109(1):105–116, 1997.

M. W. H. Remme and J. Rinzel. Role of active dendritic conductances in subthreshold input integration. *Journal of Computational Neuroscience*, 31(1):13–30, 2011.

A. Reyes, R. Lujan, A. Rozov, N. Burnashev, P. Somogyi, and B. Sakmann. Target-cell-specific facilitation and depression in neocortical circuits. *Nature Neuroscience*, 1(4):279–285, 1998.

M. G. Ritchie, M. Saarikettu, S. Livingstone, and A. Hoikkala. Characterization of female preference functions for *Drosophila montana* courtship song and a test of the temperature coupling hypothesis. *Evolution*, 55(4):721–727, 2001.

R. M. Robertson and T. G. Money. Temperature and neuronal circuit function: Compensation, tuning and tolerance. *Current Opinion in Neurobiology*, 22(4):724–734, 2012.

F. A. Roemschied, M. J. B. Eberhard, J.-H. Schleimer, B. Ronacher, and S. Schreiber. Cell-intrinsic mechanisms of temperature compensation in a grasshopper sensory receptor neuron. *eLife*, 3, 2014.

A. Rokem, S. Watzl, T. Gollisch, M. Stemmler, A. V. M. Herz, and I. Samengo. Spike-timing precision underlies the coding efficiency of auditory receptor neurons. *Journal of Neurophysiology*, 95(4):2541–2552, 2006.

H. Römer. Die Informationsverarbeitung tympanaler Rezeptorelemente von *Locusta migratoria* (Acrididae, Orthoptera). *Journal of Comparative Physiology A*, 109 (1):101–122, 1976.

H. Römer. Ecological constraints for sound communication: From grasshoppers to elephants. In F. Barth, editor, *Ecology of sensing*, pages 59–77. Springer, 2001.

H. Römer and V. Marquart. Morphology and physiology of auditory interneurons in the metathoracic ganglion of the locust. *Journal of Comparative Physiology A*, 155:249–262, 1984.

B. Ronacher. Processing of species-specific signals in the auditory pathway of grasshoppers. In B. Hedwig, editor, *Insect hearing and acoustic communication.*, pages 185–204. Springer Berlin Heidelberg, 2014.

B. Ronacher and R. Krahe. Song recognition in the grasshopper *Chorthippus biguttulus* is not impaired by shortening song signals: Implications for neuronal encoding. *Journal of Comparative Physiology A*, 183(6):729–735, 1998.

B. Ronacher and R. Krahe. Temporal integration vs. parallel processing: Coping with the variability of neuronal messages in directional hearing of insects. *European Journal of Neuroscience*, 12(6):2147–2156, 2000.

B. Ronacher and A. Stumpner. Filtering of behaviourally relevant temporal parameters of a grasshopper's song by an auditory interneuron. *Journal of Comparative Physiology A*, 163(4):517–523, 1988.

B. Ronacher and A. Stumpner. Parallel processing of song pattern and sound direction by ascending auditory interneurons in the grasshopper *Chorthippus biguttulus*. In K. Wiese, F. G. Gribakin, A. V. Popov, and G. Renninger, editors, *Sensory Systems of Arthropods.* Birkhäuser Basel, 1993.

B. Ronacher, D. v. Helversen, and O. v. Helversen. Routes and stations in the processing of auditory directional information in the CNS of a grasshopper, as revealed by surgical experiments. *Journal of Comparative Physiology A*, 158(3):363–374, 1986.

B. Ronacher, A. Franz, S. Wohlgemuth, and R. M. Hennig. Variability of spike trains and the processing of temporal patterns of acoustic signals - problems, constraints, and solutions. *Journal of Comparative Physiology A*, 190(4):257–277, 2004.

B. Ronacher, S. Wohlgemuth, A. Vogel, and R. Krahe. Discrimination of acoustic communication signals by grasshoppers (*Chorthippus biguttulus*): Temporal resolution, temporal integration, and the impact of intrinsic noise. *Journal of Comparative Psychology*, 122(3):252–263, 2008.

B. Ronacher, R. M. Hennig, and J. Clemens. Computational principles underlying recognition of acoustic signals in grasshoppers and crickets. *Journal of Comparative Physiology A*, 201(1):61–71, 2015.

P. Sabourin, H. Gottlieb, and G. S. Pollack. Carrier-dependent temporal processing in an auditory interneuron. *The Journal of the Acoustical Society of America*, 123(5): 2910–2917, 2008.

J. D. Saija, T. C. Andringa, D. Başkent, and E. G. Akyürek. Temporal integration of consecutive tones into synthetic vowels demonstrates perceptual assembly in audition. *Journal of Experimental Psychology: Human Perception and Performance*, 40 (2):857, 2014.

A. Sanborn. Acoustic signals and temperature. *Insect sounds and communication: Physiology, behaviour, ecology, and evolution. London: CRC Press, Taylor & Francis Group*, pages 111–125, 2006.

P. Schiolten, O. N. Larsen, and A. Michelsen. Mechanical time resolution in some insect ears. *Journal of Comparative Physiology*, 143(3):289–295, 1981.

A. Schmidt, B. Ronacher, and R. M. Hennig. The role of frequency, phase and time for processing of amplitude modulated signals by grasshoppers. *Journal of Comparative Physiology A*, 194(3):221–233, 2008.

K. M. Schrode and M. A. Bee. Evolutionary adaptations for the temporal processing of natural sounds by the anuran peripheral auditory system. *The Journal of Experimental Biology*, 218(6):837–848, 2015.

O. Schwartz, J. W. Pillow, N. C. Rust, and E. P. Simoncelli. Spike-triggered neural characterization. *Journal of Vision*, 6(4):13, 2006.

G. Silberberg, C. Wu, and H. Markram. Synaptic dynamics control the timing of neuronal excitation in the activated neocortical microcircuit. *The Journal of Physiology*, 556(1):19–27, 2004.

S. J. Slee, M. H. Higgs, A. L. Fairhall, and W. J. Spain. Tonotopic tuning in a sound localization circuit. *Journal of Neurophysiology*, 103(5):2857–2875, 2010.

J. W. Smolders and R. Klinke. Effects of temperature on the properties of primary auditory fibres of the spectacled caiman, *Caiman crocodilus* (L.). *Journal of Comparative Physiology A*, 155(1):19–30, 1984.

T. Sokoliuk, A. Stumpner, and B. Ronacher. GABA-like immunoreactivity suggests an inhibitory function of the thoracic low-frequency neuron (TN1) in acridid grasshoppers. *Naturwissenschaften*, 76(5):223–225, 1989.

D. L. Spavieri Jr, H. Eichner, and A. Borst. Coding efficiency of fly motion processing is set by firing rate, not firing precision. *PLoS Computational Biology*, 6(7): e1000860, 2010.

N. Spruston. Dendritic signal integration. In L. Squire, editor, *Encyclopedia of Neuroscience*, pages 445–451. Elsevier, 2009.

N. Spruston, G. Stuart, and M. Häusser. Dendritic integration. In G. Stuart, N. Spruston, and M. Häusser, editors, *Dendrites*, pages 351–399. Oxford University Press New York, 2007.

N. Stange and B. Ronacher. Grasshopper calling songs convey information about condition and health of males. *Journal of Comparative Physiology A*, 198(4):309–318, 2012.

I. B. Stiebler and P. M. Narins. Temperature-dependence of auditory nerve response properties in the frog. *Hearing Research*, 46(1):63–81, 1990.

A. Stumpner. *Auditorische thorakale Interneurone von Chorthippus biguttulus L.: Morphologische und physiologische Charakterisierung und Darstellung ihrer Filtereigenschaften für verhaltensrelevante Lautattrappen*. PhD thesis, Friedrich-Alexander-Universität Erlangen-Nürnberg, 1988.

A. Stumpner. Physiological variability of auditory neurons in a grasshopper. *Naturwissenschaften*, 76(9):427–429, 1989.

A. Stumpner and B. Ronacher. Auditory interneurones in the metathoracic ganglion of the grasshopper (*Chorthippus biguttulus*). I. Morphological and physiological characterization. *The Journal of Experimental Biology*, 158:391–410, 1991.

A. Stumpner and B. Ronacher. Neurophysiological aspects of song pattern recognition and sound localization in grasshoppers. *American Zoologist*, 34(6):696–705, 1994.

A. Stumpner and D. von Helversen. Evolution and function of auditory systems in insects. *Naturwissenschaften*, 88(4):159–170, Apr 2001.

A. Stumpner and O. von Helversen. Song production and song recognition in a group of sibling grasshopper species (*Chorthippus dorsatus*, *Ch. dichrous* and *Ch. loratus*: Orthoptera, Acrididae). *Bioacoustics*, 6(1):1–23, 1994.

A. Stumpner, B. Ronacher, and O. von Helversen. Auditory interneurones in the metathoracic ganglion of the grasshopper (*Chorthippus biguttulus*). II. Processing of temporal patterns of the song of the male. *The Journal of Experimental Biology*, 158:411–430, 1991.

A. Y. Supin, P. E. Nachtigall, and M. Breese. Evoked-potential recovery during double click stimulation in a whale: A possibility of biosonar automatic gain control. *The Journal of the Acoustical Society of America*, 121(1):618–625, 2007.

A. Surlykke and O. Bojesen. Integration time for short broad band clicks in echolocating FM-bats (*Eptesicus fuscus*). *Journal of Comparative Physiology A*, 178(2):235–241, 1996.

A. Surlykke, O. N. Larsen, and A. Michelsen. Temporal coding in the auditory receptor of the moth ear. *Journal of Comparative Physiology A*, 162:367–374, 1988.

S. M. Thompson, L. M. Masukawa, and D. A. Prince. Temperature dependence of intrinsic membrane properties and synaptic potentials in hippocampal CA1 neurons in vitro. *The Journal of Neuroscience*, 5(3):817–824, 1985.

A. M. Thomson, J. Deuchars, and D. C. West. Single axon excitatory postsynaptic potentials in neocortical interneurons exhibit pronounced paired pulse facilitation. *Neuroscience*, 54(2):347–360, 1993.

J. Tougaard. Energy detection and temporal integration in the noctuid A1 auditory receptor. *Journal of Comparative Physiology A*, 178:669–677, 1996.

J. Tougaard. Detection of short pure-tone stimuli in the noctuid ear: What are temporal integration and integration time all about? *Journal of Comparative Physiology A*, 183:563–572, 1998.

M. V. Tsodyks and H. Markram. The neural code between neocortical pyramidal neurons depends on neurotransmitter release probability. *Proceedings of the National Academy of Sciences*, 94(2):719–723, 1997.

P. van Dijk, H. P. Wit, and J. M. Segenhout. Dissecting the frog inner ear with Gaussian noise. II. Temperature dependence of inner ear function. *Hearing Research*, 114(1-2):243–251, 1997.

N. F. Viemeister and G. H. Wakefield. Temporal integration and multiple looks. *Journal of the Acoustical Society of America*, 90(2):858–865, 1991.

N. F. Viemeister, B. G. Shivapuja, and A. Recio. Physiological correlates of temporal integration. In Y. Cazals, L. Demany, and K. Horner, editors, *Auditory Physiology and Perception*. Pergamon, Oxford, 1992.

A. Vogel and B. Ronacher. Neural correlations increase between consecutive processing levels in the auditory system of locusts. *Journal of Neurophysiology*, 97(5): 3376–3385, 2007.

A. Vogel, R. M. Hennig, and B. Ronacher. Increase of neuronal response variability at higher processing levels as revealed by simultaneous recordings. *Journal of Neurophysiology*, 93(6):3548–3559, 2005.

D. von Helversen. Gesang des Männchens und Lautschema des Weibchens bei der Feldheuschrecke *Chorthippus biguttulus* (Orthoptera, Acrididae). *Journal of Comparative Physiology*, 81(4):381–422, 1972.

D. von Helversen. Acoustic communication and orientation in grasshoppers. In M. Lehrer, editor, *Orientation and communication in arthropods*, pages 301–341. Birkhäuser Basel, 1997.

D. von Helversen and O. von Helversen. Korrespondenz zwischen Gesang und auslösendem Schema bei Feldheuschrecken. *Nova Acta Leopoldina*, 54(245):449–462, 1981.

D. von Helversen, R. Balakrishnan, and O. von Helversen. Acoustic communication in a duetting grasshopper: Receiver response variability, male strategies and signal design. *Animal Behaviour*, 68(1):131–144, 2004.

A. Warzecha, W. Horstmann, and M. Egelhaaf. Temperature-dependence of neuronal performance in the motion pathway of the blowfly *Calliphora erythrocephala*. *The Journal of Experimental Biology*, 202(22):3161–3170, 1999.

G. Weschke and B. Ronacher. Influence of sound pressure level on the processing of amplitude modulations by auditory neurons of the locust. *Journal of Comparative Physiology A*, 194(3):255–265, 2008.

D. Wicher, C. Walther, and C. Wicher. Non-synaptic ion channels in insects — basic properties of currents and their modulation in neurons and skeletal muscles. *Progress in Neurobiology*, 64(5):431–525, 2001.

J. F. C. Windmill, S. Bockenhauer, and D. Robert. Time-resolved tympanal mechanics of the locust. *Journal of the Royal Society Interface*, 5(29):1435–1443, 2008.

S. Wirtssohn and B. Ronacher. Temporal integration at consecutive processing stages in the auditory pathway of the grasshopper. *Journal of Neurophysiology*, 113(7):2280–2288, 2015.

S. Wohlgemuth and B. Ronacher. Auditory discrimination of amplitude modulations based on metric distances of spike trains. *Journal of Neurophysiology*, 97(4): 3082–3092, 2007.

S. Wohlgemuth, A. Vogel, and B. Ronacher. Encoding of amplitude modulations by auditory neurons of the locust: Influence of modulation frequency, rise time, and modulation depth. *Journal of Comparative Physiology A*, 197(1):61–74, 2011.

H. Wolf. Response patterns of two auditory interneurons in a freely moving grasshopper (*Chorthippus biguttulus* L.). I. Response properties in the intact animal. *Journal of Comparative Physiology A*, 158(5):689–696, 1986.

R. Wolfenden, M. Snider, C. Ridgway, and B. Miller. The temperature dependence of enzyme rate enhancements. *Journal of the American Chemical Society*, 121(32): 7419–7420, 1999.

D. Young. *Nerve cells and animal behaviour*. Cambridge University Press, 1989.

R. S. Zucker and W. G. Regehr. Short-term synaptic plasticity. *Annual Review of Physiology*, 64(1):355–405, 2002.

J. Zwislocki. Theory of temporal auditory summation. *Journal of the Acoustical Society of America*, 32:1046–1059, 1960.

J. Zwislocki, R. Hellman, and R. Verrillo. Threshold of audibility for short pulses. *Journal of the Acoustical Society of America*, 34(10):1648–1652, 1962.

Danksagung

Mein großer Dank gilt meinem Betreuer, Prof. Bernhard Ronacher. Er hatte immer ein offenes Ohr und konstruktive Ideen bei Problemen jeder Art, und war immer unterstützend. Er hat mir großes Vertrauen entgegengebracht und mir auch die Freiheit gelassen, Ideen auszuprobieren. Seine blitzschnell angefertigten Korrekturen und kritischen Überarbeitungen meiner verschiedenen schriftlichen Arbeiten haben mir viel über Lesbarkeit von Texten und Logik von Argumenten beigebracht.

Bei Prof. Matthias Hennig möchte ich mich für seine kritischen Anmerkungen und Fragen und seine Diskussionsbereitschaft bedanken. Sie haben mich weitergebracht und mir Ideen und Anregungen gegeben. Auch danke ich ihm für seine Unterstützung in technischen Belangen und für seine Labview-Programme, die ich nutzen durfte.

Ich danke Prof. Susanne Schreiber dafür, dass sie sich stets für mich eingesetzt hat. Die Zusammenarbeit mit ihrer Arbeitsgruppe war konstruktiv und spannend, und ich habe viel Neues gelernt.

Frederic Roemschied danke ich für die Zusammenarbeit, die zur Entstehung von Kapitel 7 geführt hat. Er hat sich die Zeit genommen, mir die theoretischen Aspekte seiner Arbeit zu vermitteln. Ich danke ihm weiterhin für die gute Werbung, die er von Anfang an für die VhPhys gemacht hat und die mich in meinem Wunsch unterstützt hat, hier zu promovieren, und dass er mir Ansporn war, an meinen Kicker-Fähigkeiten zu arbeiten.

Mein besonderer Dank gilt natürlich auch den ehemaligen und aktuellen Mitgliedern der AG VhPhys. Monika Eberhard, Olaf Kutzki und Jan Clemens haben mir das intrazelluläre Ableiten gezeigt; Eileen Gabel, Nora de Camp und Florian Rau haben mich beim Erlernen des extrazellulären Ableitens unterstützt. Monika Eberhard war bei wirklich jedem Problem hilfsbereit, egal ob es um Methodik, Datenanalyse, Posteraufbau oder die ab und zu nötige mentale Unterstützung ging. Florian Raus Matlab-Tutorials und seine Spiketimes-Toolbox waren Gold wert; psychosozial förderlich in- und außerhalb der Uni war unsere geteilte Leidenschaft für Salmiak in jedwedem Aggregatzustand. Michael Reichert hat durch sein kritisches und konstruktives Korrekturlesen verschiedener schriftlicher Entwürfe oft geholfen; mit seinem enormen Fachwissen und seiner Begeisterungsfähigkeit hat er mich immer wieder motiviert. Jonas Finck war immer kreativ und hilfsbereit bei technischen Problemen. Sein kritisches Denken und sein breitgefächertes Interesse an der Biologie haben mir neue Perpektiven eröffnet. Eileen Gabel danke ich für lustige Mittagspausen mit leckerem Kaffee. Ihr moralischer Beistand hat zur Entstehung dieser Arbeit beigetragen. Stefanie Krämer hat mir das Verhalten

von Heuschrecken nähergebracht und mein Verständnis vertieft. Fleur Lebhardt und Thomas Blankers hatten bei Statistik-Fragen immer ein offenes Ohr und einen guten Rat parat. Nicole Stange danke ich für einen guten Start in der AG mit ihr als Zimmergenossin und ihr Interesse an und ihre Bereitschaft zu wissenschaftlichen Diskussionen der generellen und speziellen Art zu früher wie später Stunde. Jennifer Aufderheide war eine super Zimmergenossin, wir hatten eine gute Arbeitsatmosphäre.

Bei Jan-Hendrik Schleimer und Janina Hesse möchte ich mich für spannende Diskussionen und lustige Disziplin-übergreifende Treffen danken. Es war sehr bereichernd, über den eigenen Tellerrand zu schauen.

Ich danke Regina Lübke für die Tierpflege. Margret Franke vom BCCN Berlin danke ich für die Unterstützung im Hintergrund; es hat immer alles reibungslos funktioniert.

Außerdem danke ich Wolf Zinke. Er hat mein wissenschaftliches Denken und Arbeiten stark geprägt, und von seinen Matlab- und LaTeX-Tutorials profitiere ich noch heute.

Meiner Familie und meinen Freundinnen und Freunden danke ich dafür, dass sie mich nicht haben vergessen lassen, dass es noch ein Leben außerhalb des Labors gibt.

Ich danke Robert Kutz für seine Loyalität, seine Geduld und seine bedingungslose Unterstützung. Bei Nervenzusammenbruch-fördernden Matheformeln hat er mich gerettet. Er war immer für mich da, hat sich mit mir gefreut oder hat mich aufgefangen, wenn nichts mehr zu gehen schien. Danke für alles!

Publikationen

Artikel in wissenschaftlichen Zeitschriften

- Sarah Wirtssohn, Bernhard Ronacher (2015): "Temporal Integration at Consecutive Processing Stages in the Auditory Pathway of the Grasshopper." *Journal of Neurophysiology* 113:2280-2288.

  Author contributions: SW and BR designed experiments. SW conducted experiments, analyzed data, prepared figures, drafted manuscript. BR revised manuscript.

Artikel in Vorbereitung

- Sarah Wirtssohn, Bernhard Ronacher (2015): "Response Recovery in the Locust Auditory Pathway." *Submitted to: Journal of Neurophysiology*.

  Author contributions: SW and BR designed experiments. SW conducted experiments, analyzed data, prepared figures, drafted manuscript. BR revised manuscript.

Konferenzbeiträge

- Sarah Wirtssohn, Bernhard Ronacher (2014): "Neurophysiology of Temporal Integration in the Grasshopper Auditory System." 9th FENS Forum of Neuroscience, Mailand, Italien
- Sarah Wirtssohn, Bernhard Ronacher (2013): "Temporal Integration in the Auditory Pathway of the Grasshopper." 10th Göttingen Meeting of the German Neuroscience Society, Göttingen, Deutschland
- Sarah Wirtssohn, Bernhard Ronacher (2012): "Temporal Resolution and Integration of Short Stimuli in the Auditory Pathway of the Locust." 10th International Congress of Neuroethology, University of Maryland, USA

Selbständigkeitserklärung

Hiermit erkläre ich, dass ich diese Dissertation selbständig und nur unter Verwendung der angegebenen Literatur und Hilfsmittel angefertigt habe. Die Dissertation ist in keinem früheren Promotionsverfahren angenommen oder als ungenügend bewertet worden. Die dem angestrebten Verfahren zu Grunde liegende Promotionsordnung erkenne ich an.

Berlin, den 06.10.2015

Sarah Kaarina Wirtssohn